THE UNIVERSITY OF OKLAHOMA

GRADUATE COLLEGE

THE INTERACTION OF EXTREMELY ENERGETIC COSMIC RAY PARTICLES WITH MATTER

A THESIS

SUBMITTED TO THE GRADUATE FACULTY

in partial fulfillment of the requirements for the

degree of

DOCTOR OF PHILOSOPHY

BY

PHILIP M. FITZPATRICK

Norman, Oklahoma

1955

THE INTERACTION OF EXTREMELY ENERGETIC COSMIC RAY PARTICLES WITH MATTER

APPROVED BY

R. A. Howard

J. Rud Nielsen

[illegible]

John C. Driser

William N. Huff

THESIS COMMITTEE

ACKNOWLEDGEMENTS

It is the pleasant duty of the author to acknowledge his indebtedness to Dr. Robert Adrian Howard for his guidance, his constant encouragement and his interest during the course of this research.

His grateful thanks are due Dr. William Schriever for several helpful suggestions and discussions. He also wishes to thank his colleagues in the nuclear emulsion research group for their assistance and cooperation in various stages of the investigation. In particular he is indebted to Mr. H. Hoffman for considerable help with the calculations; to Mr. S. Urban for his assistance in processing the plates, in making measurements and in arranging for several of the photographs which are used in this thesis; to Mr. W. Osborne for the photomicrograph shown in Figure 32.

The author wishes to express his most sincere gratitude to his wife without whose patience and aid it would not have been possible to complete this work.

TABLE OF CONTENTS

LIST OF TABLES

LIST OF ILLUSTRATIONS

LIST OF ILLUSTRATIONS--Continued

LIST OF ILLUSTRATIONS--Continued

THE INTERACTION OF EXTREMELY ENERGETIC COSMIC RAY PARTICLES WITH MATTER

CHAPTER I

INTRODUCTION

The investigation reported here is a study of one aspect of the interaction of extremely energetic cosmic ray particles with matter. A large number of other investigation have been and, currently, are being performed in different laboratories, all having the common aim of gaining insight into the nature and properties of the different kinds of particles occurring in cosmic ray phenomena. The importance of the research rests upon the fact that a considerable part of our knowledge of nuclear structure is obtained from such experiments. The analysis of unusual events appearing in photographic emulsions which have been exposed to cosmic radiation at great altitudes provides the most prolific source of information concerning the aforementioned particles. The photographic emulsion technique has been used in the study described in this thesis.

The specific aims of the present research were:

1) To set up a procedure for processing nuclear emulsions exposed to cosmic rays.

2) To outline a method of correcting for the effect of distortion on the various types of track measurement.

3) To explore the potentialities of a new technique of track measurement developed in this laboratory.

4) To survey and summarize the techniques used by other research groups in making mass and energy determinations from observations of multiple Coulomb scattering.

5) To analyze a curious V-event which was observed in one of the emulsions.

6) To formulate a procedure for calculating the probable deviations of the results of the measurements which are commonly made on cosmic ray events.

In Chapter II a detailed description is given of the procedures which were used to expose and process the plates. A period of two years has elapsed since this initial work was performed and in that period more convenient methods of processing the nuclear emulsions have been developed; these will be discussed in subsequent reports. Glass-backed emulsions were used in the present research. More recently the attention of this laboratory has been directed to the examination of emulsion pellicles which provide a much larger volume of continuously sensitive medium. Although there are many important advantages to be gained from working with thicker blocks of emulsion, the technical difficulties of mounting these unsupported pellicles on glass plates (for subsequent microscopic study) without introducing excessive distortion are great. These and other related problems are now being examined.

Due to the removal of considerable amounts of silver bromide during the fixing stage the final processed emulsion suffers a large shrinkage in thickness. To make accurate measurements of the ranges of particles whose trajectories dip with respect to the viewing plane the emulsion shrinkage must be considered. The method which has been employed to take account of this effect is discussed in Chapter III. Also introduced at this point are the beginnings of a discussion of distortion which is interwoven into the remaining chapters of the thesis. A method which may be used to determine the distortion vector is described. Following this scheme the distortion vector has been determined for a particular region of interest in one of the emulsions.

Methods of obtaining estimates of mass and energy from the analysis of tracks produced by unknown particles are considered in the next two chapters. In Chapter IV the emphasis is placed upon the types of information which may be obtained from measurements of the specific ionization. Here the procedures used to calibrate the emulsions for range, grain density and gap counting are treated. A new technique of track area evaluation for severely clogged tracks is described. First attempts to explore the potentialities of the new technique appear to be most promising; discrimination is provided between alpha particles, protons and π-mesons having residual ranges of only 500 microns. This selectivity is comparable with that achieved by gap counting measurements. Plans are now underway in this laboratory aimed at refining the measurements obtainable by the method. Also described in this chapter are the procedures which have been applied to correct for the effect of distortion upon the grain and gap count observations.

A considerable amount of experimental work has been done by many emulsion research groups in which the theory of multiple Coulomb scattering has been applied as a means of securing particle identification from measurements of the small angle scattering of tracks appearing in the nuclear plates. Unfortunately the descriptions of the techniques employed and the results obtained are distributed throughout much of the literature and, thus, are not in convenient form for use. A survey has been undertaken and a summary of the general procedures in use by the various groups is presented in Chapter V. Considerable detail is given on how the results of scattering observations may be used to obtain estimates of rest mass and energy for both slow and fast particles. Also treated are the methods used to assign probable deviation to the quoted values. A description of the procedures which have been used in the present work to correct the observed scattering data for the distortion effect is included in the general discussion.

While searching the plates an unusual V-shaped track was observed. Because of certain curious aspects of the finding an extended analysis was made of the event. The results are given in Chapter VI. One of the prongs is identified as being due to a particle of approximately deuteronic mass. The second track is produced by a charged particle whose rest mass is less than 1000 electron mass units. The plane defined by the tracks contains (within 4^{o}) the center of an energetic nuclear disintegration 949 microns from the vertex of the V. A plausible explanation of the occurrence may be made by assuming that an unstable neutral particle is emitted from the nuclear disruption and subsequently decays into two charged secondaries. For such a two-body decay scheme it does not appear possible to interpret the finding in terms of previously reported V-type events because of the low Q-values involved.

Very little information has appeared in cosmic ray literature on the actual procedures used by the individual research groups to arrive at the probable deviations which they quote for physical quantities other than those quantities obtained from scattering data. This problem is examined in Appendix A. The procedures which have been developed follow from a general line of attack suggested by Schriever.*

*Wm. Schriever, Professor of Physics, University of Oklahoma.

CHAPTER II

METHODS USED IN THE EXPOSURE, PROCESSING AND SCANNING OF NUCLEAR EMULSIONS

Exposure

Electron-sensitive, Ilford, G-5, photographic emulsions, 400 microns thick, were used in the present research. An original order of one dozen 1" by 3" glass-backed emulsions was received from the manufacturer. One of the emulsions was removed from the package to be kept as a test plate. The remaining eleven plates were carefully aligned in a vertical stack, in parallel fashion, one above the other, with alternate facings of glass to glass and emulsion to emulsion. The emulsion faces were separated from each other by slender (0.5 mm thick) cardboard end strips placed along the 1" edges of the plates. Except for a few mm near the shorter edges of the plates, a 0.5 mm air gap was present between adjacent emulsion surfaces. The emulsion stack was then placed in a small rubber balloon. After the air had been exhausted from the balloon the entire unit was jacketed by a tight fitting, thin-walled cardboard container. The container was then securely bound with masking tape. The unit, thus packaged, was exposed* to cosmic radiation at an altitude of approximately 99,000 feet for 3½ hours. The plates were received in this laboratory within three days after their exposure and the processing procedure, to be described in what follows, was begun immediately, in order to minimize the possibility of latent image fading.

The "Dry" Method of Warming and Cooling Emulsions

In recent years, a considerable amount of time and effort on the part of many researchers has gone into attempting to improve the techniques of processing the nuclear emulsion with the view in mind of increasing its utility as a precision tool of research. One of the most important contributions to this work has been made by Dilworth et al. (1) of the Brussels group. These investigators have carried on an extended study of the problems of processing and have proposed procedures for handling the emulsions which have been adopted by many of the people who are investigating cosmic rays by means of photographic plates.

An outline of the processing procedure which was used in this laboratory is reproduced in Table 1. It represents

---

*The emulsions were carried aloft in a free flight balloon through the courtesy of the General Mills Co. and the office of Naval Research. The launching site and the impact point of the released load were both within 10 miles of the city of Minneapolis, Minnesota, at an approximate geomagnetic latitude of 60° N.

Table 1

Processing of 400 μ Ilford G-5 Emulsions

	Temperature	Time
Presoaking (Distilled Water)	Room $\rightarrow$ 5° C	100 min.
Penetration of Cold Developer[1]	5	100 min.
Warm, "Dry" Development	5 $\rightarrow$ 24	20 min.
Dry Cooling	24 $\rightarrow$ 5	5 min.
Acid Stop (1%)	5	100 min.
Removal of Surface Deposit		
Fixation (4 ml/cm^2 emulsion)[2]		
Clearing	5	18 hrs.
Dilution	5	24 hrs.
Washing	5	24 hrs.
Plasticizing solution ("Flexogloss")[3]	5	0.5 hrs.
Drying (Relative Humidity 69% $\rightarrow$ 63%)	23.5	7 days

[1]Developer
Distilled water.........................1000 cc
Sodium sulphite (anhydrous)..............18 g
Potassium bromide (10% solution)..........8 cc
Amidol..................................4.5 g
(Solution filtered before use)

[2]Fixing Bath
Distilled water.........................1000 cc
Sodium thiosulfate (C.P.)................400 g
Sodium bisulfite........................7.5 g
Ammonium chloride........................7 g
(Solution filtered before use)

[3]Plasticizer
10% Solution of Ansco "Flexogloss"
Ansco, Binghampton, N. Y.

but a slight modification of the Brussels technique and was suggested by Shapiro (2).

A series of experiments (A, 7-21)* was conducted to try to determine a satisfactory method of carrying out the warm "dry" development and "dry" cooling stages of the procedure. All measurements referred to below were made in a room the temperature of which was maintained at 23.5 ± 1.0 °C by means of an air conditioning unit.

To simulate the conditions which would be present during actual processing, a nuclear emulsion, affixed to its glass backing plate, was set on a stainless steel tray and the entire unit was then immersed in a cold developer bath, for a period of 2 hours. Upon removal of the tray from the bath, it was placed in an electric oven maintained at 26.0 ± 0.2 °C. The hot junction of a thermocouple** was quickly inserted in a slit between the glass and the emulsion, the cold junction being maintained at 0 °C. Data could thus be obtained to relate the rise of emulsion temperature to the time in the oven. The data points are shown in Figure 1.

---

*Reference to experimental data which is recorded in research notebooks on file in this laboratory. The identification number of the notebook is given first, followed by the pages on which the experimental data are to be found. Thus, (A, 7-21) refers to notebook A, pages 7-21 inclusive.

**A copper-constantan thermocouple was used. The thermocouple had been calibrated previously by means of a potentiometer in a conventional fashion. Before calibration the wires leading into the thermocouple junctions were insulated from each other by melted paraffin to minimize voltaic emf's.

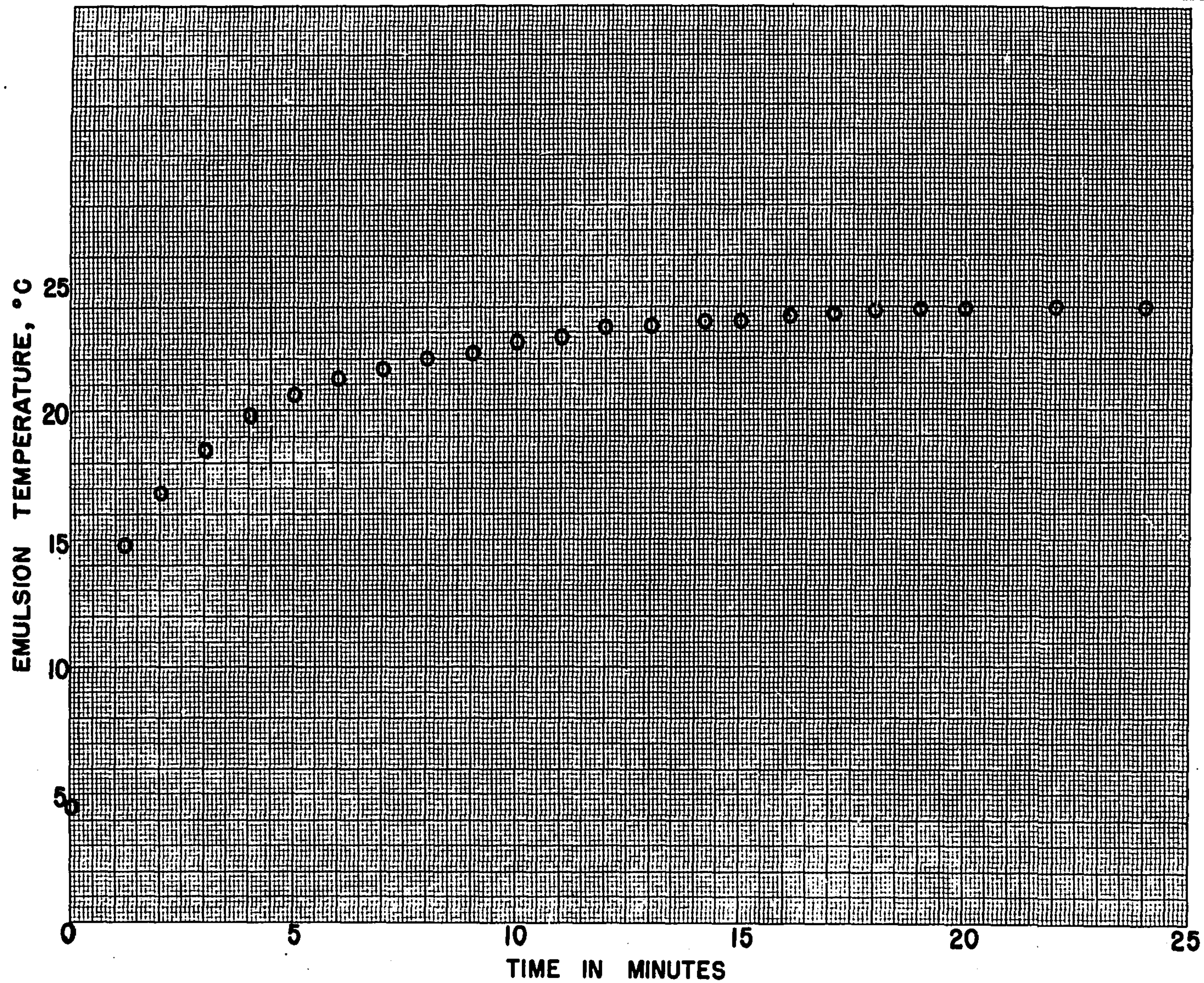

Fig. 1. Rise of emulsion temperature vs time in oven; thermocouple junction between glass backing plate and emulsion.

The experiment was repeated with the hot junction of the thermocouple being introduced between the emulsion layers rather than between the glass and the emulsion and similar results were obtained which are shown in Figure 2.

The problem of dry cooling the emulsions was examined. It was found that the main storage compartment of an ordinary household refrigerator, which was available in the laboratory, could be utilized, in a very simple fashion, to reduce the emulsion temperature from 24 °C to approximately 5 °C in a period of five minutes. For a setting of B on the refrigerator temperature control dial, the central region of the compartment after an 8 hour stabilization period was observed to have a temperature oscillation of $\pm 1\frac{1}{2}^{\circ}$ about the mean value of 3 °C. A nuclear emulsion, originally at 24 °C , was introduced into the compartment at the instant the refrigerator compressor motor cut on. The hot junction of the thermocouple was placed between the glass and the emulsion and the fall off of emulsion temperature was measured as a function of the time. The observation are shown in Figure 3. Similar measurements were made for the condition that the emulsion was introduced at the instant the compressor motor cut off. These results are also shown in Figure 3.

The exact form of the cooling curve depends on the point on the temperature cycle of the refrigerator at which the emulsion is introduced into the central compartment.

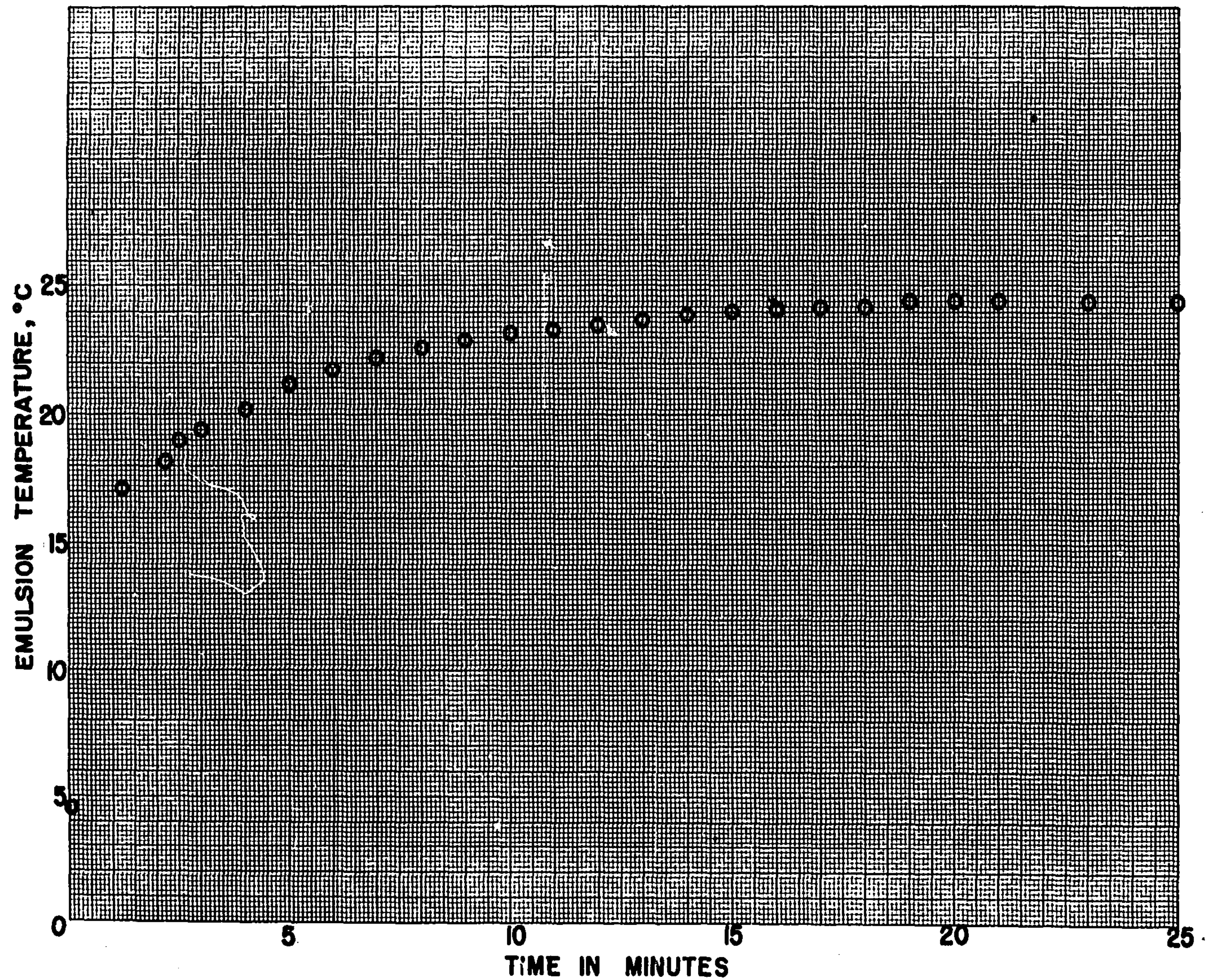

Fig. 2. Rise of emulsion temperature vs time in oven; thermocouple junction between emulsion layers.

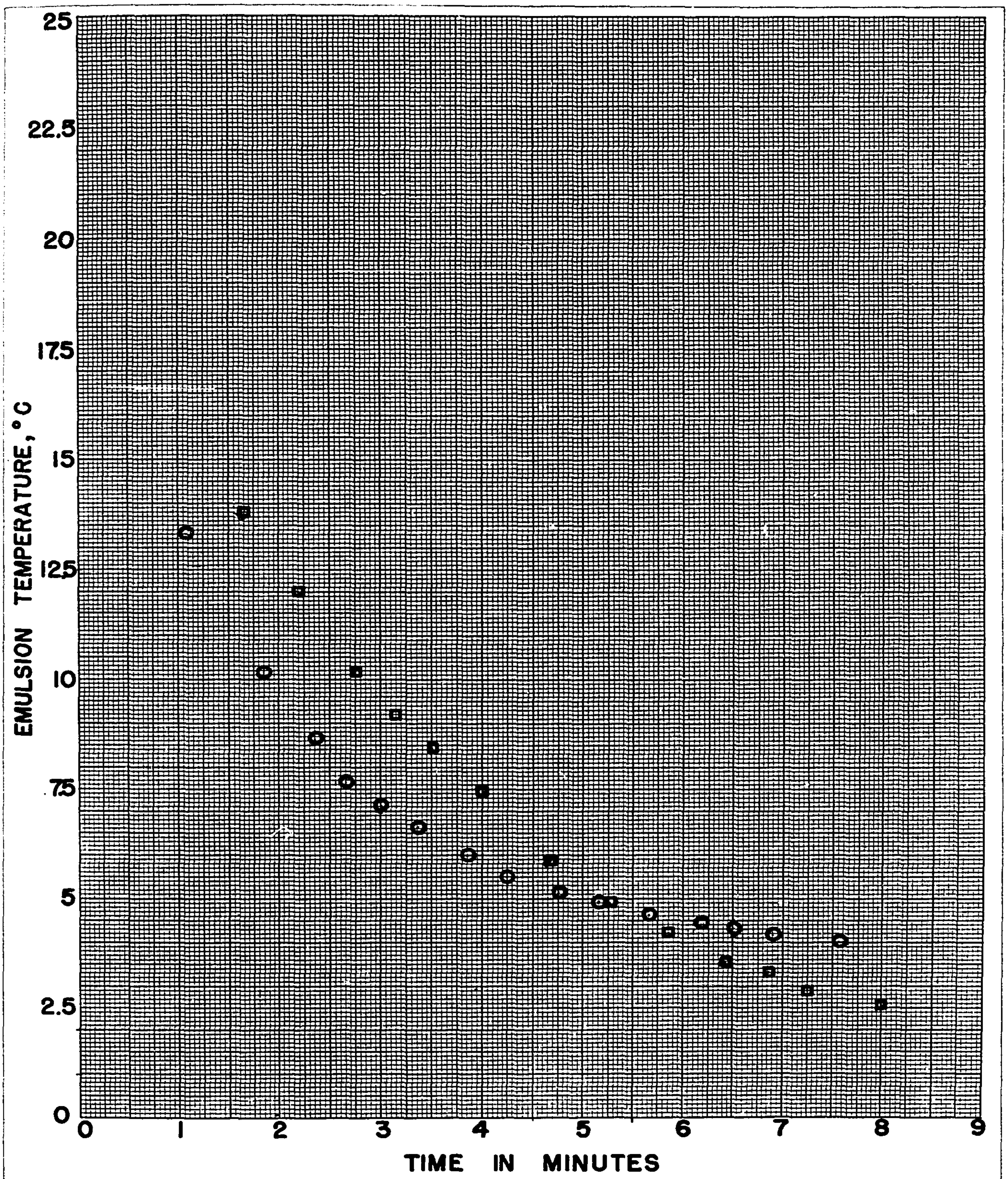

Fig. 3. Fall off of emulsion temperature vs time in cooling compartment.

From the curves in Figure 3, it is clear, however, that, regardless of where on this temperature cycle the plates are introduced into the compartment, if the emulsion temperature at the time of entry is 24 °C then after a period of 5 minutes has elapsed the emulsion temperature will have fallen to approximately 5 °C.

From the experiments described above it was concluded that the warm "dry" development and dry cooling stages of the processing procedure could be efficiently carried out in two simple stages. The nuclear plates, upon removal from the cold developer could be placed in an electric oven (maintained at 26.0 °C) for a period of 20 minutes. This would cause the emulsion temperature to be raised to approximately 24 °C. They could then be transferred to the storage compartment of the refrigerator, stabilized on setting B, for a 5 minute period, to lower their temperature to approximately 5 °C.

Processing

In order to facilitate the handling of the emulsions during processing, a special tray (shown on Figure 4) was built. The materials of the tray were chosen so as not to interact chemically with the processing solutions. Lucite end clamps are provided to hold the emulsions in position on the stainless steel base plate. The clamps are fastened to the tray bottom by means of stainless steel screws, the

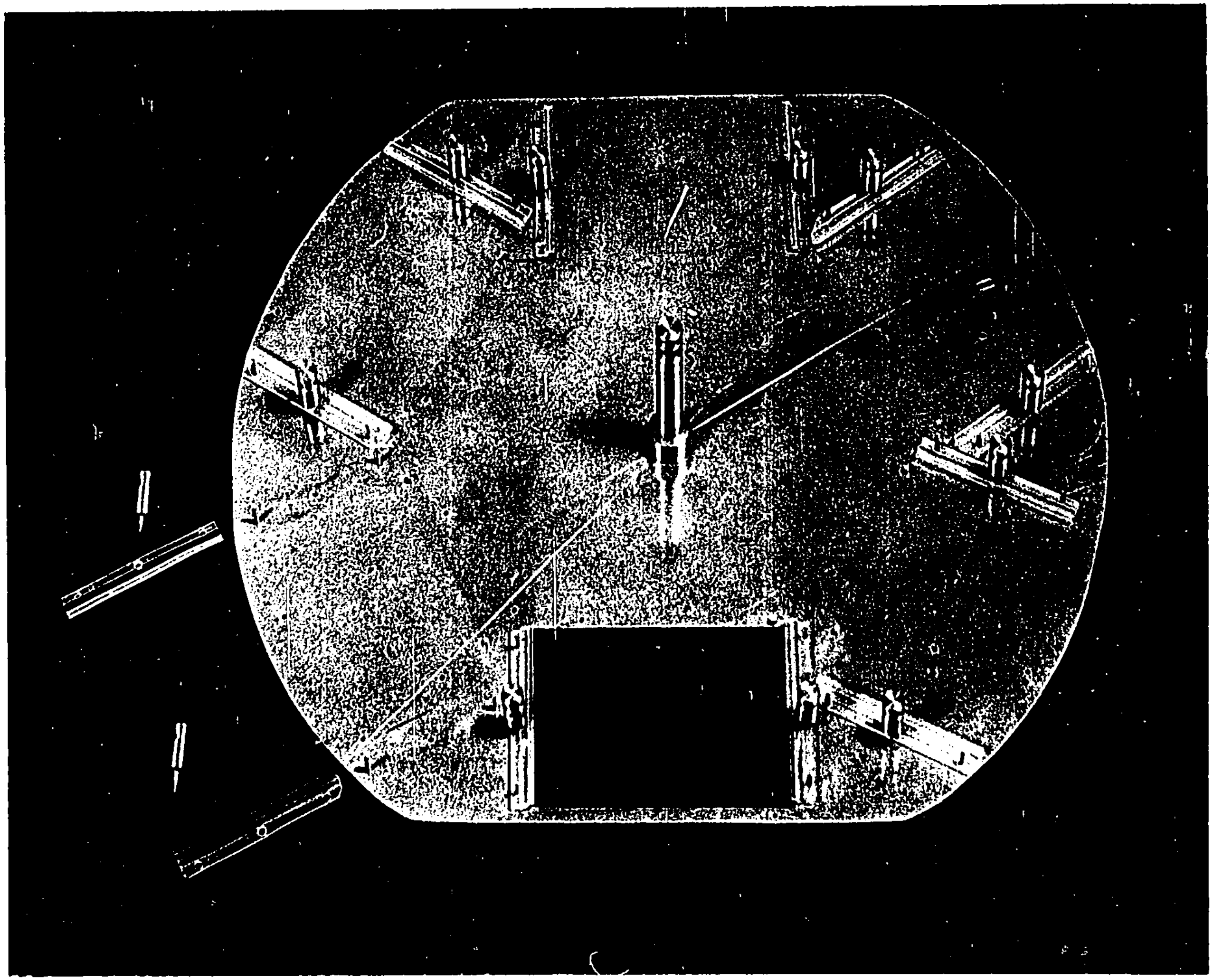

Fig. 4. Processing tray

screws also serving to control the pressure which the clamps exert on the emulsion edges.

The tray has been designed to accomodate twelve, 3" by 1", emulsions, at one time, and with the emulsions in position the assembly may be moved about quite readily by means of a detachable handle, also made of stainless steel.

As soon as the emulsions had been received in this laboratory after their high altitude exposure to cosmic rays, the processing procedure was started.* The position and orientation of each emulsion in the stack was recorded on the glass backing plate with a wax marking pencil.** The plates were then secured in position on the stainless steel platform and the assembly placed, in a horizontal position, in a larger enamel tray which contained sufficient distilled water, (at room temperature), to cover completely the emulsion surfaces.***

An ice and salt-water bath in contact with the outside surface of the enamel tray was used to lower the tem-

---

*All processing operations through the fixation stage were carried out in a photographic dark room using a low intensity red safelight as needed.

**It is necessary to maintain such a record if one is to be able to make subsequent correlations between tracks produced by cosmic ray particles which have traversed several emulsions in the stack.

***During all of the processing stages the plates were kept in a horizontal position.

perature of the distilled water. After approximately 1 hour, the temperature of the water had been reduced to $5^{\circ} \pm 2^{\circ}$ C. Thereafter, for the remainder of the pre-soaking stage, a temperature of $5^{\circ} \pm 2^{\circ}$ C was maintained by carefully controlling the ice and salt-water bath.

The purpose of the pre-soaking bath is twofold:

1) it causes the emulsion to swell, thus making it easier for the actual cold developer (used in the next stage) to penetrate uniformly the emulsion layers,

2) the gradual reduction of temperature to 5° C prepares the plates for introduction into the cold developer.

At the end of this presoak period the distilled water was replaced by an equal amount of pre-cooled developer solution already at 5° C. At this temperature, the developer is relatively inactive (2). After soaking in the cold developer for 1 hour and 40 minutes at 5° C the emulsions were transferred to an electric oven pre-set to maintain a temperature of $26.0 \pm 0.3^{\circ}$. The emulsions, at this point, were filled with absorbed developer and the actual process of development which is extremely slow at 5° C, accelerated as the temperature was raised. The "dry" method of raising the emulsion temperature has been found (3) to give more uniformity of development with depth and leave much less surface deposit of Ag than warming methods in which the emulsions are in contact with solutions. The plates were left in the oven for 20 minutes and then transferred to the central compartment of the refrigerator (stabilized on setting B). This caused a lowering of the emulsion temperature which checked the development throughout the plate. The dry-cooling also got the plates ready for the next (cold) stage of the procedure.

The assembly was removed from the refrigerator after 5 minutes and placed in a dilute acetic acid stop bath pre-cooled to 5 °C. A large cylindrical glass tank which could be conveniently employed in the subsequent fixation and washing stages was used to hold the stop bath. In this, and the following stages, the solution temperature of 5° C could be maintained readily within a few degrees by an ice and salt-water bath in contact with the outside walls of the glass tank. The plates were left in the acid solution the same length of time as that required for the cold stage development to permit complete penetration of the solution. At the beginning of this stage the emulsions were gently mopped with a sponge to remove any surface deposit which might have formed.

After 1 hour and 40 minutes, the acid bath was replaced by 5000 ml. of fixing solution at 5° C. To prevent stagnation, and thus, to provide more effective removal of the undeveloped silver bromide salt from the emulsion, the fixing solution was slowly circulated by means of two rotating stainless steel paddles immersed in a vertical position in the upper surface of the liquid. The rotary drive was furnished by a small electric motor, whose rate of rotation was controlled by a variable transformer. At 3 hour intervals, one half the volume of fixing solution was drained off and replenished by an equal amount of fresh solution at the same temperature.

After the assembly had been in the fixing bath for a total time of 18 hours, a gradual dilution of the fixing solution was begun. At regular intervals small quantities of cold distilled water were added to the tank until, after a 24 hour period, the fixing solution had been replaced by water. The plates were then washed in distilled water (at 5° C) for an additional 24 hours.

Upon completion of the washing stage the distilled water was replaced by a 10% solution of Ansco flexogloss also at 5° C. The emulsion assembly was removed from this solution after 30 minutes and the drying stage begun.

Drying

The refrigerator was well suited to serve as a drying chamber. By cutting off the compressor motor soon after the dry cooling had been accomplished and opening the door of the box, the main storage compartment was allowed to come into equilibrium with the atmosphere of the microscopy room. After loosening the lucite end clips to relieve the pressure on the emulsion edges, the emulsion tray was placed in a horizontal position on the center shelf of the refrigerator. Several trays of tap water were placed on the bottom shelf of the compartment to increase the humidity* inside the box. A 24 hour, continuous recording, Bristol, thermo-humidigraph was enclosed in the chamber with the plates to provide a record of the relative humidity variations occurring while the plates were being dried.

During the first six days of the drying stage the relative humidity remained at 69 percent ± 1 percent. On the sixth day it was observed that a slight gradient of thickness of emulsion seemed to exist between the edges of the emulsions nearest the center of the stainless steel platform and the edges nearest the outer rim. This was caused by the fact that the tray bottom was not perfectly flat. The plates were taken off the tray and placed on a wooden block which had been carefully leveled on the center shelf of the compartment. The trays of water were removed and the relative humidity in the chamber gradually dropped to 63 percent ± 1.5 percent.** After the plates had dried for 7 days they were available for study under the microscope.

---

*If the surface of the plate is dried too rapidly the moisture lower down in the emulsion tends to be trapped. This results in stresses in the soft emulsion which produce distortions. (3)

**The plates were not dried in an atmosphere of lower relative humidity because plans were underway at this time which were aimed at controlling the humidity level in the microscopy room in the neighborhood of 60 percent.

Storage

One of the most common difficulties encountered in working with nuclear emulsions is the tendency for the emulsions to peel from the glass backing plates after processing and drying, if the relative humidity to which the plates are subjected is low, or if it is allowed to vary over too wide a range. In addition, emulsions, even after processing, suffer vertical expansion and shrinkage with changes in the relative humidity, so that if precise depth measurements are to be made the relative humidity should be controlled. These and other related problems have been solved in this laboratory by storing and examining the plates in a constant-humidity, constant-temperature microscopy room. Normally the environment in this room is maintained at 70. ± 1. °F, R. H. = 60 percent ± 3 percent. The emulsions when not in use are stored in a horizontal position, on shelves, in a lucite box constructed specifically for this purpose.

Scanning

An AO Spencer Research microscope No. 5LXK was used for scanning and measuring purposes. X- and y- coordinate scales graduated in mm are rigidly attached to a circular revolving mechanical stage. Vernier attachments permit the coordinate scales to be read to 0.1 mm. The microscope optics include 10, 20 and 44 power dry objectives, a 90 power oil-immersion objective and 5, 10, 15 and 20 power eyepieces.

Since it is necessary in making many of the emulsion measurements to be able to rotate the nuclear plate independently of rotating the coordinate axes the special turntable (see Figures 5, 6) was designed and built. It may readily be interchanged with the standard plate holders provided by the manufacturer if required. Manual control makes it possible to orientate the plate at any required angle with the coordinate axes. In addition to its utility in making actual measurements, it is also a great aid when, in scanning the plates, one is checking for the possibility of related events in the emulsions. For example, if it is required to follow a track from one emulsion to the next, one plate is first superimposed upon the other upon the turntable and the plates rotated until the track in question is aligned parallel to one of the axes of the microscope stage. To be in a position to focus upon various parts of the track in the two emulsions, it is necessary only to move the microscope stage along the chosen axis.

The magnification used in surveying the plates will depend on the particular investigation being carried out. If, for example, one is interested in locating only the "black" tracks left by heavy stripped nuclei in the primary radiation, a much lower magnification is needed than would be required if one were attempting to record the "light" tracks caused by electron pairs.

In the present research, the plates were examined

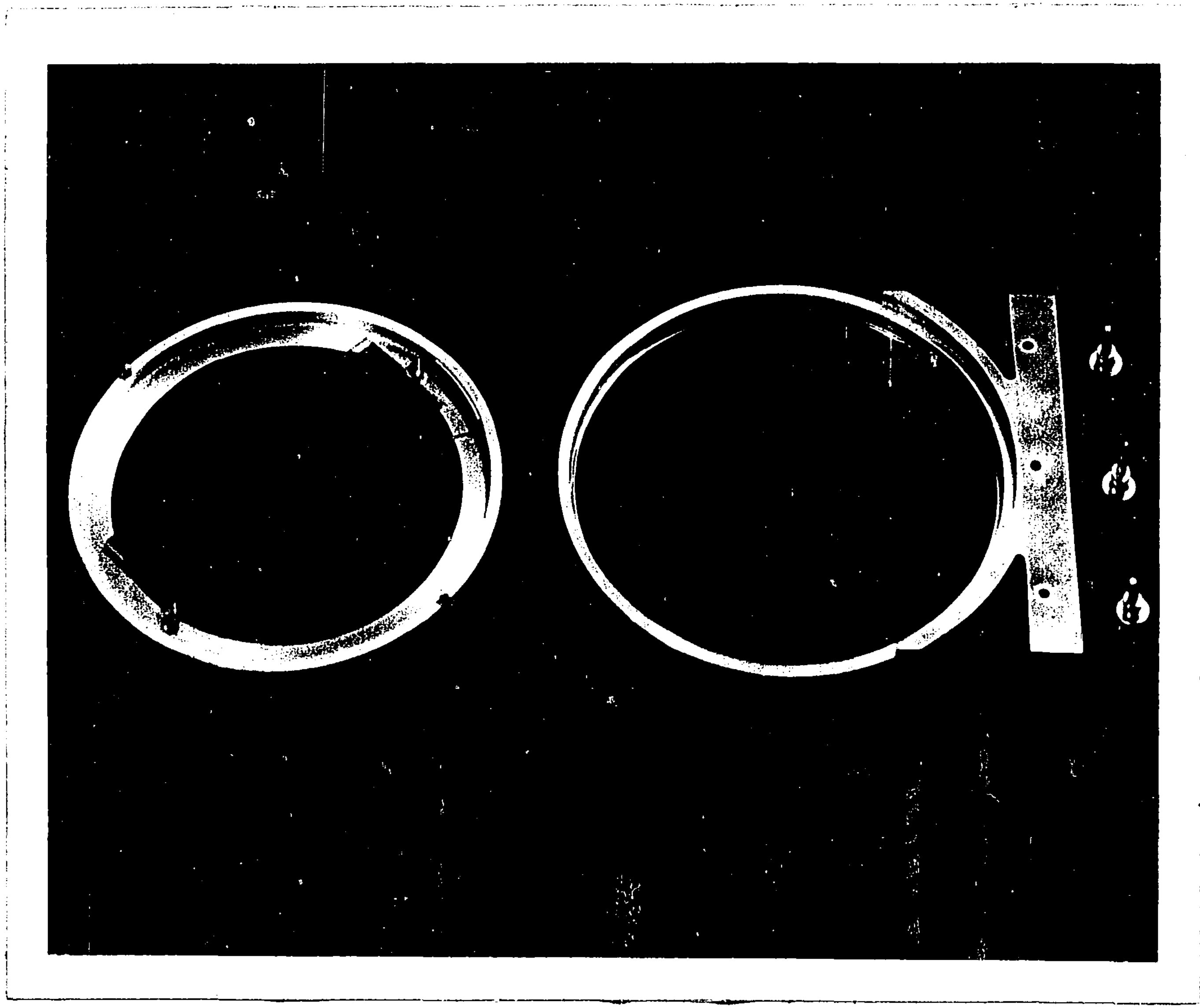

Fig. 5. Microscope turntable

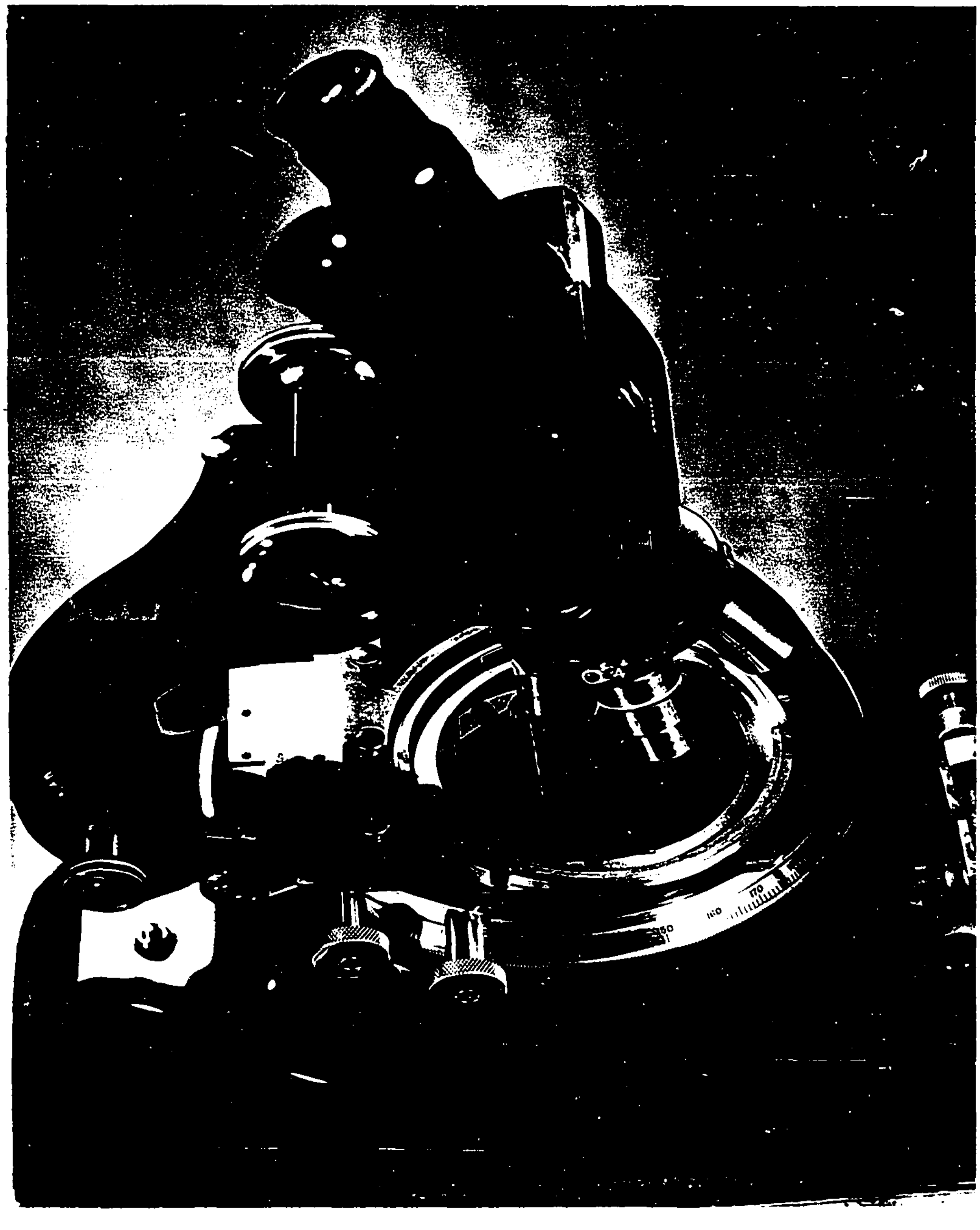

Fig. 6. AO Spencer Research microscope, No. 5LXK, with turntable.

with the two-fold purpose of recording not only curious cosmic ray events but also particle tracks which might be used subsequently for calibrating the emulsions. The use of the 44 x dry objective and 10 x eyepiece was found to be satisfactory to accomplish these ends. Careful search of the emulsions under this magnification should reveal the majority of tracks left by even the more lightly ionizing charged particles.

The scanning procedure adopted was to align the plate with its longer edge parallel to the x-axis of the microscope. Starting at either of the shorter edges of the plate successive swaths of 0.3 mm width on the x-coordinate scale were examined. This procedure results in an overlapping of the fields of view for two adjacent strips insuring against the possibility of overlooking an event. When a finding of interest was observed the event was sketched, odd features described, and the following data recorded:

1) The microscope coordinates.

2) If a star, the number of visible prongs and the depth below the air-emulsion surface.

3) Approximate ranges for the tracks of interest, and a notation as to whether or not they were arrested in the emulsion.

Tentative identifications of the particles were also made, based solely on the visual appearance of the tracks.

CHAPTER III

METHODS OF CORRECTING FOR SHRINKAGE AND DISTORTION IN NUCLEAR EMULSIONS

Emulsion Shrinkage

The thickness of a nuclear emulsion during the exposure period differs from the thickness of the same emulsion after it has been processed since the unused silver salt which constitutes a large part of the unprocessed emulsion is removed during the fixation stage. When the gelatine is well adhered to the glass backing plate the shrinkage results, approximately, in a uniform linear transformation in the z* coordinates for any point.(4).

It is necessary to correct for the effect of shrinkage when determining the length of tracks which are inclined to the viewing plane of the emulsion. This may be done by applying the formula

$$\Delta R = \left[\beta^2 + (k\delta)^2\right]^{\frac{1}{2}} \qquad (3\text{-}1)$$

---

*Conventionally, the z-axis is taken perpendicular to the viewing plane of the emulsion, and hence essentially perpendicular to the glass-gelatine interface.

which gives the original (i.e. before processing) length ΔR of an interval of track in terms of the measured projected length ρ, the shrinkage factor k, and the observed depth difference δ between the end points of the interval. Here k is defined to be the ratio of the emulsion thickness during exposure (assumed to be 400 microns in the present work) to the apparent thickness of the emulsion during observation. The apparent thickness of the emulsion is determined experimentally by measuring the difference in depth between the highest and lowest fog grains visible by means of the fine-focus control of the microscope. This procedure requires that a linear relationship exists between the vertical motion of the objective lens and the readings on the drum scale of the fine adjustment.

In order to check the relationship for the Spencer microscope a small lucite "staircase" was built which consists of a flight of 18 flat steps milled into the plastic. The average vertical separation between adjacent step levels is about 25 microns. With the staircase mounted on a 3" x 1" glass plate, the step surfaces are distinguishable readily under the microscope when the 90 x oil immersion lens is used in combination with the 10 power eyepiece. For this optical arrangement the heights of successive step levels above the base were measured by the microscope, using the fine-focus control and starting at the first step. These data (C, 2-22) were then compared with the corresponding values of step height obtained from direct measurements with a micrometer caliper and the relationship was found to be linear except at the extreme ends of the cam drive. Since the entire sweep of the fine adjustment assembly will lift the objective lens through a vertical distance of more than 2500 microns, no difficulty is encountered, if in making depth measurements with this instrument, one confines himself to the central region of the cam drive.

Emulsion Distortion

The main causes for the distortions commonly encountered in processed nuclear plates are the stresses introduced when the emulsion suffers volume changes (5). Even before processing, such volume changes may be occasioned by temperature and pressure variations. With the exception of distortions introduced when affixing emulsion pellicles to glass backing plates, most of the serious distortions undoubtedly arise in the fixation, washing, and drying stages. Although there are other effects of distortion for which no sensible methods of correction have been devised (5), the most common effect is the so-called C-type distortion. When C-type distortion is present, attempts are usually made to estimate and correct for its influence on the various types of emulsion measurements.

C-type distortion refers to the deformation of a rectilinear track passing through the emulsion layers into a track whose curvature is closely approximated by a section of a parabolic arc, due to a unidirectional shifting of the emulsion layers in planes parallel to the glass backing surface. Qualitatively, the presence of such distortion, in a region of a given plate, can be detected by inspecting steeply dipping tracks in the same region.

The effects of C-type distortion on dipping tracks has been studied by Lal et al. (6). They show that a point (x, y, z) in the undistorted emulsion will, under C-type distortion, suffer a displacement S, in the (x, y) plane, in the direction of the emulsion layer shift given by

$$S = S_o \left[2 \frac{z}{z_o} - \left(\frac{z}{z_o} \right)^2 \right] \qquad (3\text{-}2)$$

where z_o is the original emulsion thickness, S_o is the maximum value of S which occurs when the point x, y is on the air surface and z is the vertical distance of the point (x, y, z) (corrected for shrinkage) above the glass surface.

A distortion vector, $\vec{S}_o$, may then be defined as having the magnitude S_o and a sense opposite to the sense of motion of the emulsion layer shift. If (3-2) is correct, then $\left(\frac{\partial S}{\partial z}\right)_{z=z_o} = 0$, and the projected track retains its original projected direction near the air surface. The vector $\vec{S}_o$ may be determined by observations on steeply dipping tracks produced by energetic particles which pass completely through the emulsion. The method of measurement will be discussed with reference to Figure 7, (a), (b).

Consider one of the steeply dipping thin tracks which has been selected for the distortion calibration. In dia-

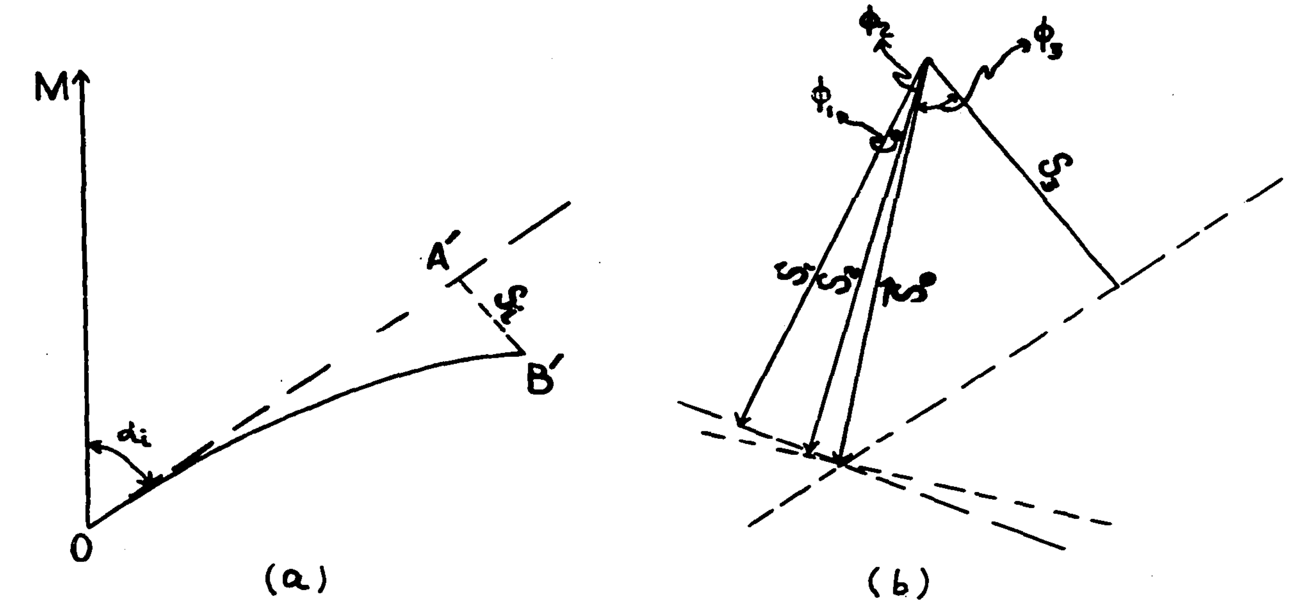

Fig. 7. Experimental procedure for determining emulsion distortion.

gram (a), Figure 7, let OA' be the projection of this originally straight track on the plane containing the air-emulsion interface and take O to be the point at which the particle entered the emulsion. Think of OM as an arbitrary but fixed reference axis in the air-emulsion interface, and let α_i be the angle between OA' and OM. The projection of the actual observed path in the common plane is represented by the arc OB'. If, for each of the several chosen tracks, it is possible to ascertain the magnitudes of S_i (the component of the distortion vector perpendicular to OA') and α_i, then the distortion vector, $\vec{S}_o$, is prescribed and may be obtained by a graphical construction. One may plot the several components S_1, S_2, etc., on polar coordinate paper at angles $90 + \alpha_1$, $90 + \alpha_2$, etc., using a common origin. Lines are now drawn through the termini of S_1, S_2, etc., perpendicular respectively to S_1, S_2, etc. See Figure 7, (b). The intersections of these normals should define a small area, and a line drawn from the origin to the center of this area will represent the distortion vector $\vec{S}_o$.

In connection with the analysis of an event described in Chapter VI, it was required to determine the distortion vector in the neighborhood of the event. A careful examination of the region of interest revealed several tracks (L, 42-43) suitable for measurement.

A readily identifiable reference direction, OM, was chosen in the plane of the emulsion and the plate was rotated on the turntable until this direction was parallel to the direction of motion provided by the x-axis drive of the microscope stage. A micrometer disc on which two finely graduated crossed scales were etched was placed in one of the eyepieces. This, in combination with a cross hair disc in the other eyepiece furnished a coordinate system in the field of view to which measurements could be referred. By rotating the eyepieces it was possible to orient the x-axis of this coordinate system so that it was parallel to the arbitrary reference direction.

It was now possible to measure the angle α_i , which the projection OA' of a given track made with OM, in the following way. The image of the first observable grain near the air-emulsion surface, of the first of the selected tracks was moved until it was superimposed on the image of the origin of the coordinate system. Several pairs of x-and y-coordinates for points on the track in the neighborhood of the origin were then read from the reticule scales.* These observations then permitted the calculation of α_i in a subsequent analysis of the data. The scheme was repeated for each of the other chosen tracks.

The next step in the procedure was to determine for each track the magnitude of S_i, the component of the distortion vector perpendicular to the projection of the original track direction. This was done, for a given track, as follows. The plate was rotated and refining adjustments made with the x and y drives of the microscope stage until the image of the x-axis of the coordinate system was made tangent to the projected direction at the air-emulsion surface of the chosen track. The track was then moved parallel to the x-axis until the image of the exit point of the track into the glass plate was superimposed on the image of the

---

*A slight approximation is involved here since the track is not perfectly straight. If, however, the track does not dip excessively and the distortion is not too severe, the effect of the track curvature on the calculated angle may be neglected.

y- axis of the coordinate system. The value of the y- coordinate at this point is the magnitude of the component of the of the distortion vector perpendicular to the projection of the original track direction. In this fashion the components of the distortion vector $\vec{S}_o$ were measured for the several tracks. By graphical construction $\vec{S}_o$ was found to have a magnitude of 79.4 microns and a direction parallel to the direction of the fixed reference axis. The results are shown in Figure 8.

Lal et al. (6) discuss the application of equation (3-2) to the problem of correcting for distortion in determining the angle between the trajectories of two particles producing intersecting tracks in the emulsion. Let $P(x', y', z')$, $P_1(x_1, y_1, z_1)$ and $P_2(x_2, y_2, z_2)$ represent the coordinates of the point of intersection, a point on track 1, and a point on track 2 respectively. It is assumed that the z-coordinates of the three points have been corrected for shrinkage. The point P_1', which is to be used for the angular calculation is found by moving from P_1 in the direction of the distortion vector by an amount obtained from equation (3-2):

$$S(z_1) - S(z') = S_o\left[\frac{2(z_1 - z')}{z_o} - \frac{(z_1^2 - z'^2)}{z_o^2}\right]. \quad (3\text{-}2a)$$

A similar correction must be made to point P_2.

When measurements are made to determine whether or not a chosen point, P_s, in the emulsion, lies in the plane defined by the two trajectories, the x- and y- coordinates

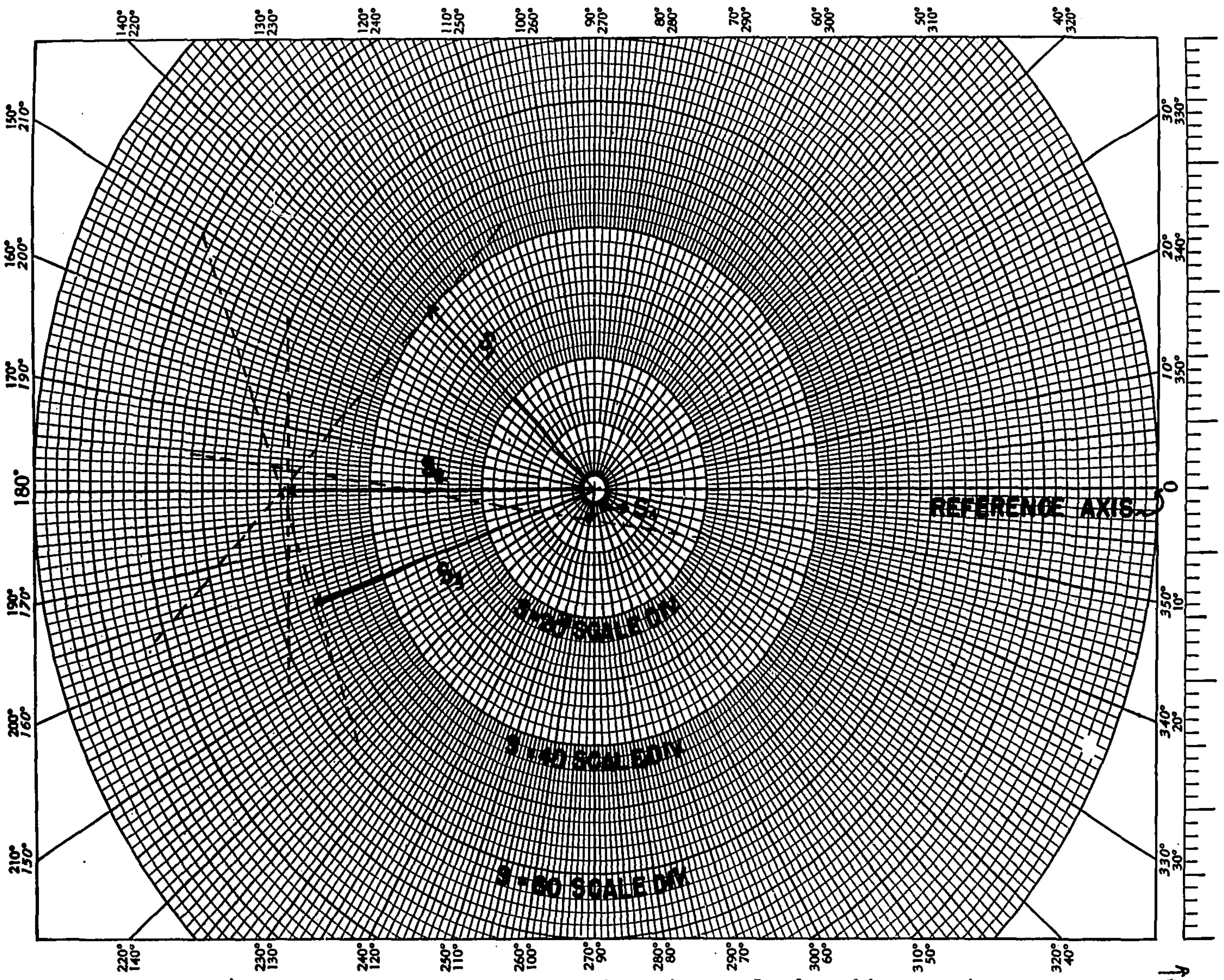

Fig. 8. Experimental determination of the distortion vector, $\vec{S}_0$. The center of the area defined by the normals drawn through the termini of S_1, S_2, S_3 and S_4 has been taken to lie on the reference axis at a distance of 35.5 scale divisions from the origin. Thus, $\vec{S}_0$ is not shown on the figure since it is essentially coincident with S_2.

of the point, P_s, must also be adjusted in the manner described above. (Several other applications of equation (3-2a) are discussed in later chapters).

The effect of C-type distortion on the various types of emulsion measurements customarily employed is appreciable only when the track or tracks involved are rather steeply dipping. Thus, for the long flat tracks used for calibration purposes (see Chapter IV) no correction for distortion was applied.

CHAPTER IV

METHODS FOR DETERMINING THE MASSES AND ENERGIES OF COSMIC RAY PARTICLES IN NUCLEAR EMULSIONS: PART (1)

General

Critical to the analysis and interpretation of any cosmic ray event is the necessity of securing reliable information about the nature and kinetic energies of the individual particles involved. Various methods and techniques have been developed which are commonly used in obtaining particle identification and making energy assignments. These methods are based essentially upon the two following considerations:

1) The energy losses suffered by the charged particle in ionizing encounters with the atomic electrons of the emulsion.

2) Small angle scattering deflections which result from Coulombian interactions with the emulsion nuclei.

The present chapter will concern itself in large part with the methods of obtaining information from the first of these considerations. The second will be discussed in detail in

Chapter V.

The Range-Energy Relation

Theoretical expressions have been derived by Bohr, Bethe, Block, Williams, Fermi, Rossi and Greisen and others (7) for the average energy loss per unit path length, $\frac{dT}{dR}$, due to inelastic collisions along the path of a charged partical traversing a given medium. In the formulation by Rossi and Greisen (8) for example, dT/dR is given by

$$\left(\frac{dT}{dR}\right) = \frac{3}{4} NZ\, m_e c^2\, \phi_0 \quad z^2 \frac{1}{\beta^2} \left[\log \frac{m_e c^2 \beta^2 T_{max}}{(1-\beta^2) I^2 Z^2} \quad 1 - \beta^2\right] \tag{4-1}$$

where T is the kinetic energy of a particle of rest mass m_o traversing the medium,

N, the number of atoms per cm^3 in the medium,

Z, the atomic number of medium,

m_e, the mass of the electron,

c, the velocity of light,

$\phi_0 = \left(\frac{e^2}{m_e c^2}\right)^2 = 6.57 \times 10^{-25}\ cm^2$, where e is the electronic charge,

z, the charge of the particle traversing the medium,

$\beta = v/c$ where v is the velocity of the particle traversing the medium,

$I = 13.5$ eV,

$T_{max} =$ maximum energy transferable in a direct collision between the particle and a free electron.

Since β is a function of T/m_o equation (4-1) may be rewritten in the form

$$(dT/dR) = z^2 f(T/m_o, z). \qquad (4\text{-}1a)$$

Integration of (4-1a) then leads to the range-energy relation

$$R = \frac{m_o}{z^2}\, g(T/m_o, z) \qquad (4\text{-}2)$$

where $g \neq f$ is a different function of the indicated variables. Here R is called the residual range and is measured backward from the terminus of the track, (i.e., R = 0 at the point of arrest).

Experiments have been carried out (9)(10) with nuclear emulsions in which the residual ranges corresponding to protons of known energy have been measured. The experimental data for proton energies up to 40 Mev are well represented by the power law relation,

$$R = CT^{\nu}.$$

A combination of this result with equation (4-2) leads to the expression for <u>singly charged particles</u>

$$R = hm_o^{1-\nu}\, T^{\nu} \qquad (4\text{-}3)$$

where the particle mass is expressed in units of the electron mass and h and ν are emulsion constants which are independent of the processing of the emulsion.

Appropriate values of h and ν were required for the particular set of plates which were being studied. To secure a value of ν , use was made of the fact that, for Ilford emulsions, Brown et al., (11) had calculated the variation with energy of the rate of loss of energy of a particle of charge $|e|$. They employed the Bloch (12) formula as modified by Halpern and Hall (13). Their results are reproduced in Figure 9. In the energy interval $0.01 \leq T/m_o \leq 0.10$ the curve may be approximated closely by a straight line. Two values of T/m_o near the end points of this interval were chosen and the corresponding values of dT/dR taken from the graph. Then differentiation of equation (4-3) leads to

$$\log \left[\left(\frac{dT}{dR}\right)_1 \Big/ \left(\frac{dT}{dR}\right)_2 \right] = (1 - \nu) \log \left[\left(\frac{T}{m_o}\right)_1 \left(\frac{m_o}{T}\right)_2 \right] \tag{4-3a}$$

where the subscripts refer to evaluation at the chosen points. Inserting the numerical values one has

$$\log \left[9.2/2.4 \right] = (1 - \nu) \log \left[0.013/0.076 \right]$$

from which $\nu = 1.761$.

It was possible to obtain a value of h in the following way. The characteristic appearance of the tracks of the π-μ-ϵ decay* in a nuclear emulsion permits an unambiguous identification of the event and hence of the particles involved. While scanning the plates such a decay process had been located and recorded.** Several measurements of the

---

*A well established decay process in which a π-meson decays at rest with the emission of a monoergic μ secondary, the μ-meson subsequently decaying at rest with the production of a positron.

**The event referred to is to be found on plate 8-53-2U. The turntable coordinates are (19.9, 110.9).

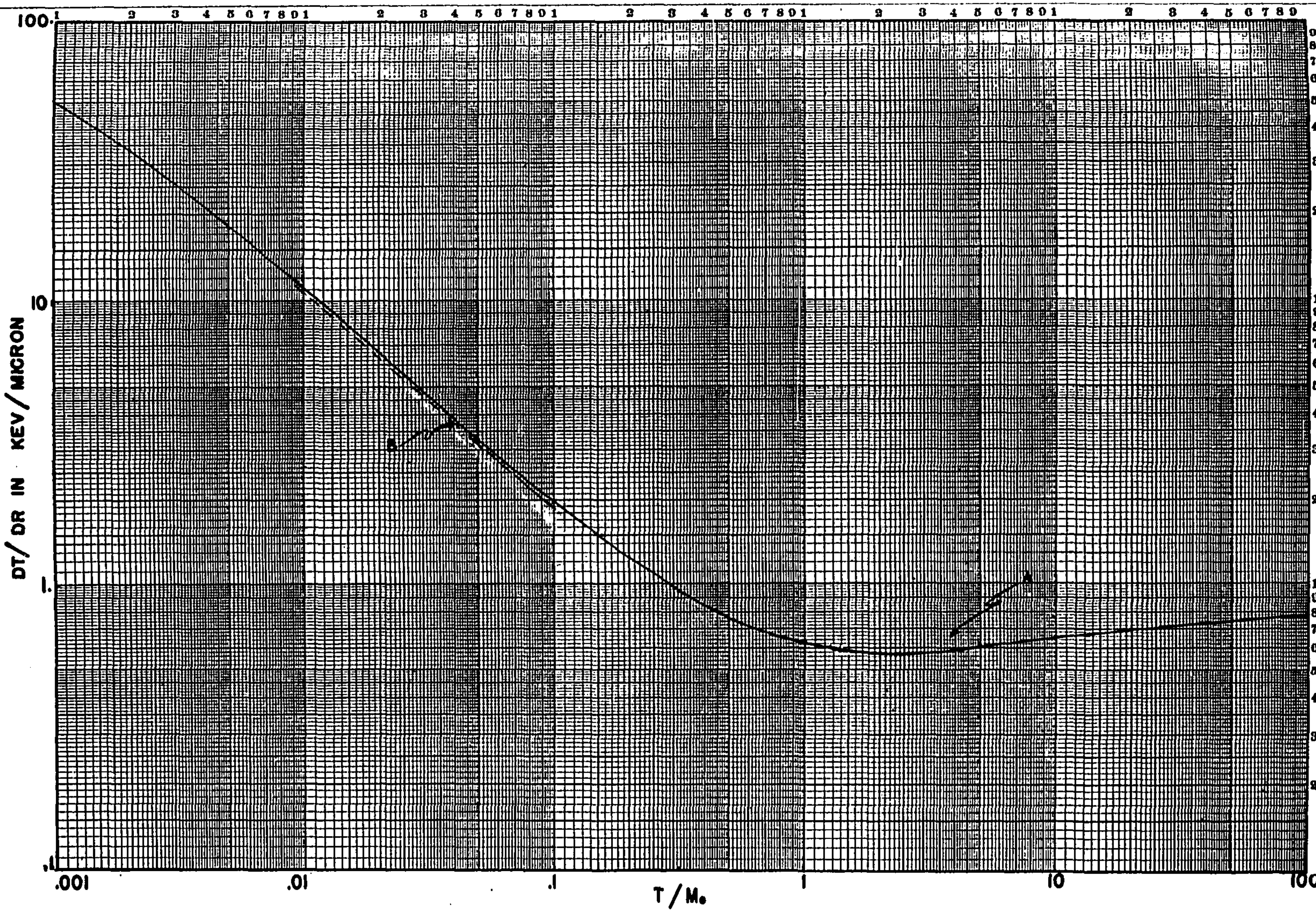

Fig. 9. The variation of the rate of energy loss, dT/dR, of a singly charged particle as a function of T/m_o. (T is the kinetic energy of the particle and m_o its rest energy in Mev. The solid curve A is the theoretical probable ionization in G-5 emulsions; the broken curve B is derived from the slope of A and the measuredrange of the muon from a π-μ-ϵ decay.)

residual range of the μ-meson were made and a mean value of 590 microns was obtained. Range straggling brought about by fluctuations in the energy losses suffered by the particle as it traverses the emulsion makes the determination of range based on a single value unreliable. A length of 590 microns has been used, however, because it is in good agreement with other reported ranges in G-5 emulsions. This range information, in conjunction with the fact that the kinetic energy of the μ-meson is unique (4.085 ± 0.044 Mev) (14) was used to calculate h from equation (4-3). A rest mass of 206.6 m_e was assumed for the μ-meson and ν was taken to be 1.761. A value of h = 2859.7 was determined. Thus, the range-energy relation for the given batch of emulsions may be written as

$$R = 2859.7\ m_o^{-0.761}\ T^{1.761} \qquad (4\text{-}3b)$$

where R is in microns when m_o is in units of electron mass and T is in Mev.

Range-energy curves have been plotted for the more commonly observed singly charged particles for energies up to 30 Mev. The results are shown in Figure 10 where the rest masses which were assumed for the various particles are given in connection with the individual curves.

After differentiating equation (4-3b) one can calculate dT/dR for a given value of T/m_o. This has been done and the results plotted on Figure 9 for comparison with the theo-

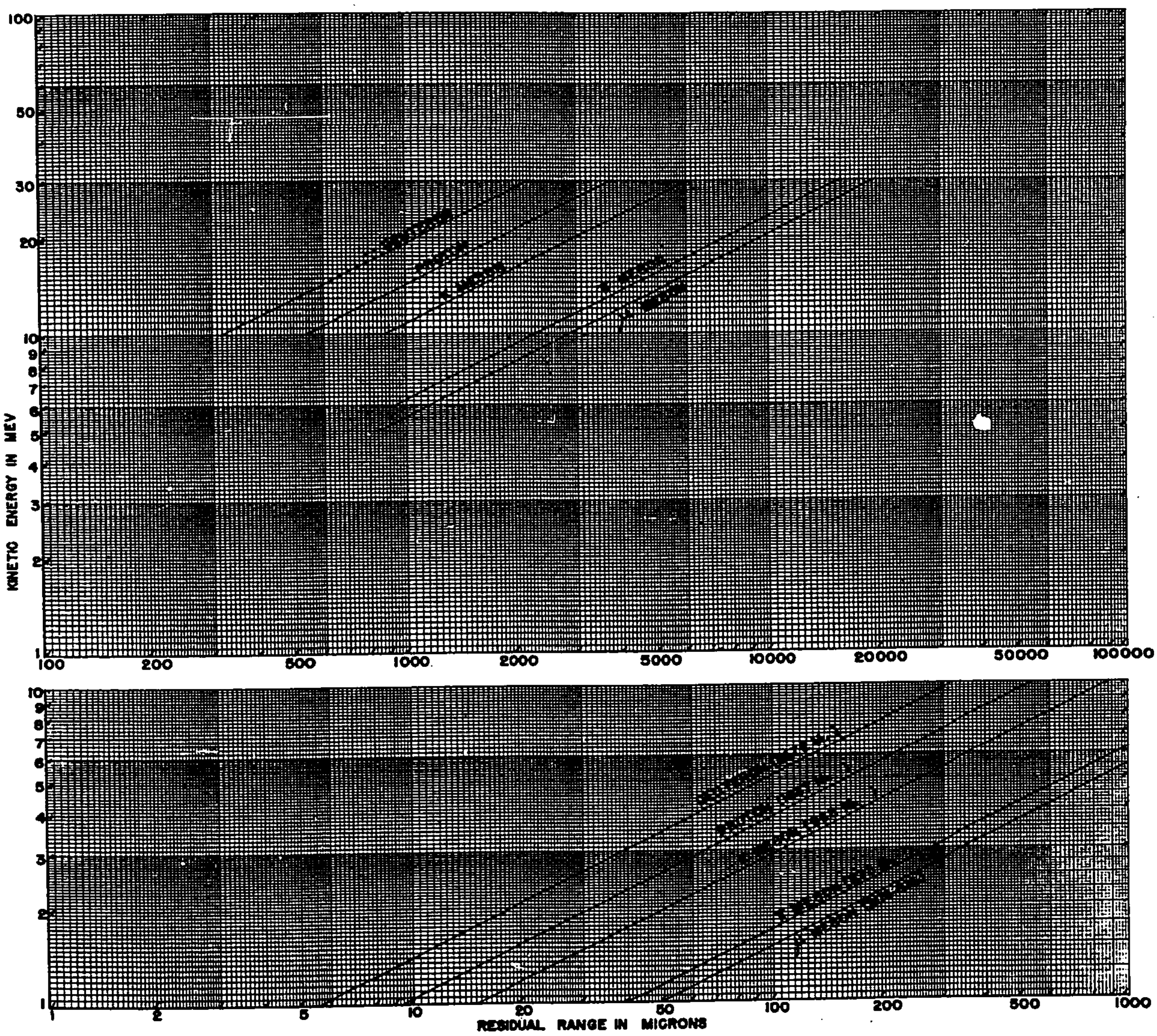

Fig. 10. Range-energy relation for various singly charged particles in G-5 emulsions.

retical curve.

Mass and Energy Determinations from Ionization Loss Calibration

While traversing a nuclear emulsion an unknown charged cosmic ray particle will surrender energy in a large number of ionizing encounters with the atomic electrons of the emulsion. These energy losses are reflected in the processed plate by the appearance of a track composed of developed silver grains distributed along the original trajectory.

For the non-relativistic case the energy lost by a singly charged particle in traversing a given range interval in the emulsion is a single-valued function (Figure 9) of its velocity only, increasing as the particle velocity decreases. This increase in energy loss as the particle slows down is accompanied by an increase in the number of developed grains associated with the track.

As the charged particle approaches the end of its range in electron-sensitive emulsions, such as the Ilford G-5, the increasing grain density is observed in the form of an increasing number of irregularly shaped blobs or clusters in which the grains are no longer resolvable as individual elements. Furthermore, as the particle approaches the point of arrest in the emulsion the blobs tend gradually to coalesce and the track appears much as a thick column of developed silver interspersed with occasional small spacings or gaps between adjacent grain clumps. The more massive the particle the longer is the extent of track over which the severe clogging persists and the more pronounced is the track broadening. Thus it is possible, for example, to resolve individual grains on light meson tracks much closer to the track termini than is possible for the tracks of protons and deuterons.

These considerations have led to the development of various techniques of measurement (15)(16)(17) which are commonly used to obtain information concerning the nature and energy of the responsible particle from the ionization density associated with its track in the nuclear emulsion. The particular type of measurement which is used in a given case will depend to a large extent on the appearance of the track in the range interval being studied.

In the heavily clogged sections of a track the measurements are usually confined to determining either the total length of the gaps per interval of length or the track opacity per interval of length. Photometric means are normally employed in this latter type of measurement. In the less congested sections of a track the number of developed silver grains occurring in successive intervals along the trajectory is counted directly. Counting grains is an easier and more rapid method than either of the types of measurement commonly used in the heavily clogged sections of track. Thus it is desirable to employ this method to the highest possible grain densities which in practice are found to be in the region of 1.5 grains per micron. (16)

The name used to describe a given measurement technique is derived from the particular ionization parameter which is determined, e.g., grain counting, gap counting, etc. Underlying the application of each of the various methods is a common scheme which involves a comparison of the track of the unknown particle with the tracks of identifiable calibration particles such as π-mesons and protons. Quantitative estimates of rest mass and kinetic energy for unknown non-relativistic singly charged particles may be obtained from these comparisons in favorable cases. These estimates are based essentially upon the predictions of ionization theory.

If one assumes that the space rate of change of the ionization parameter is a function only of the space rate of energy loss then it can be shown that at points on the tracks of two different singly charged particles a and b where the ionization densities, and hence the space rate of change of the ionization parameters, are equal, the relations

$$P_a/P_b = R_a/R_b = T_a/T_b = m_a/m_b \qquad (4\text{-}4)$$

will hold.* Here R refers to residual range, T to kinetic energy and m to the rest mass of the particle in question.

---

*These and related expressions are derived for the case of grain counting by J. M. Fowler (17). It is clear from the discussion in this reference, however, that other ionization parameters may be substituted for N, the total number of grains in a track of residual length R.

P represents the cumulative value obtained by measuring a given ionization parameter (e.g., total grain count) from R = 0 to R = R. The subscripts have the usual significance.

Equation (4-4) has been employed in combination with calibration curves which have been developed for our emulsions to aid in determining the identities and the kinetic energies of the non-relativistic charged particles associated with the twin tracks of the V-event* described in Chapter VI of this thesis.

The selection of the calibration tracks and the determination of the types of measurement which were made on these tracks had been dictated by preliminary measurements on the event. To minimize the effects of differential emulsion development, calibration tracks were selected, where possible, which were located at approximately the same depths and regions of the emulsions as the tracks with which they were to be compared. The procedures employed in obtaining the calibration curves and some comments on their application are described in what follows.

(a) <u>Grain Density Calibration Curves</u>. Due to the relative paucity of long recognizable π-meson tracks termi-

---

*A phenomenological term used to describe a cosmic ray event in which an uncharged particle decays in flight with the production of two observable charged secondary particles or, alternatively, an event in which a charged particle decays in flight with the production of one observable charged secondary.

nating in the emulsion it was not possible to select tracks which completely satisfied the double criteria that they be at the same depth and in the same regions of the emulsions as one of the tracks to be compared. Grain counts were made, however, on the tracks of three π-mesons, most nearly meeting the stipulated conditions, in the residual range interval from 2010 to 4000 microns. Each of the three particles had come to the end of its range in the emulsion, and could readily be identified as a π-meson from the appearance of the track curvature and the fact that a characteristic π interaction was observed to take place at the point of arrest. In two of the examples the π-meson had been absorbed by an emulsion nucleus with the production of a low energy star.* In the third case the π-meson had decayed at rest into a μ-meson. The location of the chosen tracks is given in Table 2.

The oil immersion 90 x objective (N.A. 130) used in conjunction with the 10 power eyepieces provided sufficiently high resolution for grain count measurements. The plate was first rotated on the turntable until the track to be studied was aligned approximately parallel to the x-axis of the microscope stage. A 50 scale division graticule placed in one of the eyepieces was used to measure the length of the intervals on the projected track, starting at a residual range of 2010 microns. The number of grains in successive sections

---

*A nuclear disintegration induced by a cosmic ray particle.

Table 2

Location of Grain Count Calibration Tracks

Track No.	Plate No.	Turntable coordinates of terminus	Type of particle	Average depth below air-emulsion surface*	Residual range in emulsion	Remarks
1	8-53-1u	(63.1, 106.2)	π^+meson	60μ	>5500μ	Decays into μ-meson (J, 57-58)
2	8-53-2D	(22.0, 95.4)	π^-meson	158μ	>8000μ	Results in π^--induced star (D, 4-15)
3	8-53-6D	(24.3, 99.7)	π^-meson	89μ	>5000μ	Results in π^--induced star (J, 61-62)

*Apparent depth in processed emulsion, as measured with microscope fine-focussing adjustment, of section of track used in grain counting.

(cells) of the track was counted.

The presence of occasional clusters of grains along the track introduced a subjective feature into the counting procedure. The convention adopted in assigning a count to a given cluster was to estimate the number of times the cross sectional area of the cluster contained the cross sectional area of a mean grain.*

The projected cell length was permitted to vary, if required, to allow for changes in the dip of the track, but for most sections a value of projected cell length of 71.5 microns was used which, for the stated magnification, coincided with 50 scale divisions on the eyepiece reticule. The difference in depths at which the end points of each successive cell were in sharp focus was also recorded from readings on the drum scale of the vertical fine adjustment. These latter data, when combined with information on the shrinkage factor of the emulsion, were required to make subsequent corrections to the projected cell lengths for vertical dip of the track in the unprocessed plate. During the course of making the grain counts the apparent depth of the emulsion in the region of the track was determined as described in

---

*When clearly resolvable the individual grains in a track exhibit an approximately circular appearance as viewed through the microscope. If the tracks of high energy particles are examined in regions where little clogging exists one can calculate a mean grain diameter for the emulsions by averaging the measured diameters of a large number of individual grains. When this was done a value of 0.57 microns was obtained for the mean grain diameter (C, 24-25).

Chapter III. A typical tabulation of grain count data is given for track (1) in Appendix B, Table 15.

The grain count observations made on each of the tracks of the three π-mesons have been plotted using a logarithmic scale. These data are shown in Figures 11, 12 and 13 where the experimental points have been fitted visually. Here $(N-N_K)$ and $(R-R_K)$ represent the total number of grains and total track length respectively which have accrued from the point at which the grain count was begun. For the particular measuring scheme which was used, R_K = 2010 microns and N_K is the unknown number of grains in the track from the terminus to R_K.

The three grain count curves, just described, were used in the construction of a mean curve of $(N-N_K)$ vs $(R-R_K)$. An arbitrary point on the $(R-R_K)$ axis having been selected a correspondent point $(N-N_K)$ was read on each individual curve. The mean value of $(N-N_K)$ for the chosen value of $(R-R_K)$ was then taken to be the average of the three equally-weighted values of $(N-N_K)$ so obtained. This procedure was repeated and mean values of $(N-N_K)$ were calculated for various choices of $(R-R_K)$. The results are set forth in Figure 14. Curves of grain density, dN/dR, plotted as a function of $(R-R_K)$, are shown in Figures 15, 16, 17 and 18. The data points for a given graph were obtained by measuring the slope of the associated grain count-residual range curve for various chosen

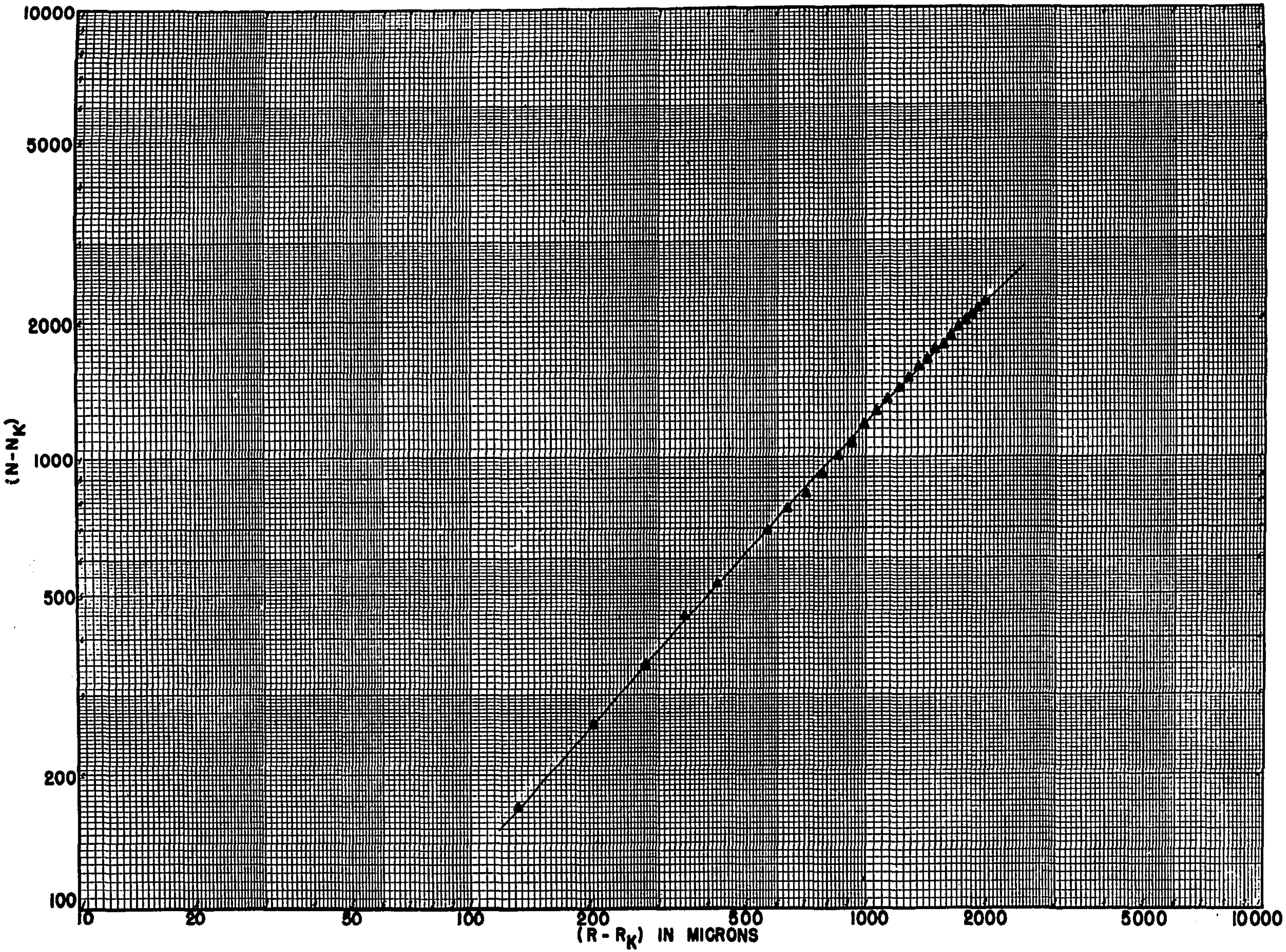

Fig. 11. Grain count vs residual range for track 1, Table 2.
(R_k = 2010 microns)

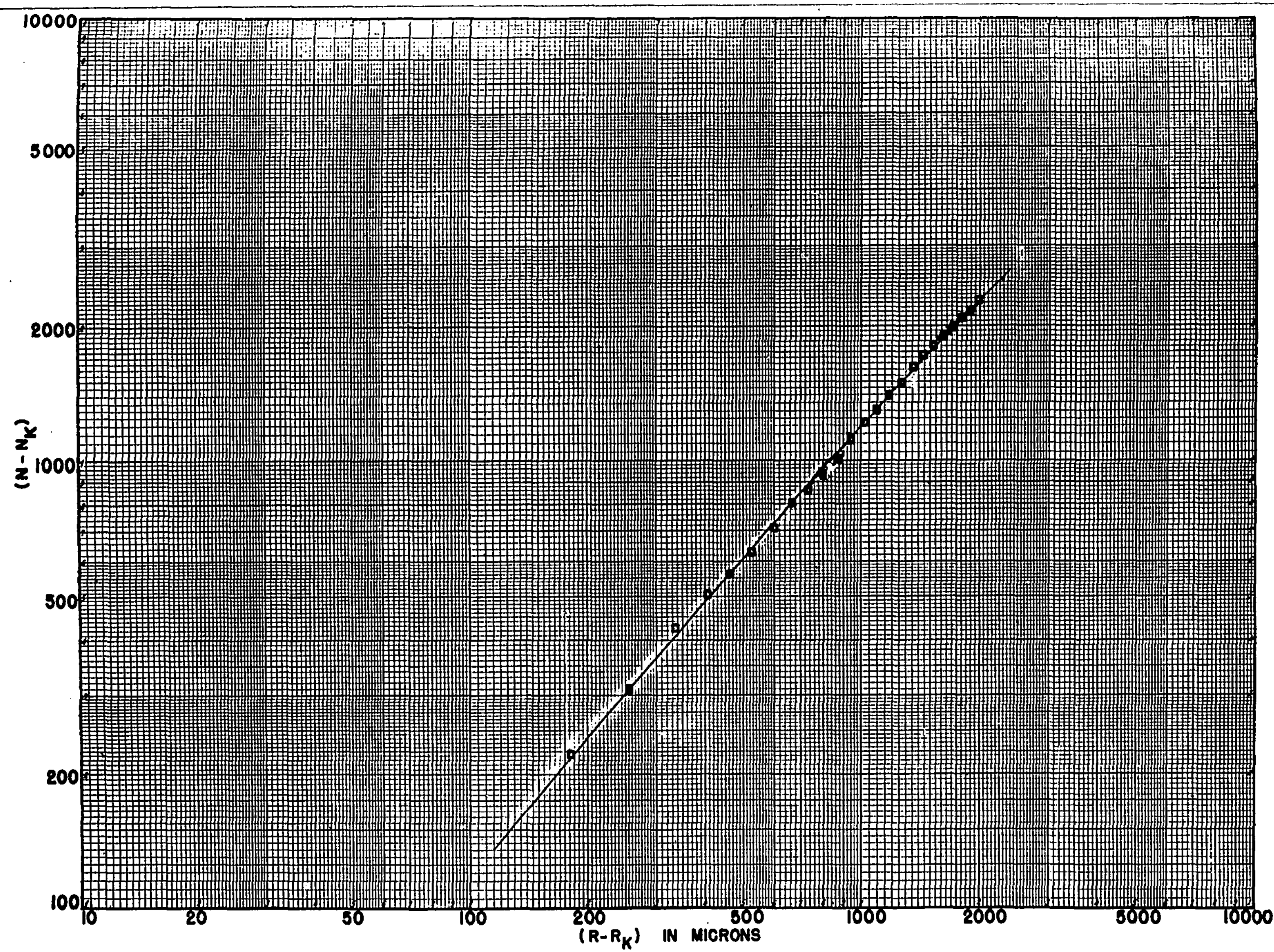

Fig. 12. Grain count vs residual range for track 2, Table 2.
(R_k = 2010 microns)

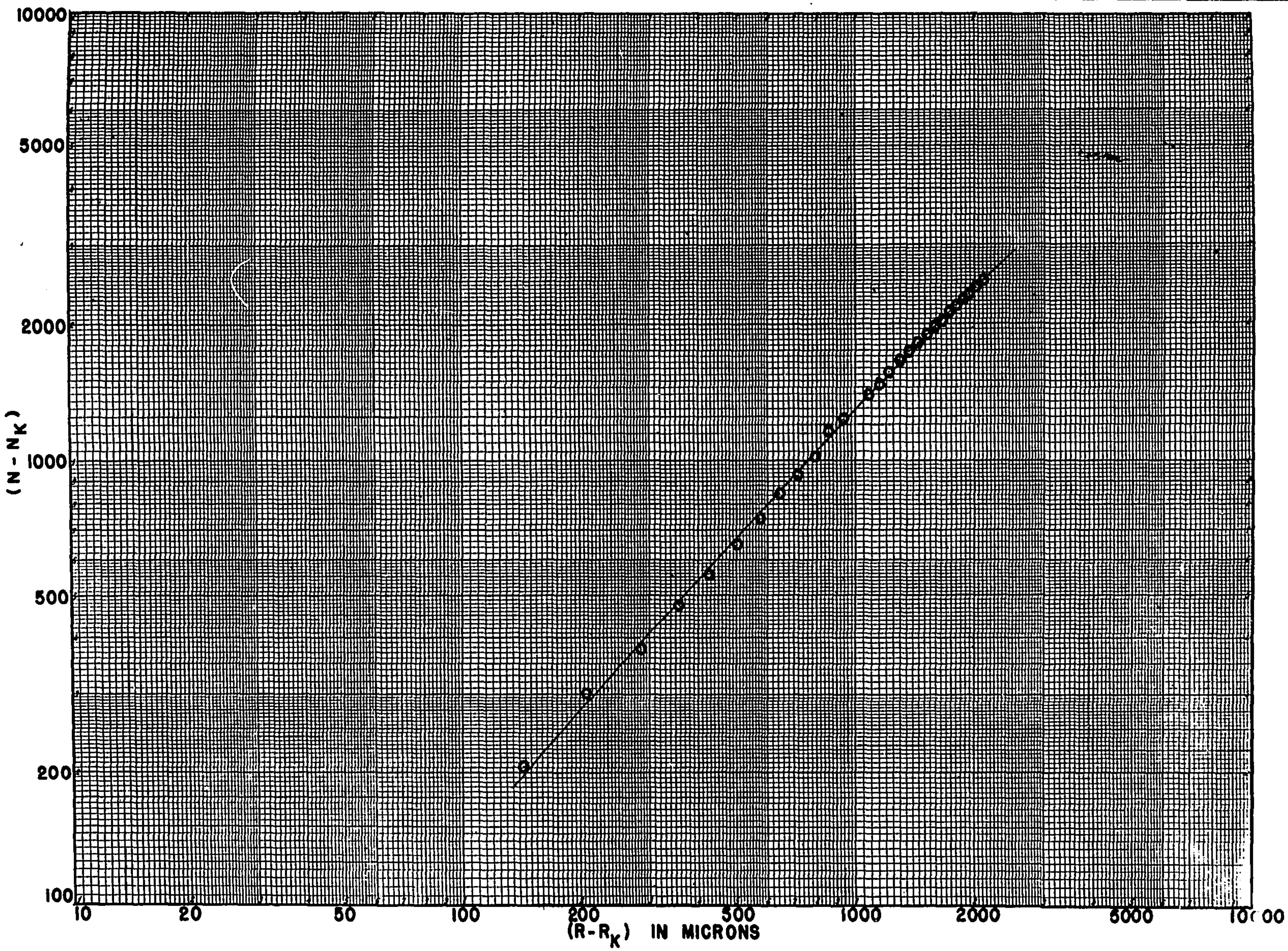

Fig. 13. Grain count vs residual range for track 3, Table 2.
(R_k = 2010 microns)

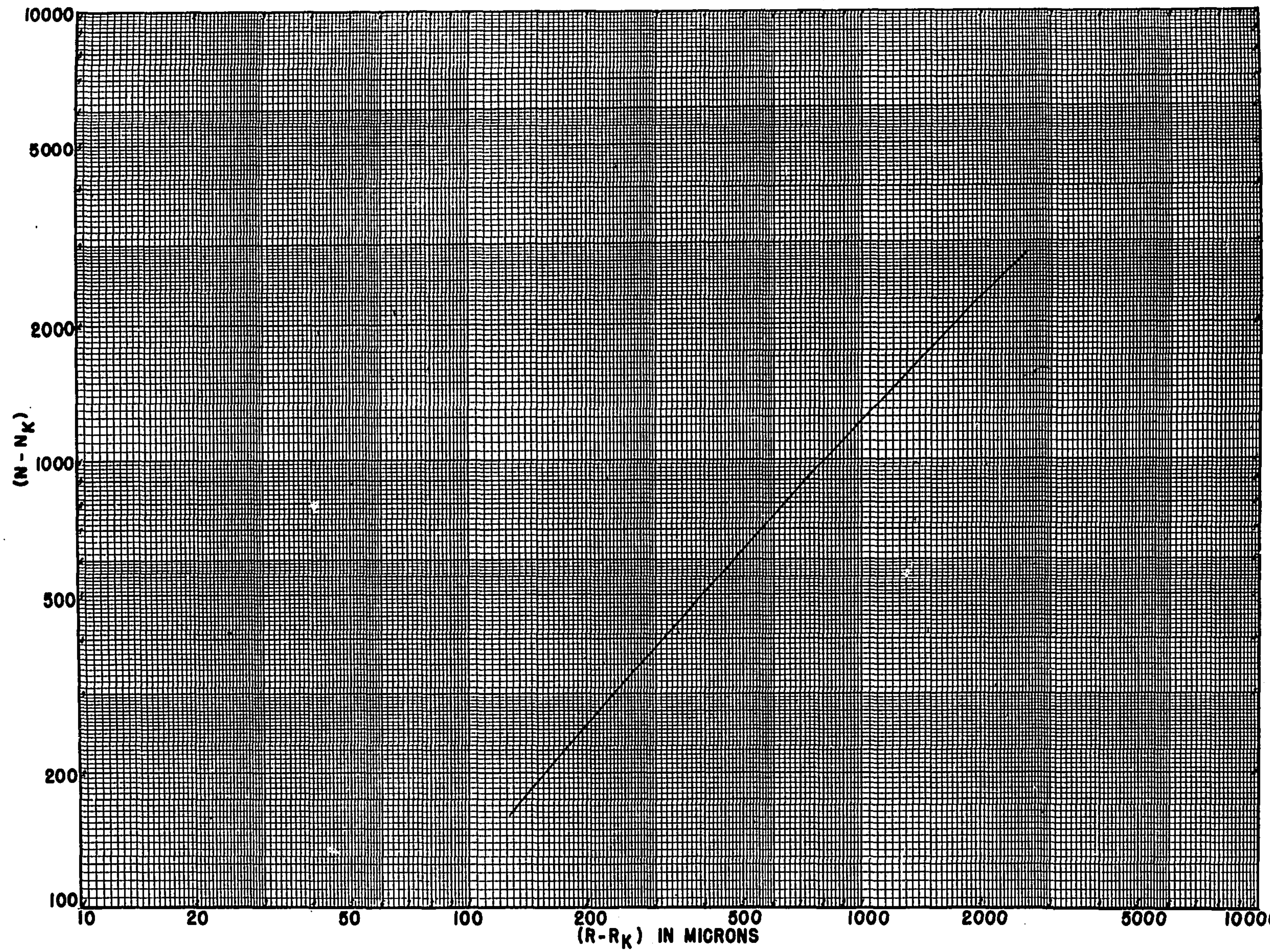

Fig. 14. Mean grain count-residual range relation for π-mesons (R_k = 2010 microns)

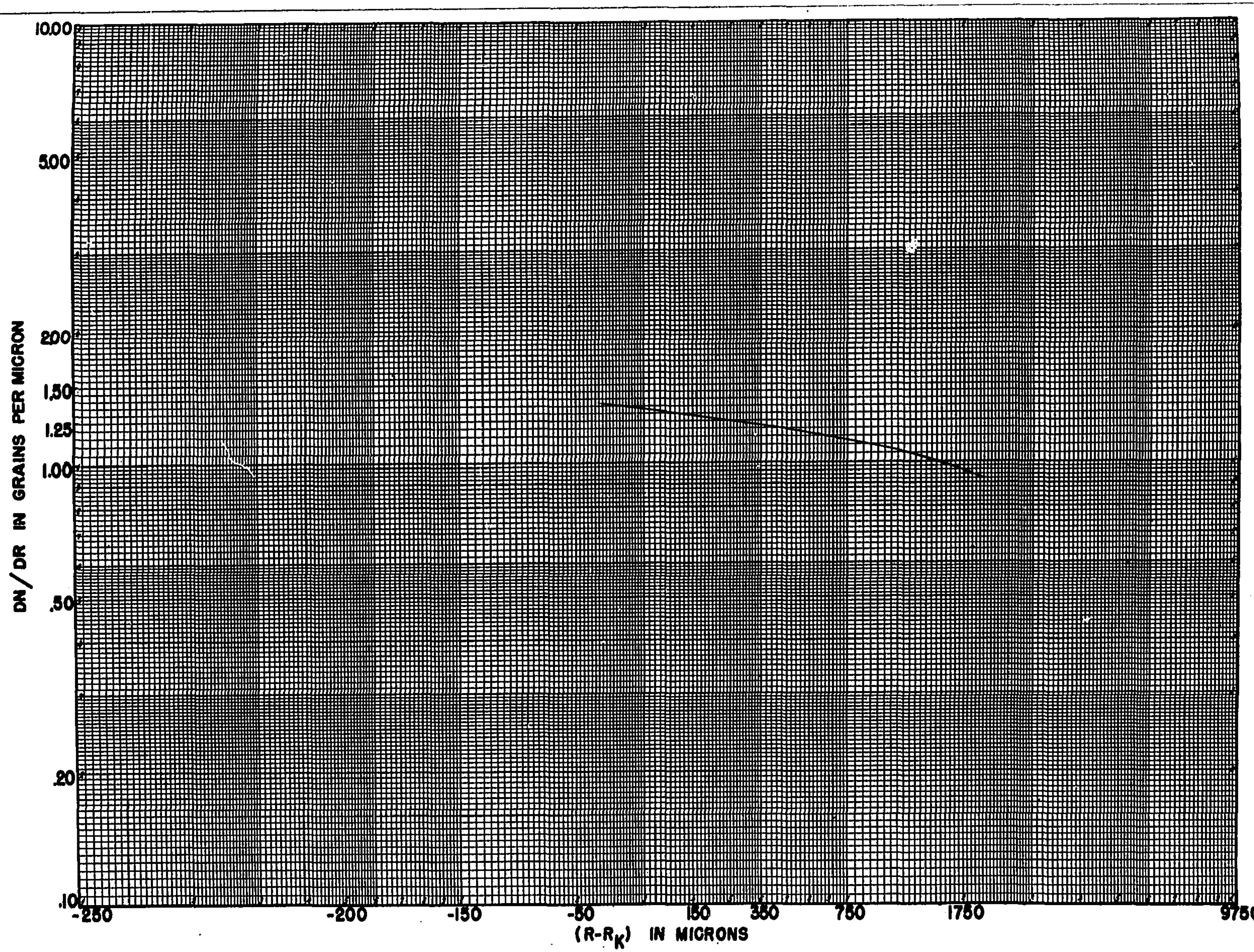

Fig. 15. Grain density vs residual range for track 1, Table 2. (R_k = 2010 microns)

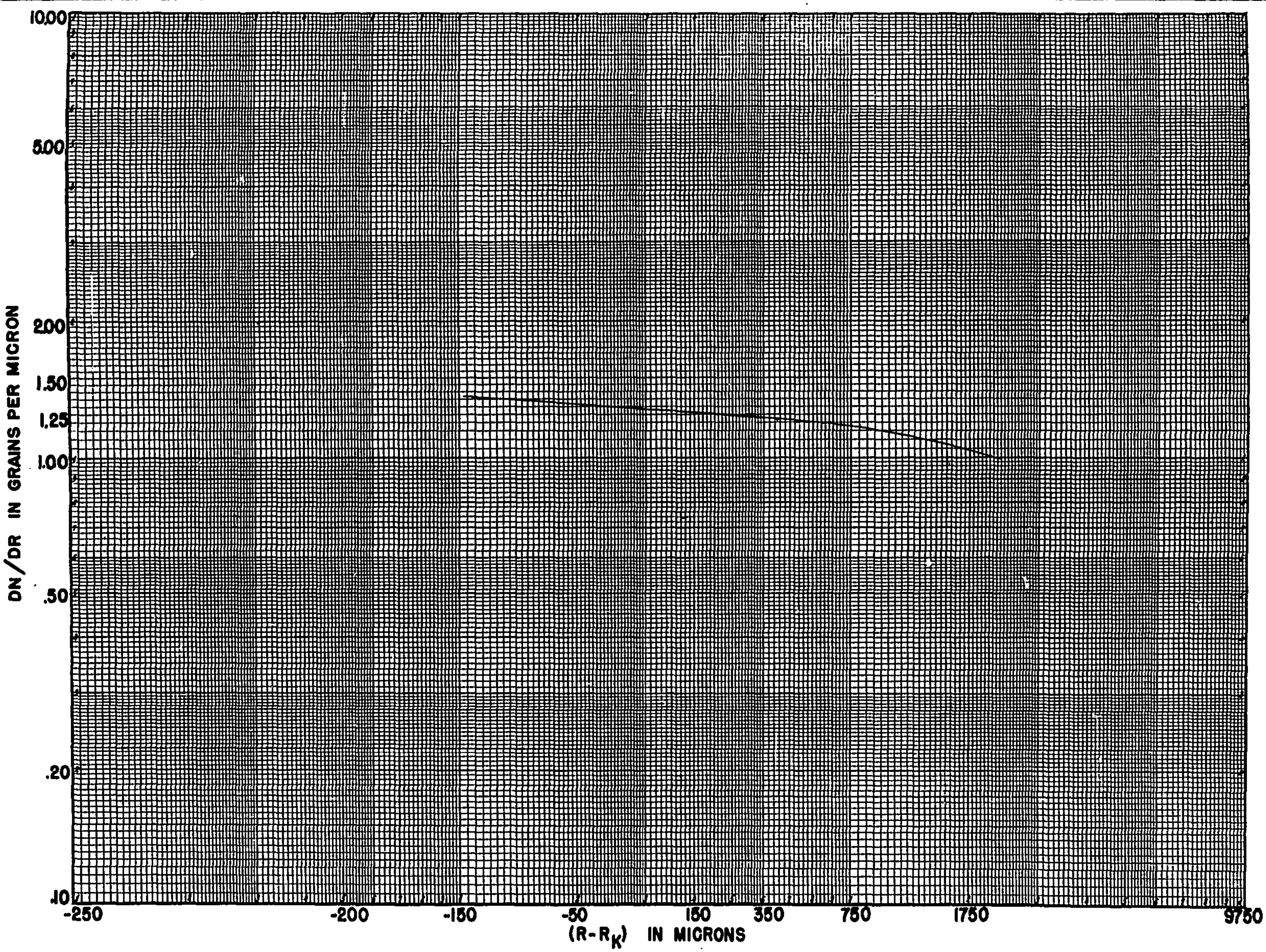

Fig. 16. Grain density vs residual range for track 2, Table 2.
(R_k = 2010 microns)

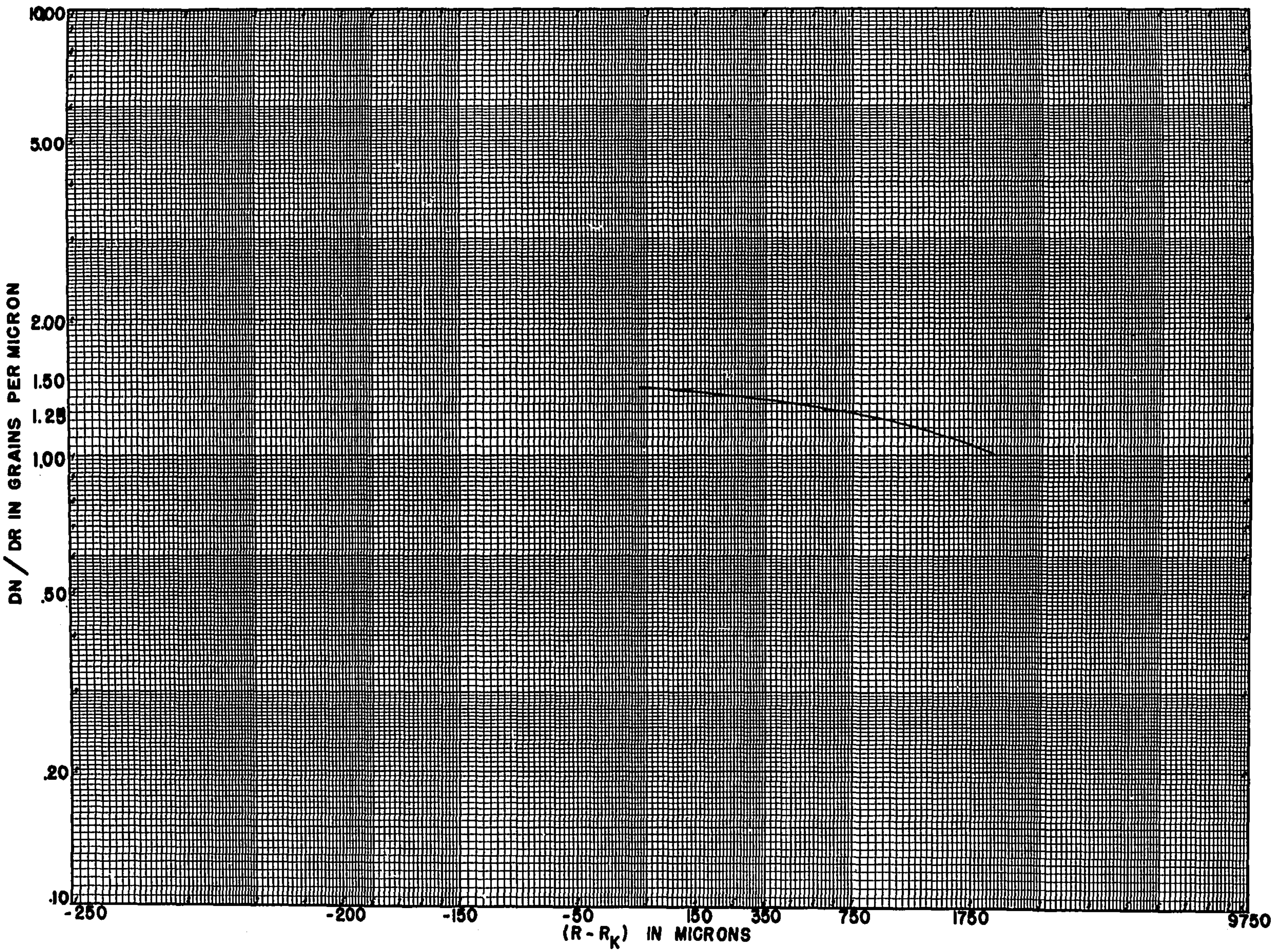

Fig. 17. Grain density vs residual range for track 3, Table 2. (R_k = 2010 microns)

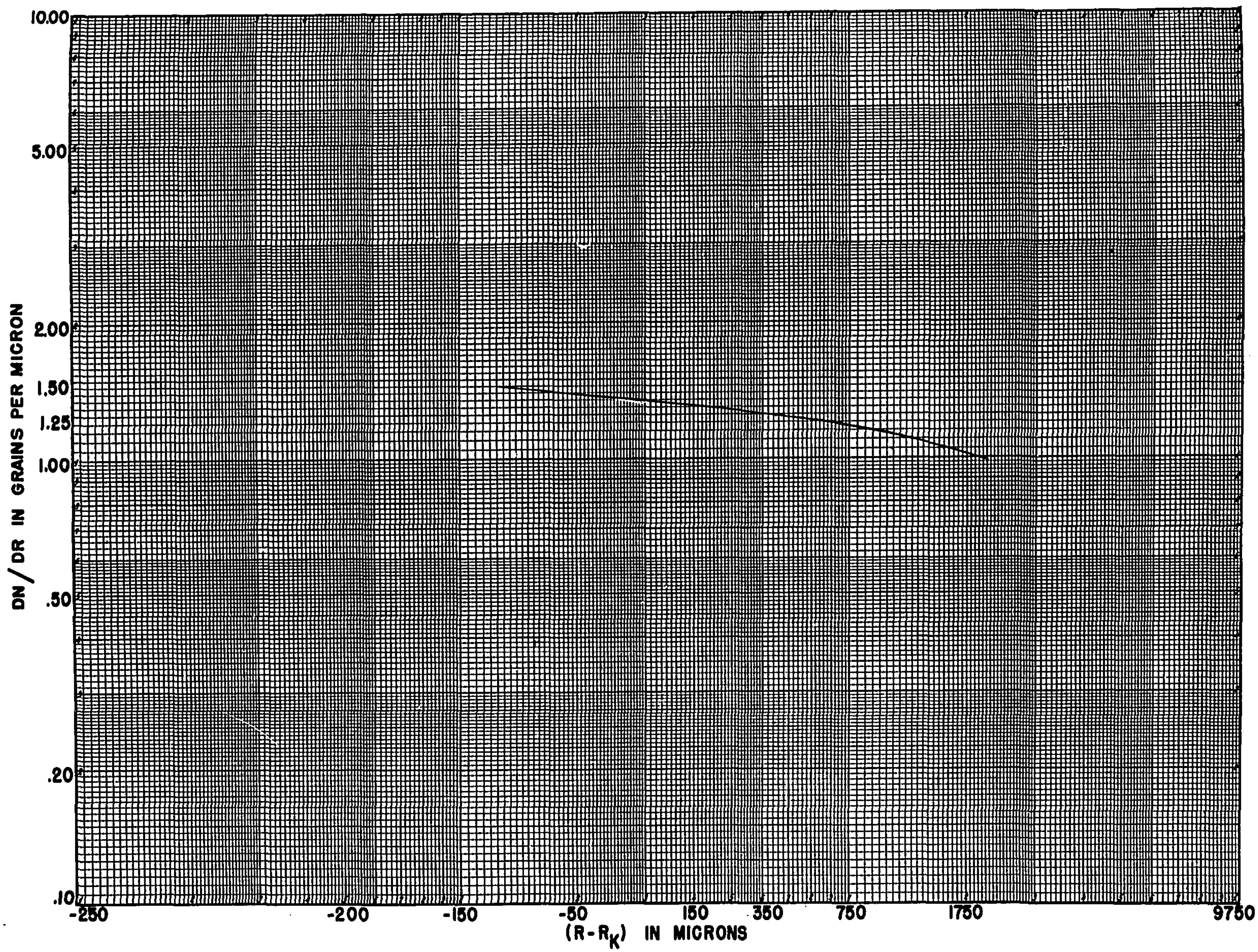

Fig. 18. Mean grain density-residual range relation for π-mesons. (R_k = 2010 microns)

values of $(R-R_K)$.

If a measurable change in grain density has occurred over a segment of track of an unknown singly charged particle, the mean grain density calibration curve for the π-mesons may be employed, in conjunction with equation (4-4), to obtain an estimate of the unknown rest mass. If ΔR_u is the observed length of the segment on the track of the unknown particle and $(dN/dR)_u^A$ and $(dN/dR)_u^B$ are the respective graindensities at the end points of this segment then the range interval ΔR_π over which a π-meson suffers a change in grain density from $(dN/dR)_u^A$ to $(dN/dR)_u^B$ can be secured from Figure 18. It is then an immediate consequence of equation (4-4) that

$$m_u = (\Delta R_u/\Delta R_\pi)\ m_\pi \tag{4-5}$$

where m_u is the rest mass of the unknown particle. Additional estimates of rest mass may be obtained by using the individual π-meson grain density curves to determine ΔR_π. This procedure yields a dispersion of values which may be used to calculate the probable deviation in the quoted mass.

As will be seen in Chapter V, observations on small angle scattering deflections along the track of an unknown charged particle m_u which does not come to the end of its range in the emulsion may be employed to obtain an estimate of its kinetic energy T_u at the midpoint (M) of its trajectory in the plate. Figure 18 may be used to determine the residual range R_π which a π-meson should have at a point on its track where the grain density is equal to the observed grain density in the neighborhood of (M). The kinetic energy T_π corresponding to the residual range R_π may then be calculated from equation (4-3b) by assuming a value of rest mass for the π-meson. Then from equation (4-4) one has

$$T_u/m_u = T_\pi/m_\pi \qquad (4\text{-}6)$$

This result when combined with the information procured from scattering measurements will yield an estimate of the unknown rest mass. As before, the dispersion of T_u/m_u values obtained by use of the individual π-meson grain density curves will serve as a basis for assigning a probable deviation to the ratio obtained from equation (4-6).

(b) Gap Count Calibration Curves. To obtain gap count calibration curves the plates were first scanned for long flat tracks which appeared to be made by protons stopping at depths and at positions relative to the edges of the plates, approximately the same as those of the track with which they were to be compared. Three tracks were selected which satisfied the stated criteria. The three particles were first identified as protons by scattering measurements using the constant sagitta method.* Pertinent information on the three chosen tracks is set forth in Table 3. Track (4) is thought to be produced by an alpha particle. Although the gap count data on this track is not used in any subsequent analysis it is included for purposes of comparison.

*A measuring technique described in Chapter V (19).

Table 3

Location of Gap Length Calibration Tracks

Track No.	Plate No.	Turntable coordinates of terminus	Type of particle	Average depth below air-emulsion surface*	Projected track length in emulsion	Mass from scattering in m_e	Remarks
1	8-53-1u	(47.2, 102.5)	proton	78μ	3790μ	2142 ± 447**	Emitted from star (J, 43-47)
2	8-53-1u	(56.9, 102.1)	proton	49μ	14610μ	1656 ± 229	(J, 23-29)
3	8-53-2D	(50.0, 97.5)	proton	69μ	7520μ	2089 ± 348	(J, 19-21; 34-35)
4	8-53-1u	(57.2, 100.9)	alpha	71μ	1560μ		Emitted from star (J, 32-33)

*Apparent depth in processed emulsion, as measured with microscope fine-focussing adjustment, of section of track used in gap counting.

**Scattering data for track (1) is tabulated in Appendix B, Table 16.

Gap count measurements were made under the same magnification and using the same eyepiece scale as that employed for grain counting. Here the procedure followed was the same as for grain counting with the exceptions that measurements were begun at the track terminus and the projected length of each visible gap in a given cell was recorded instead of the number of grains in the cell. The individual gaps were first shifted to the center of the field and their length estimated in eights of a scale division (1 scale division = 1.43 microns). It is important to record the length of each gap separately because of a small correction which must be made to the gap count on dipping tracks. This correction arises from the fact that a gap of length, g_i, appers of length $(g_i + A) \cos \theta' - A$, where θ' is the angle between the normal to the original particle trajectory and the viewing direction and A is the mean grain diameter.*

A calibration curve of the mean cumulative gap length G, vs residual range, R, was obtained from the gap measurements on the three proton tracks in a fashion similar to that already explained in connection with the discussion on grain counting. From this experimental curve it was possible to calculate an expected deuteron curve making use of relation (4-4). These results are shown in Figure 19. Also shown

---

*A derivation of the correction which is required and an example of its application to the observed gap data of track (1) is given in Appendix B, pg. 195 to 196. See also (16).

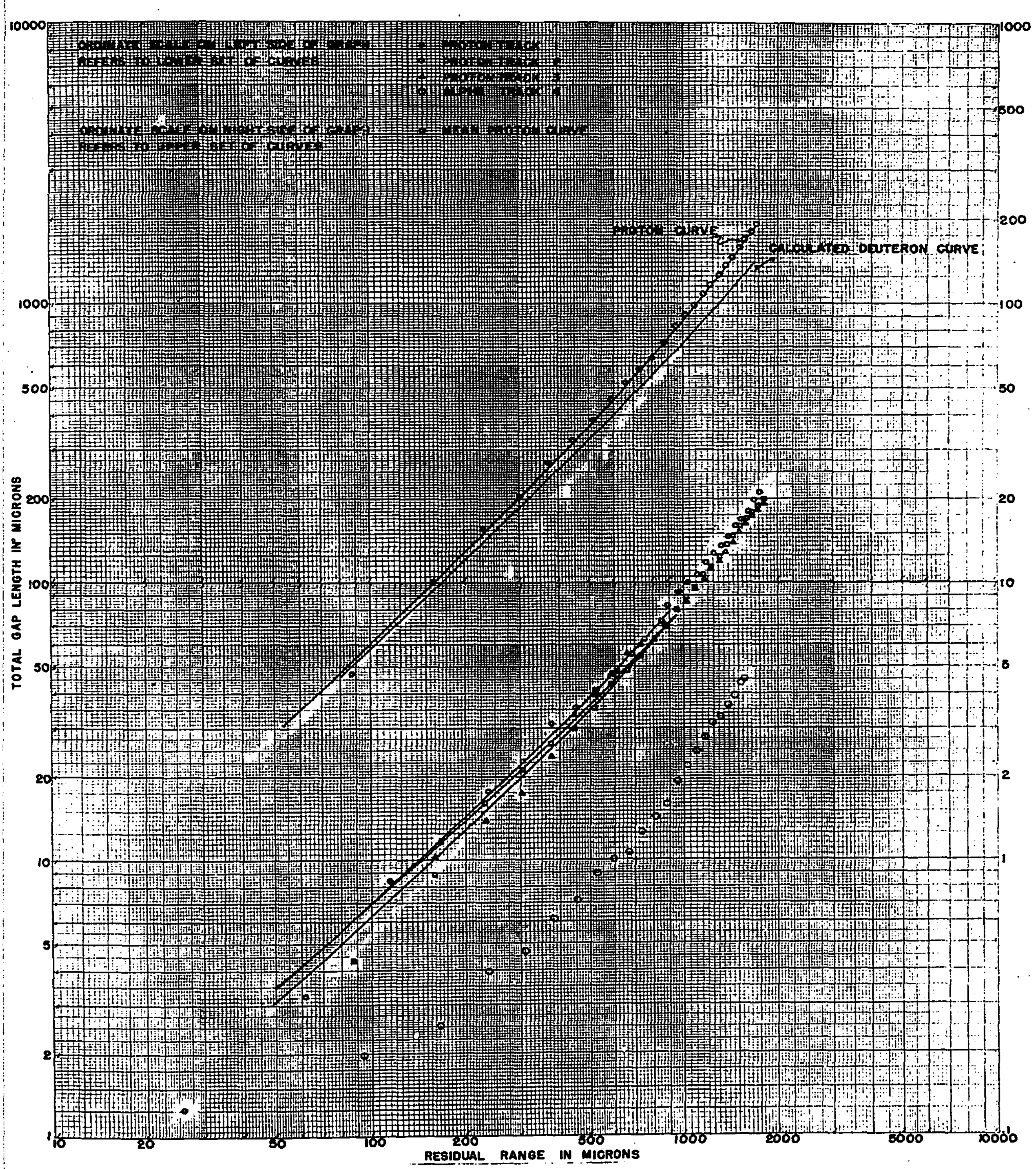

Fig. 19. Cumulative gap length-residual range relations for three protons and an alpha particle. Also shown is the expected value of total ionization for a deuteron.

are the individual G vs R data for tracks (1) through (4).

Area Measurements

It is observed experimentally that along the trajectories of charged particles arrested in the emulsion there is an increase in the cross-sectional area of the metallic silver blobs as the particle slows down. First attempts have been made in this laboratory to explore the possibility of utilizing this area property as a means of discriminating between tracks which are produced by particles of different mass which come to the end of their range in the emulsion. In this preliminary investigation "area" measurements have been confined to sections of tracks within ~ 1100 microns of the terminus. The method of measurement and the results will be discussed.

Of the six tracks selected for the calibration, four appeared to be caused by slow protons coming to rest in the emulsion, one was interpreted as an alpha particle and the remaining track could be identified with a π-meson which had decayed at rest. The pertinent information on the tracks is given in Table 4.

The binocular assembly of the microscope was replaced by the vertical monocular tube and a camera lucida fastened in position on the eyepiece tube which permitted the simultaneous viewing of the microscope field and a drawing surface which was aligned perpendicular to the optic axis of the micro-

Table 4

Location of Area Measurement Calibration Tracks

Track No.	Plate No.	Turntable coordinates	Assumed particle	Residual range in emulsion	Remarks
1	8-53-2D	(48.4, 170)	proton or deuteron	$\sim 2000\mu$	Emitted from star (E, 14)
2	8-53-2D	(48.4, 170.0)	proton or deuteron	$\sim 1050\mu$	Emitted from star (E, 10)
3	8-53-1u	(60.6, 108.6)	proton or deuteron	$\sim 2000\mu$	Emitted from star (E, 16)
4	8-53-2u	(60.6, 99.2)	proton or deuteron	$\sim 1800\mu$	(E, 15)
5	8-53-2D	(19.7, 111.7)	π-meson	2566μ	π-μ-ϵ decay (E, 20)
6	8-53-1u	(57.2, 100.9)	alpha	1560μ	Emitted from star (E, 12)

scope. A piece of plate glass of suitable dimensions, onto which strips of light weight paper had been securely taped, served as a drawing surface upon which "blob perimeters" could be sketched directly. A small incandescent lamp, fixed in position beneath the glass plate, was used in order that the drawing surface could be more clearly seen. The camera lucida was equipped with two sets of neutral density filters which provided a means of obtaining a satisfactory balance between the light coming to the eye from the microscope and light coming to the eye from the drawing surface.

By making the tracings of the grain cluster boundaries enclose as large an area as possible the percentage of deviation associated with subsequent measurements of these areas is made as small as possible. This means that, consistent with good resolution, the highest magnification which the microscope can supply is required during the sketching operation. After trying several optical arrangements, it was found that the best results could be obtained by using a 20 power eyepiece, with reticule insert, in conjunction with the 90 x oil immersion objective lens.

Starting at the track terminus, outlines of the images of the grain clusters were traced in successive cells of the track. This was done by causing the image of the tip of a sharply pointed (hard) pencil to move around the boundary of the cluster image as seen in the microscope field. See

Figure 20. (In the sketching procedure it is necessary to bring each blob image into sharp focus with the vertical fine adjustment knob of the microscope before one attempts to trace the outline.) As in previous ionization density measurements the cell length was permitted to vary if required. Again the depth differences between cell end points were recorded so that in a later analysis of the data adjustments could be made for the dip of the track.

The areas encompassed by the outlines which had been traced were measured with a planimeter. The procedure employed was to tape the strips of paper upon which the tracings had been made to a flat glass plate, illuminated from below by a small source of light. The "blob perimeters" corresponding to a given cell were first connected by fine straight lines drawn approximately parallel to the track direction so that the area of the entire cell could be measured in a single continuous motion of the planimeter guide point. A hand magnifier was mounted in position over the cell to be studied in order to improve the ease and accuracy of measurement.

The guide point of the planimeter was made to trace out three complete circuits of the cell outlines and the total area (in arbitrary units) corresponding to the entire traversal was read directly from the instrument. The average value obtained by dividing the total area by the number of

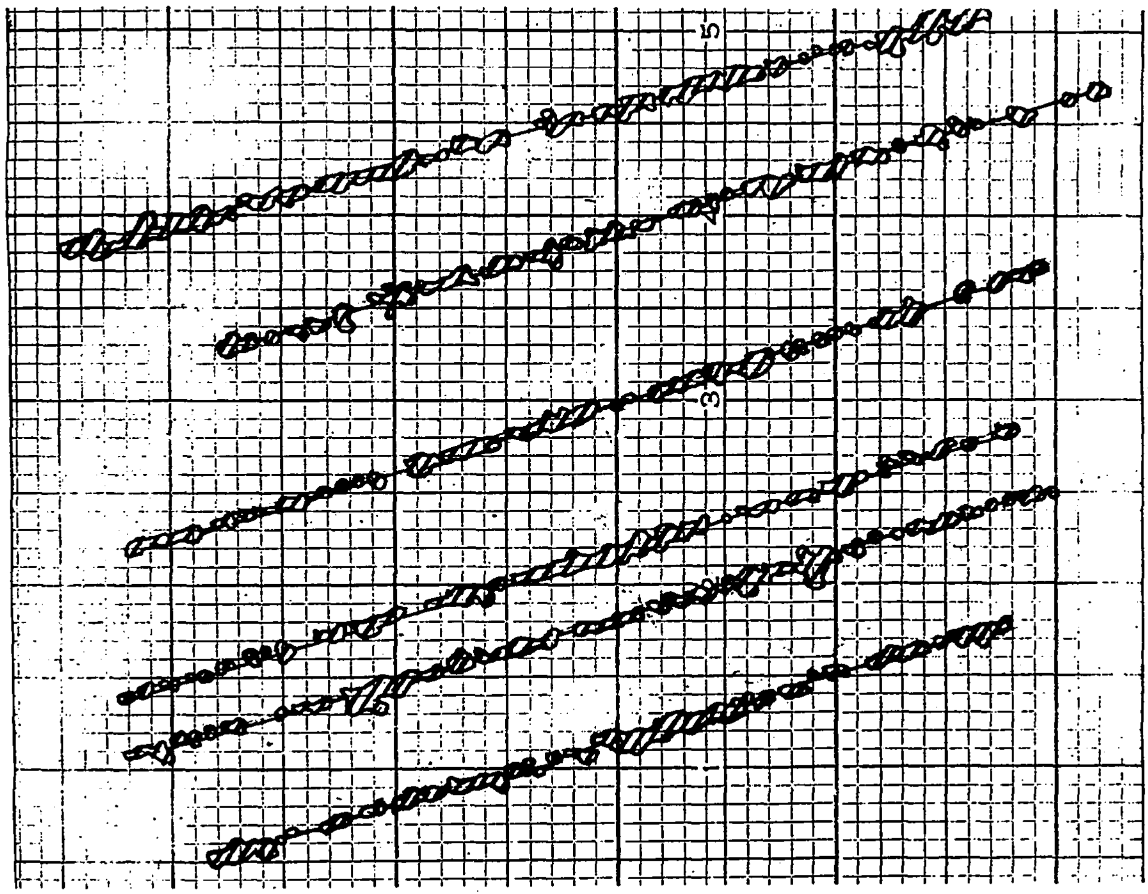

Fig. 20. Reproduction of typical area sketches for a proton track.

complete circuits was taken to be the projected area (in arbitrary units) of the cell. A typical tabulation of the data so obtained for track (1) is given in Appendix B, Table (18). The results obtained from measurements on the six tracks are shown in Figure 21. Also included in this figure for comparison is a plot of the area measurements made on one of the tracks of the event described in Chapter VI.

Because of the random nature of the choice of calibration particles (1) through (4) it is quite probable that these tracks are produced by a mixture of protons and deuterons so that the question of the length of track needed to discriminate between protons and deuterons remains unsettled. Nonetheless, an examination of Figure 21 indicates quite clearly that the area method is capable of differentiating between tracks produced by protons, light mesons and alpha particles which terminate in the emulsion, when only some 500 microns of track is available for study, a selectivity quite comparable with the gap count technique.

These first findings are considered to be quite promising and, at present, work (to be discussed below) is underway in this laboratory aimed at improving the actual measuring technique. Two additional factors, independent of the way the measurements are made, which should tend to improve the discrimination provided by the area method involve the choice of:

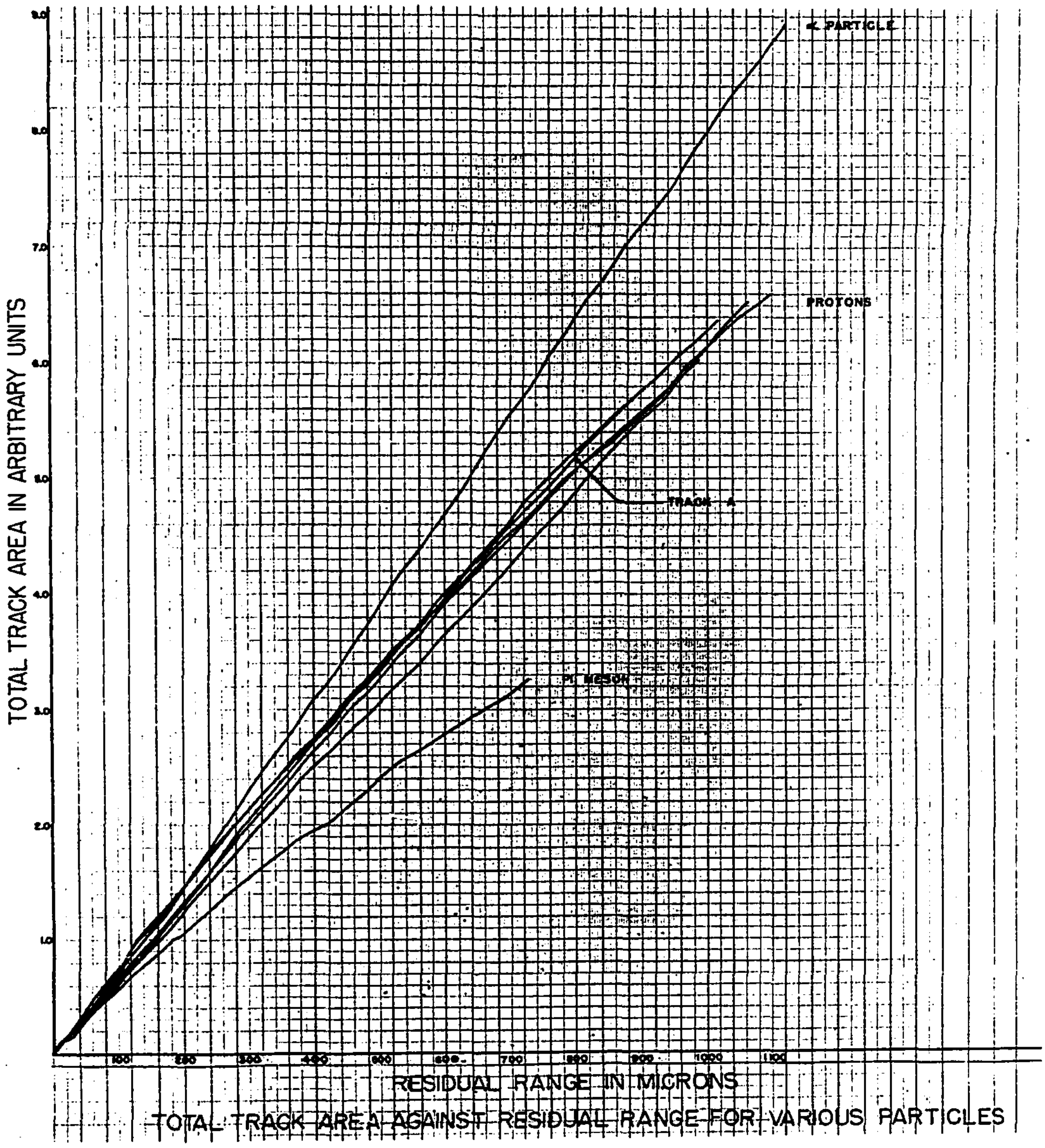

Fig. 21. Total track area vs residual range for various calibration particles.

1) Long tracks for use in the calibration so that the identities of the responsible particles may be cross-checked by other means.

2) Calibration tracks which are located in the same region and at approximately the same depths of the emulsion as the tracks with which they are to be compared.

A feature common to both the grain and gap counting techniques is the subjectivity involved in the taking of the data. For this reason, measurements made on the track of an unknown particle by one observer should not be compared with calibration curves made by another observer. No information is available, as yet, in this laboratory, to assess the degree of subjectivity associated with the making of the tracings in the area method. Because of the small size of the blob image which was traced, however, there is no reason to believe that the tracing technique as described, would reduce the subjective factor.

Three observers participated in making the planimeter measurements discussed earlier. It was found that an individual operator could reproduce his own area measurements on a given cell to within eleven percent and that different observers making measurements on the same cell would also agree within eleven percent. This would imply that insofar as the actual measurements <u>from the tracings</u> are concerned, the element of subjectivity essentially has been eliminated.

An accurate reproduction of the blob or cluster images on an enlarged scale should result in:

1) Increased discrimination between tracks produced by charged particles of different mass.

2) Reduction, if not complete elimination, of the subjective factor involved in the measuring procedure.

3) Reduction of the probable deviation of the measurements made with the planimeter.

To this end, beginning attempts have been made to project a magnified cluster image onto a screen or drawing surface by using a high intensity light source in combination with the appropriate optical arrangement, but, at present, no satisfactory method of projection has been devised which will give proper resolution of the image. An alternative procedure currently is being investigated in this laboratory in which the cluster areas are to be measured by a planimeter from highly magnified photomicrographic reproductions* of the track made under controlled illumination and processing conditions.

Corrections for Distortion to Grain Count and Gap Length Measurements Made on Dipping Tracks

Within a given cell of a track upon which either grain count or gap length measurements are made the apparent track direction can be well represented by a straight line joining

---

*The author wishes to express his indebtedness for this suggestion to Wm. Schriever, Professor of Physics, University of Oklahoma.

the end points of the cell. If the distortion vector, $\vec{S}_o$, has a component parallel to this apparent track direction x', then either a stretching or foreshortening of the cell has occurred in the x' direction which should be taken into account. A possible method of correcting for this effect will be discussed with reference to Figure 22.

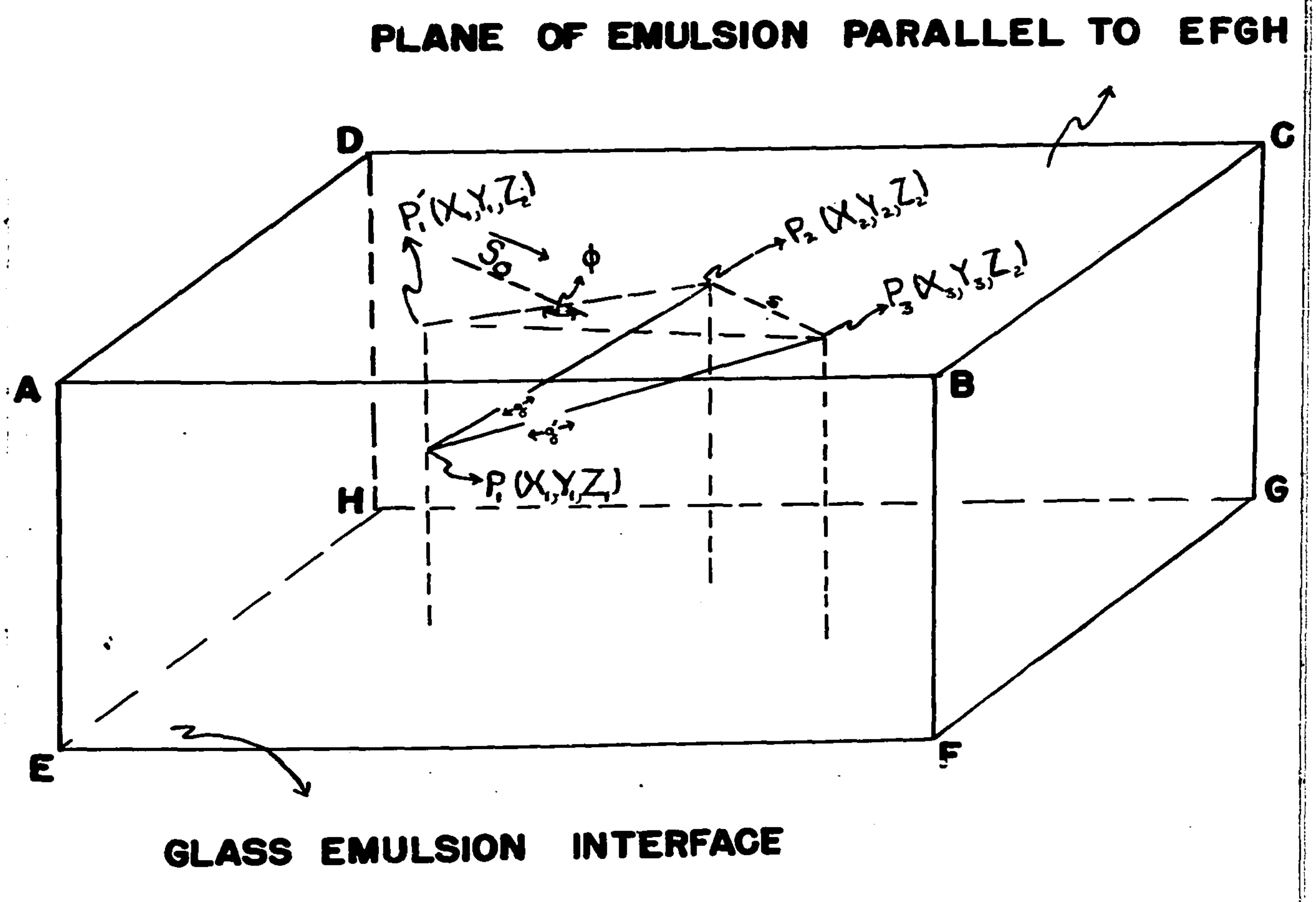

Fig. 22. The method of correcting grain and gap counts for distortion.

Let $\overline{P_1P_2}$ be the apparent length of a cell used in the measurement as determined from equation (3-1). Consider z_1 and z_2 ($z_2 > z_1$) to be the vertical distances, corrected for shrinkage, of the end points, P_1 and P_2, of the cell above the glass-emulsion interface. The distortion vector $\vec{S}_0$, parallel to the plane ABCD, is assumed to make an angle ϕ with the projection $\overline{P_1P_2}$ of the apparent track direction as indicated. Because of distortion, the (x,y) coordinates of points along the original trajectory of the particle are different after the emulsion has been processed. If this coordinate shift were the same for each depth in the emulsion, no correction would be necessary. Since the emulsion is bonded to the glass, there can be no shift at $z = 0$, so that any observed distortion will have to be a function of z. To correct for changes in cell length produced by distortion one need only take account of the differential coordinate shift between the two ends of the cell at depths z_1 and z_2*. Thus, P_3, a point on the original trajectory of the particle has suffered a differential shift with respect to P_1 to some other point P_2, the z-coordinate of P_3 remaining unchanged.

---

*This statement is strictly true only if the shrinkage of the emulsion associated with the processing of the plates results in a uniform linear transformation of the z-coordinates for any point. It is believed, however, that any distortion contribution due to higher order terms in the transformation will be negligibly small except near the edges of the plate. This is borne out by the fact that visual inspection of steeply dipping tracks produced by high energy particles reveals no perceptible evidence of curvature in planes perpendicular to the viewing plane.

The magnitude of this displacement, s, may be calculated from equation (3-2a). Hence, the corrected cell length $\overline{P_1P_3}$ can be obtained from the formula

$$\overline{P_1P_3} = \left[(\overline{P_1'P_3})^2 + (z_2 - z_1)^2 \right]^{\frac{1}{2}} = \left[(\overline{P_1'P_2})^2 + s^2 - 2(\overline{P_1'P_2})\ s \cos\phi + (z_2 - z_1)^2 \right]^{\frac{1}{2}}. \tag{4-7}$$

In practice, a track which does not exhibit excessive curvature, may be rotated until it is aligned approximately parallel to a chosen reference axis and the angle, ϕ, between the reference axis and the direction of the distortion vector determined as described in Chapter III. This angle, ϕ, may then be assumed constant for the successive cells when determining the corrected cell lengths from equation (4-7).

When the ionization parameter which has been measured is the gap length, an additional correction must be made to the data over and above the corrections which are introduced due to the apparent dip of the track. In Figure 22, if g is the length of a gap on the apparent track then the same gap on the undistorted track had a length g' where

$$g' = \frac{\overline{P_1P_3}}{P_1P_2}\ g$$

or, more generally, for n gaps in the same cell

$$\sum_{i=1}^{i=n} g_i' = \frac{\overline{P_1P_3}}{\overline{P_1P_2}} \sum_{i=1}^{i=n} g_i. \tag{4-8}$$

CHAPTER V

MEHTODS OF DETERMINING THE MASS AND ENERGY OF COSMIC RAY PARTICLES IN NUCLEAR EMULSIONS: PART (2)

Introduction

A charged particle passing through a photographic emulsion will, in general, undergo deviations from a rectilinear path due to Coulombian type interactions* with the nuclei of the medium. It is possible quite frequently to obtain meaningful estimates of the rest mass and kinetic energy of an unknown particle traversing a segment of emulsion by measuring these deflections or scatterings and then coupling such experimental scattering data with information about the

*In what follows neither the effect of inelastic electronic scattering due to the atomic electrons nor the effect of non-electric forces is considered. The intensity of the inelastic electronic scattering has been shown by E. J. Williams (20) to be at most of the order of $1/z^*$ of the Coulomb scattering by the nuclei where z^* is the effective nuclear charge for a mixed medium. For nuclear emulsions $z^* \cong 41$ so the effect is of order of 2.5%, and one may apply a correction if desired (21). Williams (20)(22), shows further that the scattering arising from short-range non-electrical interactions with nuclear particles would take place at comparatively large angles where there is practically no scattering due to the electrical forces.

energy loss of the particle obtained from measurements of the ionization produced by the particle along its track. An outline of the usual procedures employed is given in the following sections. The next four sections are concerned primarily with the application of the scattering theory to the study of fast particles. The term, fast particle, as used here, refers to particles possessing sufficient kinetic energy so that over the entire interval of measured scattering the energy loss due to ionization may be neglected. The more difficult problem of applying the theory to the treatment of slow particles where the ionization loss must be taken into account, is considered in some detail in the next to last section. In the final section the methods of arriving at assignments of probable deviation for the mass and energy estimates obtained from scattering is considered.

Fundamental Equation of Multiple Scattering Theory

A change in direction, α_t, suffered by a charged particle in traversing a medium of thickness t may be accounted for in several ways. Here, α_t, is the projection of the deflection of the particle on a plane perpendicular to the line of sight* and containing the initial direction and is measured by the angle between tangents drawn to the points

*The quantity α_t is not readily measured directly in the emulsion but a related quantity is easily obtainable by the coordinate technique discussed in a later section of this chapter.

of origin and terminus of the projected path. The deflection, α_t, may be the resultant of a series of single small-angle deviations brought about by elastic collisions with the different atomic nuclei in the matter traversed, or alternatively, the resultant deflection may be due predominantly to scattering from a single nucleus. The former type of scattering is known as multiple, or plural, Coulomb scattering, according as the number of contributing collisions is large or small; the latter type is known as single or large-angle Coulomb scattering.

Theories of Coulomb scattering have been developed by Williams (20), Rossi and Greisen (8), Goudsmit and Saunderson (23), Snyder and Scott (24)(25), Lewis (26), and Moliere (27), which lead to results identical within a few percent (21). Because of their simpler mathematical presentations and convenience of form, the theories of Williams and Moliere or some combination thereof (21) are most frequently used in studying the scattering problem in photographic emulsions. The fundamental equation of multiple scattering common to the aforementioned theories, to be given below as equation (5-1) can perhaps be best understood from the following discussion.

Consider a charged particle traversing a thin layer of scattering medium of thickness t. Let T_t be the average value of the kinetic energy in the medium and let α_{it} represent the angle between the direction of incidence and the projected angle of emergence. Visualize, n identical charged particles, each with the same average kinetic energy, T_t, traversing the same thin layer of medium of thickness t. Let α_{1t}, α_{2t}, --- α_{nt}, be the deflection angles corresponding to the n particles. Then, if $\bar{\alpha}_t$ is the arithmetic mean of the α_{it}* taken without regard to sign, the theories predict

$$\bar{\alpha}_t = \delta L. \qquad (5\text{-}1)$$

In (5-1)

$$\delta = \frac{2e^2 \; z t^{\frac{1}{2}} \; (\Sigma_j N_j Z_j^2)^{\frac{1}{2}}}{T_t \left(\frac{2+\sigma}{1+\sigma}\right)}$$

where N_j is the number of atoms per unit volume,

Z_j is the atomic number of the j^{th} atomic species,

e is the electronic charge,

z is the number of unit charges on the scattered particle,

t is the thickness of absorber traversed,

T_t is the average energy of the scattered particle in the medium, and

$\sigma = T_t/m_oc^2$ is the ratio of the average kinetic energy to the rest energy of the scattered particle.

The explicit form of L differs in the theoretical investigations referred to above, leading to slightly differing values for its calculated magnitudes, but, in general, for a given value of z, L is a slowly varying function of the thickness t of the absorber and the velocity of the scattered

---

*The distribution of the α_{it} is given approximately by a Gaussian function (20).

particle.

The application of equation (5-1) to the scattering of fast particles in nuclear emulsions will be seen to be immediate. In Figure 23, let the track of a fast multiply scattered charged particle, passing successively through points P_1, P_2, --- P_{n+1}, as projected onto the defined plane, be represented by the curved granular path between points A and B.

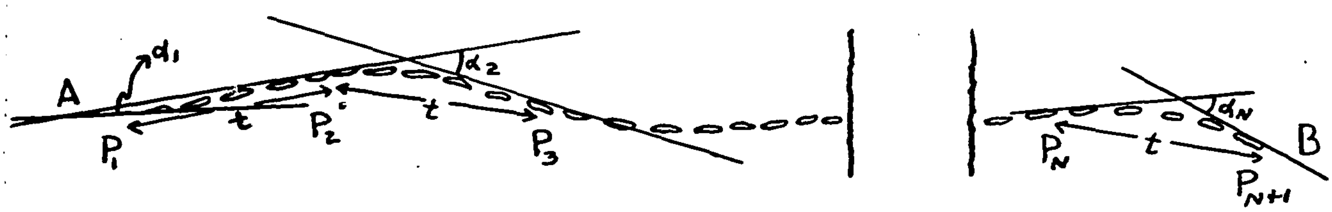

Fig. 23. Multiple Coulomb scattering of fast particles in nuclear emulsions.

Let S designate the entire arc length as measured along the track between A and B. The track is then subdivided into n cells of equal arc length t, such that S = nt. Points P_1, P_2, --- P_n, represent initial points on the track of the cells 1,2, ---, n, respectively. The angles α_1, α_2, --- α_n, are assumed to be small ($<10^\circ$) and correspond to angles between sucessive tangents drawn to the track at points P_1, P_2, --- P_{m+1}. Here, one considers each α_i to be the resultant deflection due to all scattering encounters with the Coulombian fields of the nuclei of the emulsion. If, now, the kinetic energy of the particle over the entire arc length, S, can be considered essentially constant, and one designates by $\bar{\alpha}_t^{tan}$ the average deviation of the set of successive α_i's it is clear that

$$\bar{\alpha}_t^{tan} = \frac{\sum_{i=1}^{i=n} |\alpha_i|}{n} = \bar{\alpha}_t = \delta L \qquad (5\text{-}2)$$

for a homogeneous medium.

In applying the theory to multiple scattering in an emulsion, it is impossible to draw accurate tangents to the track at points of equal separation, t, since the track is not truly a continuous curve but is actually defined by a finite number of grains, hence the quantity α_t^{tan} is not measured directly. In practice, one commonly measures* (see)

---

*An alternative procedure (not used in making the scattering measurements described in the subsequent chapters of the present research) is to determine the average deviation $\bar{\alpha}^{exp}$ of the angles between best fit lines of length t drawn through the track grains lying in the cell length t(28)(29). This may be accomplished by direct microscopic measurement using an eyepiece goniometer or by measuring the angles on large scale fascimile drawings obtained by using either a projection microscope or a camera lucida. In general, the mean line will be intermediate between a chord and a tangent and the upper and lower limits of $\bar{\alpha}_t^{exp}$, will be fixed by the next section) the average deviation $\bar{\alpha}_t^{chord}$ of the angles between successive chords of length t. Rossi and Greisen (8) have shown theoretically that in a sufficiently extended series of measurements the ratio $\bar{\alpha}_t^{tan}/\bar{\alpha}_t^{chord}$ tends to $(3/2)^{\frac{1}{2}}$ so that equation (5-2) may be written

$$\bar{\alpha}_t^{chord} = (2/3)^{\frac{1}{2}} \quad \delta L. \tag{5-3}$$

The quantity $T\left(\frac{2+\sigma}{1+\sigma}\right)$ may readily be shown to be equal to pv where p is the momentum and v the velocity of the scattered particle, so that in terms of the product pv equation (5-3) becomes

$$\bar{\alpha}_t^{chord} \quad \frac{pv}{zt^{\frac{1}{2}}} = (2/3)^{\frac{1}{2}} \; 2e^2 \; (\Sigma_j N_j Z_j^{\,2})^{\frac{1}{2}} \; L. \tag{5-4}$$

For no compelling reason, it has become standard in emulsion measurements to multiply both sides of (5-4) by the factor 10 and reformulate the equation as

---

mean values of the tangents and the chords, i.e.,

$$\bar{\alpha}_t^{tan} > \bar{\alpha}_t^{exp} > (2/3)^{\frac{1}{2}} \quad \bar{\alpha}_t^{tan}$$

or

$$\bar{\alpha}_t^{exp} = 0.91 \;\; \bar{\alpha}_t^{tan} \pm 0.04 \;\; \bar{\alpha}_t^{tan}.$$

Thus the measured angles must be increased by 9 ± 4% to correspond to $\bar{\alpha}_t^{tan}$. Slight modifications of the method resulting from the introduction of smoothing procedures are discussed in detail in the references cited.

$$\bar{\alpha}_t^{chord} \; \frac{pv}{z} \left(\frac{100}{t}\right)^{\frac{1}{2}} = (8/3)^{\frac{1}{2}} \; 2e^2 \; (\Sigma_j N_j Z_j^{\;2})^{\frac{1}{2}} \; (100)^{\frac{1}{2}} \; L = K_{chord} \tag{5-5}$$

where K_{chord} is called the "scattering constant" of the medium for angles measured between successive chords. Because of the nature of L, it is seen that K_{chord} depends primarily on the properties of the emulsion and but slightly on t and the velocity of the scattered particle. Customarily, $\bar{\alpha}_t^{chord}$ and pv are expressed in degrees and Mev respectively, so that with t in microns, the usual units of K_{chord} are Mev-degrees-(t microns)$^{-\frac{1}{2}}$.

A knowledge of $\bar{\alpha}_t^{chord}$ and K_{chord} of (5-5) permits one to express the kinetic energy of a singly charged particle in terms of its rest mass. The next two sections will concern themselves with a discussion of the methods used both to determine $\bar{\alpha}_t^{chord}$ and to select the appropriate value of K_{chord} for the conditions of the experiment. In what follows it will be convenient to drop the subscripts and superscript and refer to $\bar{\alpha}_t^{chord}$ and K_{chord} as $\bar{\alpha}$ and K respectively, unless it be specified otherwise.

Method of Determining $\bar{\alpha}$

(a) Procedure. A very rapid and convenient technique described by Fowler (4) is quite frequently used to measure angles between successive chords. In this scheme, the section of track along which the kinetic energy of the scattered particle may be considered constant is aligned approximately parallel to one of the directions of microscope stage motion, say the x-axis. An eyepiece scale is then oriented so that it is perpendicular to the x-axis. The track is moved by successive displacements, t_p, along the x-axis. The displacement, t_p, may be measured by either a micrometer drum calibrated in microns, or if a binocular microscope is used, by a graticule in the second eyepiece. As each displacement is executed, the intersection of the track with the eyepiece scale is recorded as a y-coordinate*. The difference in depth between the end points of the cell should also be recorded so that the actual cell length, t, may be calculated in a later analysis of the data. This procedure is carried out along the entire section of the track under analysis. The second differences in the y-coordinates then yield a measure of the angle between successive chords as can be seen by reference to Figure 24.

Consider the projection of the track on the defined plane of the emulsion to be represented by the curved dotted line, and let y_1, y_2 ---, represent coordinates of the track obtained as discussed above. Then the first differences in

---

*There is some latitude employed in the methods used to record the track position; e.g., Menon et al. estimate the mean line through a small, arbitrary section of track and interpret the position as the intersection of this imagined line with the eyepiece scale. Such a procedure results in a smoothing effect and the ratio $\bar{\alpha}_t^{tan}/\bar{\alpha}_t^{chord} = (3/2)^{\frac{1}{2}}$ no longer holds except for small (<50 microns) cells (30).

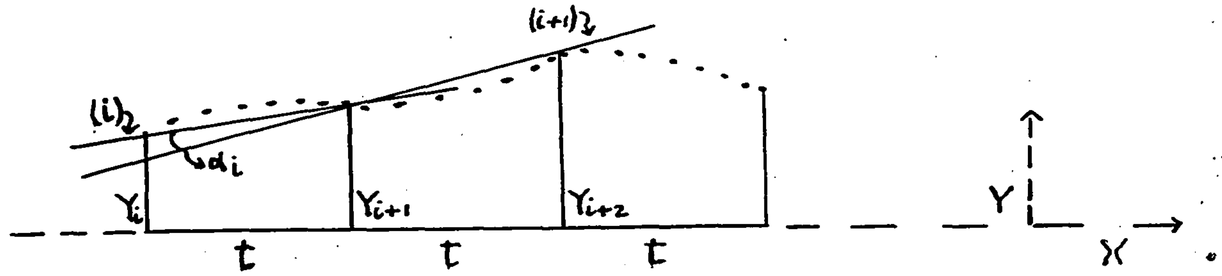

Fig. 24. The coordinate method of multiple scattering measurements.

the y-coordinates are $S_1 = y_1 - y_2$, $S_2 = y_2 - y_3$, ---, $S_n = y_n - y_{n+1}$ and the second differences are $D_1 = S_1 - S_2$, $D_2 = S_2 - S_3$, ---, $D_n = S_n - S_{n+1}$. The slopes of the chords 1, 2, ---, n, are given by S_1/t, S_2/t, ---, S_n/t, respectively. From analytic geometry, for small angles, if α_i is the angle between the i^{th} and $(i + 1)^{th}$ chord, then

$$\alpha_i = \frac{S_i/t - S_{i+1}/t}{1 + \frac{S_i \, S_{i+1}}{t^2}} \cong \frac{D_i}{t} \tag{5-6}$$

and the average deviation between successive chords is given by

$$\bar{\alpha} = \frac{\sum_{i=1}^{i=n} |\alpha_i|}{n} = \frac{\bar{D}}{t} \tag{5-7}$$

with $\bar{D} = \frac{\sum_{i=1}^{i=n} |D_i|}{n}$. Here $\bar{\alpha}$ is in radians if $\bar{D}$ and t are expressed in the same length unit.

The method just described of obtaining $\bar{\alpha}$ is called the "coordinate" method and represents a notable advance in the application of multiple scattering measurements to determining the mass and energy of charged particles in nuclear emulsions. Usually, in practice, y-coordinate readings are taken at small displacements, t'_p, ($\sim$ 5 microns) on the x-axis, where t'_p is a sub-multiple of t_p. When one then later analyzes the data, $\bar{D}$ is calculated from overlapping values of second difference which are obtained by using all those pairs of primed cell coordinate readings which are separated by an interval t. The procedure as described above was adopted in the present investigation in several instances which are discussed in Chapter VI.

(b) <u>Choice of Appropriate Value of t; Correction for Noise</u>. The decision as to the proper value of t to choose in evaluating $\bar{\alpha}$ is controlled by two conflicting factors. In order to give $\bar{\alpha}$ the greatest statistical weight, the largest possible number of values of second difference, D_i, should be included in determining $\bar{D}$ which would mean the smallest possible value of t should be chosen. In practice, however, the value of $\bar{D}$ calculated from the measured values of the y-coordinates contain apparent fluctuations in track direction which are superimposed on the actual multiple Coulomb scattering. The mean of the absolute values of these apparent fluctuations, termed "noise-level" scattering, $\bar{D}_n$, are due mainly to three effects:

1) Deviations (ϵ_1) in reading the eyepiece scale when determining the y-coordinates.

2) Deviations (ϵ_2) due to the random departure of the microscope stage motion from linearity.

3) Deviations (ϵ_3) due to the distribution of developed grains about the true particle trajectory.

It will be seen below that the result of this "noise-level" scattering is to impose a lower limit on the length of the cell, t, which may be used so that the actual value of t employed in determining $\bar{\alpha}$ represents a compromise between the deviations due to statistical fluctuations and those due to measurement.

Levi-Setti (31) has conducted a systematic study of "noise-level" scattering by analyzing measurements on an extremely high energy ($>$ 250 Bev) track of over 70,000 microns in the emulsion. He finds that, when scattering measurements are made using the "coordinate" method, the "noise-level," $\bar{D}_n$, is constant for cells of length $t < 200$ microns while for $t > 200$ microns it increases approximately as $t^{\frac{1}{2}}$ for conventional microscope stages with ball-bearing movements. The amplitude of $\bar{D}_n$ at a given cell size is strongly affected by the quality and condition of the microscope being used.

The experimental data of Fowler (4) show that for small cell sizes there is no significant difference between the value of $\overline{D}$ and the noise level, $\overline{D}_n$. Excluding extreme relativistic particles, increasing the cell size results in an increase in the difference $(\overline{D} - \overline{D}_n)$. He also finds that the values of $\bar{\alpha}$ corresponding to observed values of $\overline{D}$ tend to become constant as one employs larger and larger cells. This constant value of $\bar{\alpha}$ is reached for a signal/noise ratio of about 4:1, so the minimum value of t which yields the condition $\overline{D} > 4\overline{D}_n$ is frequently adopted in the determination of $\bar{\alpha}$. This value of t may normally be selected on the basis of preliminary observations.

Since the amplitude of $\overline{D}_n$ at a given value of t differs for different instruments and different operators, in order to apply the criterion $\overline{D} > 4\overline{D}_n$, the variation of $\overline{D}_n$ with cell length must be determined by calibration for a particular microscope by the observer who is to make the scattering measurements. To test for noise, the track of a very high energy particle with a long range, say > 20,000 microns, in the emulsion may be selected for measurement of scattering. If one measures the mean angle of scattering, $\bar{\alpha}$, using a cell of length ~ 3000 microns and obtains an extremely small value of $\bar{\alpha}$, it is a reasonably good approximation to assume that values of $\bar{\alpha}$ for t < 1000 microns represent spurious scattering effects (32). Under this assumption one can obtain a "noise-level" calibration curve by plotting $\overline{D}_n$ as a function of t. This scheme has been applied and a noise-level curve obtained for the x-axis of the Spencer microscope used in the present research (H, 3-17). The results are shown in Figure 25.

There is some latitude employed by different investigators in the application of the signal/noise criterion given above. For normal cosmic ray experiments, Gottstein (32) considers a ratio 2:1 to be an acceptable figure while in calibration experiments a ratio greater than 4:1 is more common particularly where sufficiently long tracks are available for study. Quite often a compromise must be effected, especially when there is but a short sample of high energy track available for analysis. In order to get a statistically meaningful estimate of $\bar{\alpha}$ one may be forced to choose a cell length, t, so small that the signal/noise ratio is less than 2:1. In such cases, a more empirical method to be discussed shortly would seem to be a reasonable procedure to use. A modification of the method of Fowler was used by Berger (33) to eliminate the effect of noise. Where the subscripts sc, obs, and n refer to the actual multiple scattering, observed multiple scattering and noise level scattering respectively, he makes use of the relation $\bar{\alpha}^2_{sc} = \bar{\alpha}^2_{obs} - \bar{\alpha}^2_n$. It is not clear from his paper, however, exactly what criterion he uses to determine the value of t at which he evaluates $\bar{\alpha}^2_{obs}$ and $\bar{\alpha}^2_n$.

If the scattering data are analyzed using small values of t, an alternative method of noise elimination may be used, which does not require calibration curves for $\bar{D}_n$. The scheme

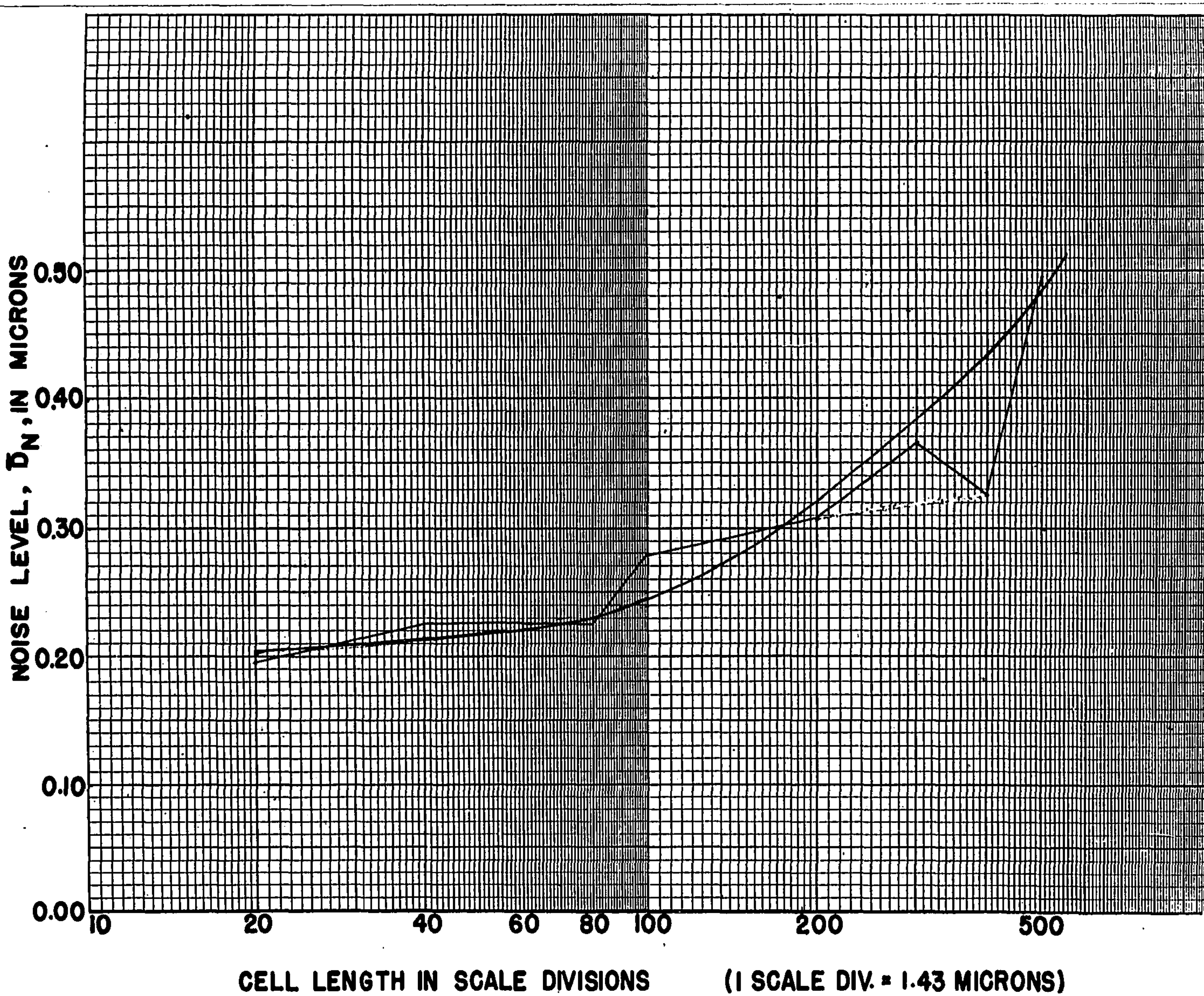

Fig. 25. Noise-level data for x-axis of Spencer Research microscope as a function of cell length.

follows closely a suggestion of Fowler (unpublished) which has been discussed by Menon (30). Careful studies of the various components contributing to the noise level $\bar{D}_n$ have been carried out by both the Brussels Group (29)(34) and the Bristol Group (30), and their results seem to indicate that, ($\epsilon_n^i = \epsilon_1^i + \epsilon_2^i + \epsilon_3^i$) has a Gaussian distribution with zero mean and the same standard deviation in every cell (35).

Assuming a Gaussian distribution and writing

$$\epsilon_n^i = \epsilon_1^i + \epsilon_2^i + \epsilon_3^i$$

as the total random deviation of the y-coordinate of the i^{th} cell one has with the same subscript notation as before

$$y_{obs}^{i} = y_{sc}^{i} + \epsilon_n^{i}, \quad y_{obs}^{i+1} = y_{sc}^{i+1} + \epsilon_n^{i+1}, \text{ etc.}$$

The i^{th} second difference will be

$$D_{obs}^{i} = D_{sc}^{i} + D_{n}^{i}.$$

Under the further assumption that the actual multiple scattering of the track has an approximately Gaussian distribution* one can show that the measured values of second difference (D_{obs}^i) will then satisfy a Gaussian distribution whose average deviation is designated by the symbol $\bar{D}_{obs}$ where $\bar{D}_{obs}$ satisfies the relation

$$(\bar{D}_{obs})^2 = (\bar{D}_{sc})^2 + (\bar{D}_n)^2. \qquad (5\text{-}8)$$

---

* See footnote Pg. 79, also part C this section.

From (5-5) one may write

$$\overline{\alpha}_{sc} = \left(\frac{t}{100}\right)^{\frac{1}{2}} \frac{z}{pv} K = \gamma K(\eta, t, \beta) t^{\frac{1}{2}}$$

where $\gamma = \dfrac{z}{(100)^{\frac{1}{2}} pv}$ and the functional notation reflects the dependence of K on the emulsion properties, η, the velocity $v = \beta c$ and the cell length, t. From (5-7) one has that

$$(\overline{D}_{sc})^2 = (\overline{\alpha}_{sc} t)^2 = \gamma^2 K^2(\eta, t, \beta) t^3$$

so that (5-8) may be rewritten as

$$(\overline{D}_{obs})^2 = \gamma^2 K^2 t^3 + (\overline{D}_n)^2. \qquad (5\text{-}9)$$

Levi-Setti's (31) results, already referred to, indicatethat if y-coordinate readings are taken by the "coordinate" method* as previously described, the noise level $\overline{D}_n$ is constant for cells of length $t < 200$ microns. If one evaluates $(\overline{D}_{obs})^2$ for cells of length t_1 and t_2, ($t_1, t_2 <$ 200 microns), ~~treat~~ing $\overline{D}_n$ as constant the noise contribution may be eliminated between the two equations

$$(\overline{D}_{1obs})^2 = \gamma^2 K^2(\eta, t_1, \beta) t_1^3 + (\overline{D}_n)^2 \qquad (5\text{-}9a)$$

$$(\overline{D}_{2obs})^2 = \gamma^2 K^2(\eta, t_2, \beta) t_2^3 + (\overline{D}_n)^2 \qquad (5\text{-}9b)$$

to obtain

$$\gamma^2 = \frac{(\overline{D}_{2obs})^2 - (\overline{D}_{1obs})^2}{K^2(\eta, t_2, \beta) t_2^3 - K^2(\eta, t_1, \beta) t_1^3} = \frac{(\overline{D}_{sc})^2}{K^2(\eta, t, \beta) t^3} . \qquad (5\text{-}9c)$$

*The y-coordinates are taken from readings on a single point of intersection of the track with the eyepiece scale.

If now (5-9c) is solved for $\bar{D}_{sc}$, one has the result that

$$\bar{D}_{sc} = K(\eta,t,\beta)t^{3/2}\left[\frac{(\bar{D}_{2obs})^2 - (\bar{D}_{1obs})^2}{K^2(\eta,t_2,\beta)t_2^3 - K^2(\eta,t_1,\beta)t_1^3}\right]^{\frac{1}{2}}. \tag{5-10}$$

Thus, $\bar{\alpha}_{sc}$ may be expressed in degrees through the relation

$$\bar{\alpha}_{sc} = \frac{\bar{D}_{sc}}{t}\left(\frac{180}{\pi}\right)$$

$$= \left(\frac{180}{\pi}\right) t^{\frac{1}{2}} K(\eta,t,\beta)\left[\frac{(\bar{D}_{2obs})^2 - (\bar{D}_{1obs})^2}{K^2(\eta,t_2,\beta)t_2^3 - K^2(\eta, t_1,\beta)t_1^3}\right]^{\frac{1}{2}}. \tag{5-11}$$

Methods for obtaining the appropriate value of $K(\eta,t,\beta)$ for a fixed cell length, t, will be discussed in the next section. Quite often, in practice, the variation of $K(\eta,t,\beta)$ with cell-size may be neglected. When such approximation is justified (5-11) reduces to

$$\bar{\alpha}_{sc} = \left(\frac{180}{\pi}\right) t^{\frac{1}{2}}\left[\frac{(\bar{D}_{2obs})^2 - (\bar{D}_{1obs})^2}{t_2^3 - t_1^3}\right]^{\frac{1}{2}}. \tag{5-12}$$

(c) Application of Cut-off. The average deviation $\bar{\alpha}$, determined as was just described, is subject to still further modification for the following reason. From theoretical considerations (20)(21) (see Figure 26) the projected deflections α distribute themselves in a way which is well represented by a probability function $P(\alpha) = G(\alpha) + S(\alpha)$.

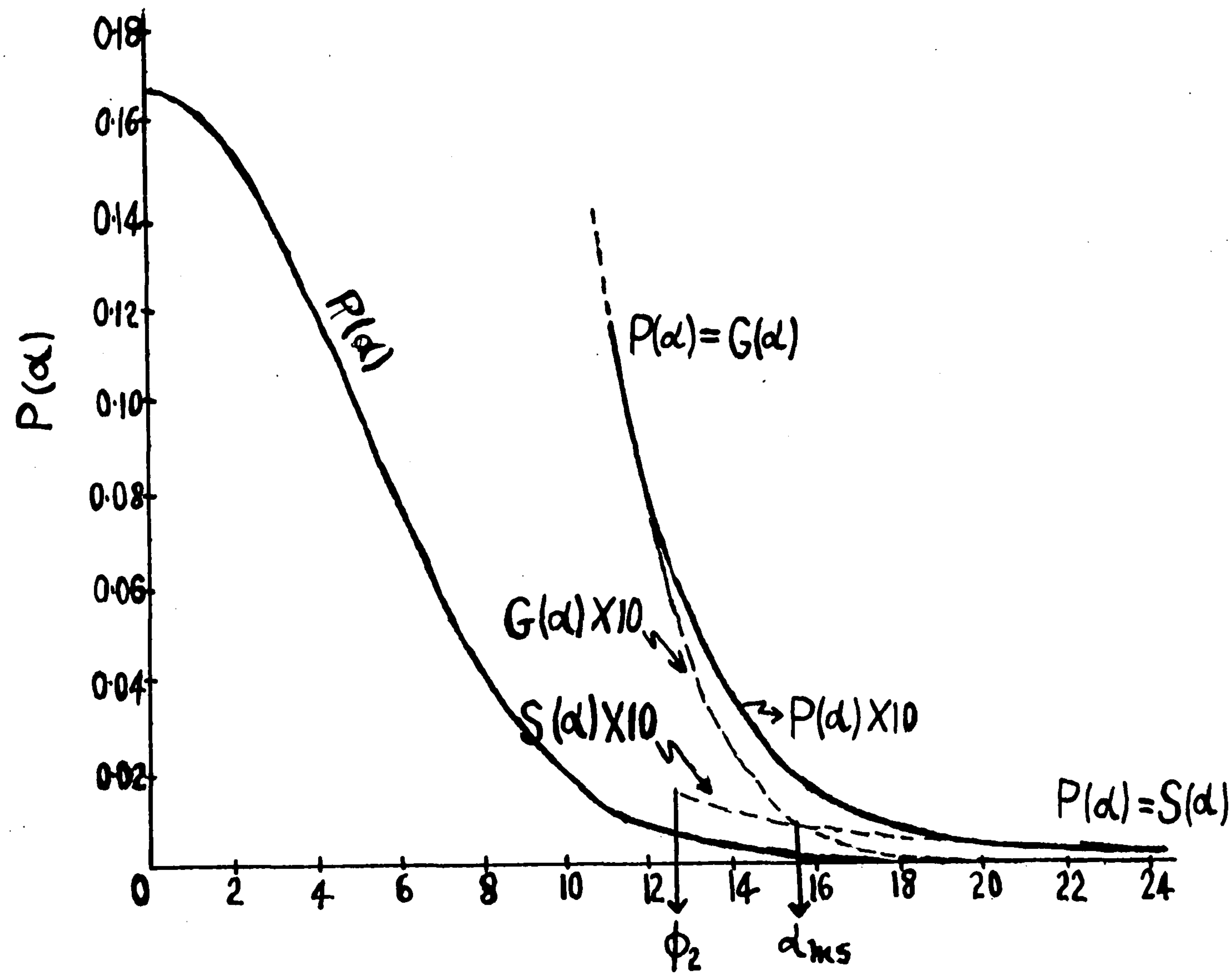

Fig. 26. Theoretical distribution of scattering (Williams).

Here $G(\alpha)$ is to a close approximation Gaussian and $S(\alpha)$ is a single collision scattering contribution starting at an angle $\alpha = \phi_2$ and given by π/α^3 for angles greater than ϕ_2 where, following Williams (20),

$$\phi_2 = 6.375\,\bar{\alpha} - 13.24$$

with angles expressed in units of δ. For particles of unit charge in Ilford G-5 emulsion δ has been evaluated by Voyvodic (21) and is given by

$$\delta = 1.006\ t^{\frac{1}{2}}/pv \text{ degrees.} \qquad (5\text{-}13)$$

In this equation, t is the cell length in microns and pv is expressed in Mev.

In figure 26, α_{ms} represents the value of α corresponding to the intersection of $G(\alpha)$ and $S(\alpha)$. For values $\alpha > \alpha_{ms}$, $S(\alpha)$ rapidly dominates $G(\alpha)$ due to the fact that the fall-off of the single scattering tail, $S(\alpha)$, is far less steep than the Gaussian fall-off of $G(\alpha)$. The presence of this non-Gaussian tail means there is an appreciable probability of large deflections occurring due to single collisions, which, if included in the statistics of a small sample, would give rise to large fluctuations in the value of pv. In analyzing scattering data, attempts are usually made to minimize the effects of this tail by cutting out of the statistics those angles α greater than a certain prescribed amount.

~~The experimental analysis carried out by Goldschmidt-~~

Clermont (29) appears to have established an arbitrary cut-off criterion which has become more or less standard in emulsion measurements. Where $\bar{\alpha}_{co}$ represents the average deviation after cut-off their work suggests deleting all values of $\alpha > 4\bar{\alpha}_{co}$. The distribution so truncated at $4\bar{\alpha}_{co}$ is very close to Gaussian with the value of $\bar{\alpha}_{co}$ usually being obtained by successive approximation (36).

A simpler method of obtaining $\bar{\alpha}_{co}$ is proposed by Voyvodic and Pickup (21) who calculate $\bar{\alpha}_{co}$ from the approximate expression

$$\bar{\alpha}_{co} = \frac{(\bar{\alpha} - \pi/4\bar{\alpha})}{(1 - \pi/32\bar{\alpha}^2)} \tag{5-14}$$

with angles in units of δ. The authors state that the equation is obtained from the analogous expression derived by Williams (20) for a cut-off at the angle ϕ_2. Williams obtains the expression (in units of δ)

$$\bar{\alpha}_m = \frac{\bar{\alpha} - \pi/\phi_2}{1 - \pi/2\phi_2^2}$$

as the average deviation of a distribution from which values of $\alpha > \phi_2$ had been dropped. Actually, then, the application of (5-14) to measurements of scattering on an individual track is equivalent to deleting from the statistics all values of $\alpha > 4\bar{\alpha}$. The average deviation of the distribution so truncated will be $\bar{\alpha}_{co}$ as given by (5-14).

Still another cut-off procedure suggests itself which can nullify the effect of the single scattering tail. When a sufficiently large number of measures of α are available one can plot the logarithm of the number of measures m having values between α and $\alpha + d\alpha$ as a function of α^2. For a Gaussian distribution a straight line should result on a semi-logarithmic graph. The best-fit straight line is drawn through the raw data and the value of α^2 for which ln m = 1, say α', is then selected as the cut-off angle, i.e., all angles $\alpha > \alpha'$ are deleted.

For tracks of particles possessing only moderate energy the value of $\bar{\alpha}$ is of the order of 0.5°. Thus it is possible to have a track aligned approximately parallel to the axis of stage motion which includes single scattering values of $\alpha > 4\bar{\alpha} \sim 2^{\circ}$ without invalidating the assumption of small angles or, equivalently, approximate parallelism, in the formation of $\bar{\alpha}$. When such is the case, the procedures discussed are adequate for determining $\bar{\alpha}_{co}$. It is not unusual, however, to observe single scatterings which cause sharp deflections through angles sufficiently large that by virtue of the encounter the track is no longer approximately parallel to the direction of stage motion. In this case, an arbitrary scheme is frequently adopted of "cutting" the track at the position of any such single scattering and measuring the scattering of each side independently. This procedure has the advantages not only of permitting one to rotate the stage to a new base line but also allows for possible energy loss at the point of scattering.

(d) Corrections for Distortion. Although the corrections for distortion now to be discussed are actually made on the raw data before "noise-level" corrections and cut-off are applied, it seemed advisable to defer the treatment of this matter until now because much of the understanding of the method of applying corrections depends upon ideas introduced in earlier sections of this chapter.

When the direction of the distortion vector, $\vec{S}_o$ makes some arbitrary angle, ϕ, with the axis, x', to which the scattering observations, y_i, on a given track, are referred, the effect of distortion on the measurements is most conveniently treated in terms of the rectangular components of the displacements, due to distortion, of the track grains in the x', y- coordinate system. In Figure 27 consider x' to be the reference axis for the scattering observations and y_i, y_{i+1} and y_{i+2} to be three successive y-coordinates of the track grains observed at the end points of two adjacent projected intervals of length t_p each. Assume that t_p is the projected apparent cell length corresponding to the apparent cell length, t, which satisfies the chosen noise criterion, and that the angle θ between the trajectory of the particle and the plane of the emulsion is approximately constant.

If the distortion vector, $\vec{S}_o$, makes an angle ϕ with the reference axis, each y-coordinate, y_i, must be replaced by a new coordinate, $y_i' = y_i + S_{i\perp}$, where $S_{i\perp}$ represents the

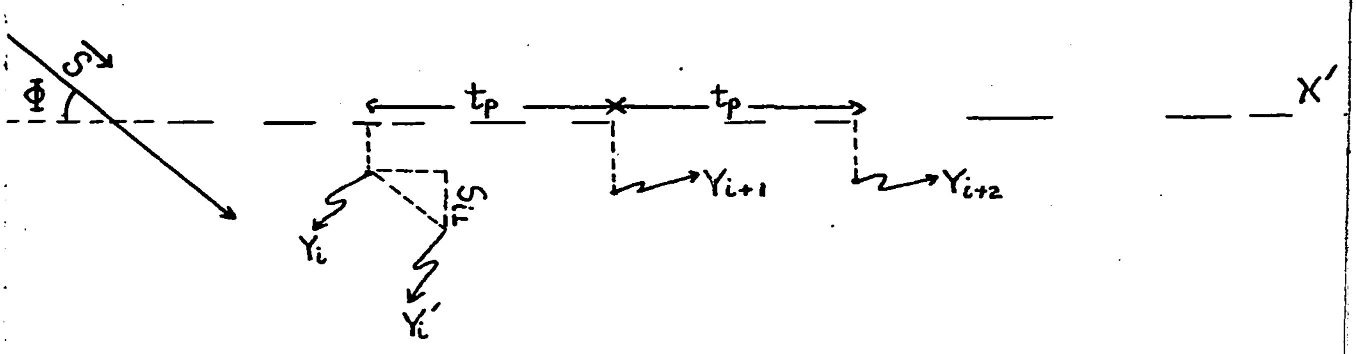

Fig. 27. The method of correcting scattering observations for distortion.

component of the displacement, due to distortion, perpendicular to the x'-axis, which, from equation (3-2a), is given by

$$S_{i\perp} = S_o \sin\phi \left[\frac{2(z_i - z_1)}{z_o} - \frac{(z_i^2 - z_1^2)}{z_o^2} \right]$$

$$= a(z_i - z_1) - b(z_i^2 - z_1^2). \qquad (5\text{-}15)$$

Here $a = \frac{2S_o \sin\phi}{z_o}$ and $b = \frac{a}{2z_o}$ are constant for the given region of the emulsion and z_1, is the height, above the glass emulsion interface, of the first point on the track at which a scattering observation was taken.

One may express the i^{th} corrected second difference, $(D^i_{obs})'$, in terms of the i^{th} apparent second difference

(D^i_{obs}) since

$$(D^i_{obs})' = y_{(i)} + S_{(i)\perp} + y_{(i+2)} + S_{(i+2)\perp} - 2y_{(i+1)} - 2S_{(i+1)\perp}$$

$$= (D^i_{obs}) + (D_{S_{i\perp}}). \qquad (5\text{-}16)$$

By use of equation (5-15) it is possible to express $(D_{S_{i\perp}})$ in a form more convenient for calculation. One obtains the expression

$$(D_{S_{i\perp}}) = \left[b(z_{i+1} + z_i) - a\right](z_{i+1} - z_i) - \left[b(z_{i+2} + z_{i+1}) - a\right](z_{i+2} - z_{i+1}). \qquad (5\text{-}17$$

Since the displacements of the track grains have components parallel to the x'-axis, the value of $(D^i_{obs})'$ obtained from equation (5-16) will now correspond to a new projected cell length, t_p'. If the distortion is not excessive and the trajectory of the particle is not too steeply dipping* it is a sufficient approximation to assume that each apparent projected cell length, t_p, has been altered by a constant amount Δt_p. The value of Δt_p may be obtained by dividing the total projected change in length over the entire portion of

---

*When these conditions are not met a constant cell length, t_p, may not be assumed to correspond after correction to a constant projected cell length, t_p'. In such a case, it would appear necessary to construct, in advance of making the scattering measurements, a scheme whereby variable apparent cell lengths would, under correction, yield constant cell lengths.

track used in making the scattering observations by the number, n, of successive cells of projected length, t_p, lying within the interval. Then $t'_p = t_p \pm \Delta t_p$ and the appropriate cell length t', is obtained in the usual way from equation (3-1).

Determination of Appropriate Value of Scattering Constant K_{co}

The question of choice of the appropriate value of the scattering constant, K, corresponding to the average deviations, $\bar{\alpha}$, may now be examined briefly. From equation (5-5) the scattering constant may, for singly charged particles, be expressed as

$$K = \delta' \, L\,(\beta,t) = (2/3)^{\frac{1}{2}} \, 2e^2 \, (\Sigma_j N_j Z_j^2)^{\frac{1}{2}} \, (100)^{\frac{1}{2}} \, L(\beta,t).$$

Since the atomic composition of Ilford, G-5, nuclear emulsions is known, for given values of t and β, K, and/or K_{co} corresponding to the cut-off average deviation, $\bar{\alpha}_{co}$, can be calculated for the various scattering theories by using the appropriate explicit expression for $L(\beta,t)$. This has been done (25)(21)(37)(32) and there appears to be general agreement, within a few percent, for the scattering constants as given by the various theoretical expressions.

Voyvodic and Pickup (21) have plotted some very convenient theoretical curves which may be used for determining K_{co} under most of the experimental conditions encountered in emulsion investigations. From the theory of Williams, with a slight modification due to Moliere, they calculate for Ilford, G-5, emulsions an explicit expression for K_{co} as a function of t and β for singly charged particles. They find

$$K_{co} = 8.21\left[\frac{\bar{\alpha} - \pi/4\bar{\alpha}}{1 - \pi/32\bar{\alpha}^2}\right]$$

where in units of δ, for the coordinate method, $\bar{\alpha} = \left(\frac{2}{3}\right)^{\frac{1}{2}}\left\{1.45 + 0.80\,(\log_e 0.723\, t_1)^{\frac{1}{2}}\right\}$ and where $t_1 = \left(\frac{1.30}{\beta^2 + 0.30}\right)t = Q(\beta)\, t$ is an equivalent cell length which is equal to t for $\beta = 1$.

A graph of K_{co} vs $\log_{10} t_1$, for use with the coordinate method, is shown in Figure 28. $Q(\beta)$ is called the velocity factor and is plotted against the relative ionization in Figure 29*. Here the relative ionization is measured with respect to relativistic or plateau value. The plateau value is approximately 10 percent higher than the minimum observed ionization values. The experimental data used in obtaining the curve of Figure 29 are taken from grain density calibrations on tracks of particles of known mass, charge, and energy. Alternatively, one might plot the velocity factor against any other measure of energy loss, such as gap density or area density.

If then, one wishes to select an appropriate value of K_{co} to use with the scattering data for a cosmic ray track of interest, the following procedure may be employed. If the particle has relativistic energy $\beta \cong 1$, $Q(\beta) = 1$ and t_1 is

---

*Figures 28 and 29, based on the work of Voyvodic and Pickup, are taken directly from (37).

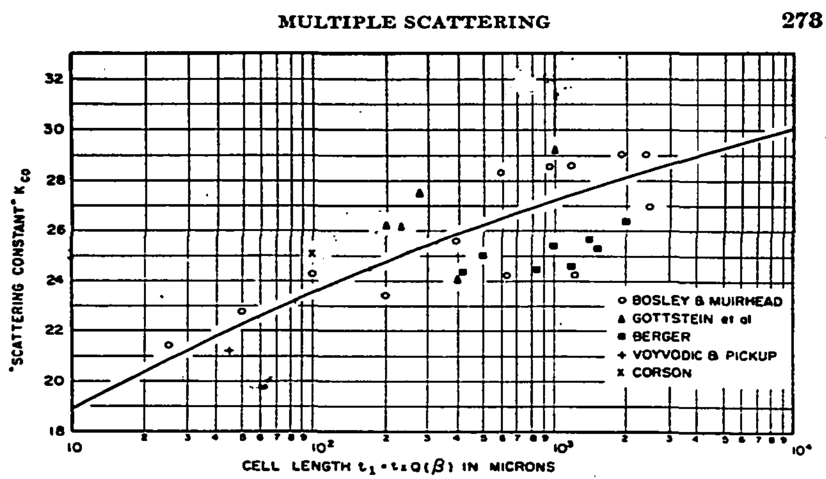

Fig. 28. Theoretical and experimental determinations of the "scattering constant" in G-5 emulsions.

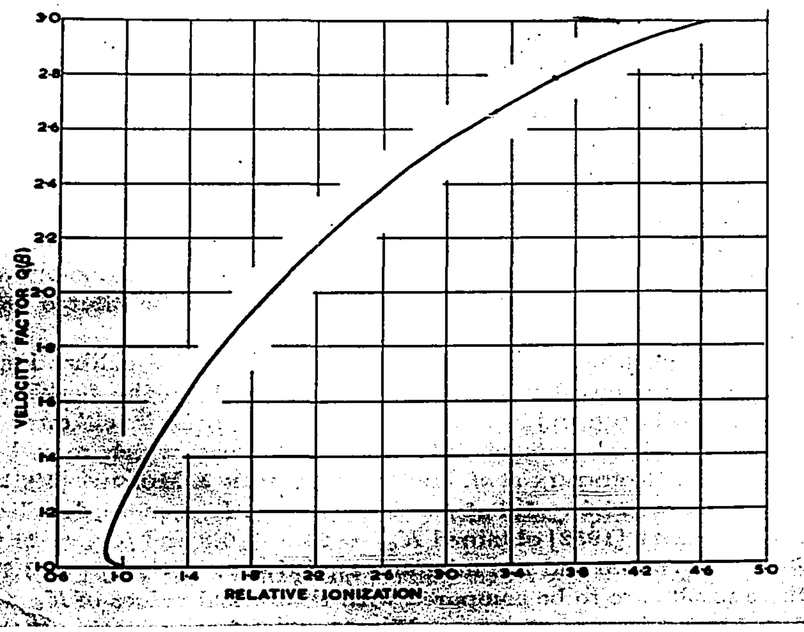

Fig. 29. The velocity factor, $Q(\beta)$, vs relative ionization in G-5 emulsions.

taken equal to t. The t value has been previously determined in the formation of $\bar{\alpha}_{co}$ and hence a K_{co} value may be read directly from the curve. For slow particles (see later section) $\beta^2 << 0.30$ and $t_1 \cong 4t$. For non-relativistic particles of intermediate energies the specific ionization must be determined. Then the appropriate value of $Q(\beta)$ is procured from Figure 29. Since $t_1 = Q(\beta)t$, K_{co} may be selected from Figure 28.

A considerable number of calibration experiments (38) (32)(39)(40)(33)(21) have been carried out for the purpose of comparing experimental and theoretical values of both K and K_{co}. In all of the calibration experiments conducted up to the present writing, singly charged particles of different mass and of different but known energies have been used, and values of the scattering constant obtained for varying cell-lengths. In these investigations, positrons, electrons, mesons and protons have been used with an overall energy spectrum from 5-337 Mev and cell lengths varying from 25-800 microns. In general the agreement with theory is good. The experimental results of Gottstein (32), however, differ significantly from the experimental results of Berger (33) for 337 ± 1 Mev protons. The source of protons for both investigations was the Berkeley cyclotron. Gottstein obtains a value of $K_{co} = 29.2 \pm 1.0$ at t = 600 microns while Berger reports $K_{co} = 24.5 \pm 0.8$ and $K_{co} = 24.6 \pm 0.9$ at t = 500 and 750 microns respectively. The various calibration results are also included in Figure (28).

Although, in principle, there is a variation in the scattering constant, K_{co}, with cell-size and velocity, Gottstein (32) points out that the effect of this variation is lessened because of the experimental procedure which has been generally adopted. He reasons that the product $Q(\beta)t$ will be essentially constant in practice for most routine measurements involving non-relativistic particles. For those particles with energies on the higher side of the non-relativistic band there is a decrease in $Q(\beta)$ but an increase in t is required to keep the signal/noise ratio at the minimum acceptable value. On the other hand, for particles of lower energy, $Q(\beta)$ is larger but one may use a smaller cell-size which will offset the increase in $Q(\beta)$. Except for extreme relativistic particles, he suggests the use of the constant $K_{co} = 26.0$ Mev-degree/$(100\mu)^{\frac{1}{2}}$ over the whole range of measurement. This procedure will not introduce a systematic error greater than ± 8 percent which for most cases will be less than the statistical uncertainty introduced due to the small number of angles normally available for use in forming $\bar{\alpha}_{co}$.

Estimation of Energy and Rest Mass of Fast Particles from Scattering Measurements on a Track Segment

Assuming that values of $\bar{\alpha}_{co}$ and K_{co} for a particular track of interest have been determined as described in previous sections, one may next consider the question of estimating the energy and rest mass of the particle producing the track. If the energy of the particle is assumed constant over the entire interval in which the scattering is measured, one has from equation (5-5) for singly charged particles

$$pv = \frac{K_{co}}{\alpha_{co}} \left(\frac{t}{100}\right)^{\frac{1}{2}} \qquad (5\text{-}18)$$

where the R. H. S. of the equation is known. It is convenient in what follows to consider two cases.

(a) Extreme Relativistic Singly Charged Particles. For extremely high energy particles, scattering measurements will yield an estimate of energy but, in general, it is not possible to determine a value of rest mass for the unknown particle. If one plots the relative ionization of a singly charged particle as a function of $\sigma = T/m_oc^2$, it is found experimentally (41)(42)(43) that as σ rises from low values, the relative ionization produced by the particle passes through a minimum value when $\sigma \cong 3$. For particle energies giving values of $\sigma > 3$, there is a slow rise in the relative ionization until a saturation value occurs for $\sigma \cong 20$. This saturation or "plateau" value is about 10 percent higher than the minimum relative ionization. This means that for relative ionization values less than or equal to the "plateau" value, it is not possible to make an unambiguous choice of σ, or equivalently, pv/m_o. An energy estimate may readily be made, however, since

$$pv = T\left(\frac{2+\sigma}{1+\sigma}\right) \rightarrow T \text{ as } \beta \rightarrow 1$$

and T is given directly by equation (5-18).

(b) Fast Singly Charged Particles Ionizing at Greater than Plateau Value. Grain, area and/or gap density measurements are made on the unknown particle. With the values of dN/dR, dA/dR and/or dG/dR thus obtained, one consults the calibration curves in which these slopes are plotted as a function of pv/m_o. This procedure yields a value of pv/m_o corresponding to the measured ionization. This value of pv/m_o in conjunction with equation (5-18) then determines the rest mass, m_o, of the unknown particle. When the identity of the particle is considered to be established, the relation $pv = T\left(\frac{2+\sigma}{1+\sigma}\right)$ then gives an estimate of the kinetic energy T. Alternatively, once the particle's identity is known, the energy may be obtained from calibration curves of dN/dR, dA/dR and/or dG/dR vs T/m_o.

Estimation of Energy and Rest Mass of Slow Particles from Scattering Measurements on a Track Segment

Thus far, the discussion has been concerned with scattering measurements on sections of high energy tracks where the energy loss over the section was small enough that the energy could be considered essentially constant. For slow particles the loss of energy along the track due to ionization is not negligible. In such cases, this energy loss must be considered and further refinements in procedure must be made since the variation in energy results in a variation of $\bar{\alpha}$ along the trajectory.

Goldschmidt-Clermont et al. (28) were the first investigators to examine this problem in applying the multiple scattering theory of Williams (20) to slow singly charged particles in nuclear emulsions. They consider an arbitrary segment of track for an unknown particle of mass M. The segment is divided into n cells of equal length t. In terms of the "coordinate" method the analysis proceeds as follows: a statistical variable, ϵ, is defined for each adjacent pair of cells by

$$\epsilon_i \equiv \frac{\alpha_i}{\bar{\alpha}_i} = \alpha_i \left(\frac{100}{t}\right)^{\frac{1}{2}} \frac{pv}{K(\eta,\beta_i,t,)} = \frac{\alpha_i T_i}{K'(\eta,\beta_i,t,)}$$

where α_i is the observed projected angle of deflection between chords drawn for the i^{th} and $(i + 1)^{th}$ cell. T_i is the average kinetic energy of the particle over the i^{th} cell and $\bar{\alpha}_i$ is given by equation (5-1).

If one had n' observed measures of α_i for the i^{th} and $(i + 1)^{th}$ cells, by definition, the average deviation of such a distribution would be

$$\bar{\epsilon}_i = \sum_{j=1}^{j=n} \frac{|\epsilon_i|}{n'} = \frac{\sum_{j=1}^{n} |\alpha_i|}{\bar{\alpha}_i\, n'} = 1.$$

Designating by $\bar{\epsilon}_M$ the average deviation of n successive values of ϵ_i along the arbitrary segment of track, they apparently assume,

$$\bar{\epsilon}_M = \bar{\epsilon}_i = 1.$$

It is desired to estimate the rest mass, M, of the unknown particle. At points on the trajectories where two particles of mass m and M have the same residual range the ratio of their kinetic energies is given by

$$\frac{T_m}{T_M} = \left(\frac{m}{M}\right)^{1-1/\nu}$$

from the range-energy relation, $R = hm_o^{1-\nu} T^{\nu}$. With this in mind, and neglecting the slight variation in K' with velocity for low values of β, one has

$$\bar{\epsilon}_M = 1 = \frac{\sum_{i=1}^{i=n} |\epsilon_i|}{n} = \frac{\sum_{i=1}^{i=n} |\alpha_i| \, T_{Mi}}{K'(\eta,t,\beta)n}$$

$$= \frac{1}{K'(\eta,t,\beta)n} \left(\frac{M}{n}\right)^{1-\frac{1}{\nu}} \sum_{i=1}^{i=n} |\alpha_i| \, T_{mi}. \qquad (5\text{-}19)$$

Consider, now, an unknown singly charged particle which does not come to rest in the emulsion. The summation on the R. H. S. of (5-19) may be carried out by first determining the ionization loss at each cell through grain, area and/or gap density measurements. With these values of ionization, corresponding ranges R_{mi} and/or energies T_{mi} may be determined from the calibration curves of ionization loss vs residual range and/or kinetic energy for the known particle. The α_i are, or course, obtained from the scattering data and $K'(\eta,t,\beta)$ is determined as discussed in an earlier section. Thus (5-19) may be solved for the unknown mass M.

The initial energy of the unknown particle is then taken from calibration curves of ionization loss vs T/M by making use of the ionization loss at the high energy end of the track.

If the unknown particle comes to rest in the emulsion the residual range R_{Mi} can be measured. One can then, using the range-energy relation, express the kinetic energy T_{Mi} in terms of the rest mass M and the residual range R_{Mi}. Substituting in the expression

$$1 = \frac{\sum_{i=1}^{i=n} |\alpha_i| T_{Mi}}{nK'(\eta, t, \beta)}$$

one can evaluate the R. H. S. and solve for the rest mass. Once the rest mass, M, has been determined, the initial kinetic energy is obtained from the range- energy relation using the appropriate measured value of residual range.

Before one can obtain values of α_i and $K'(\eta, t, \beta)$ a decision must be reached as to the proper choice of cell length, t, for the arbitrary segment of track under analysis. The procedure for such determination is essentially as discussed earlier where the value of t which is chosen depends on the signal/noise criterion which has been adopted. In principle, at least, this method permits one to carry on measurements to the very end of the track if the particle comes to rest in the emulsion. The trajectory can be divided into a small number of arbitrary segments and the scattering of each segment measured separately. The cell length, t, to be used in a given segment can, subject to keeping the signal/noise ratio at the proper level, be decreased as the track terminus is approached. The assumption of negligible variation in $K'(\eta,t,\beta)$ with velocity can be maintained and appropriate values of $K'(\eta,t,\beta)$ for different cell lengths obtained as before. Thus, one could get several estimates of the particle's rest mass and energy, each segment yielding an estimate of these two quantities. As a practical matter, however, energy is lost very rapidly as the particle approaches the point of arrest, so that, even when one chooses a small cell length t, the energy may vary considerably over the cell as the particle slows down. In addition, it becomes increasingly difficult to eliminate effectively from the measurements, the contribution of large angle deflections due to single collisions. If such large angle deviations are included in the statistics, it results in large fluctuations in the estimates of energy and rest mass. Thus the scattering measurements are usually confined to a part of the trajectory where the change of energy is not too large. The exact cut-off point is arbitrary and depends on the general appearance of the track near the terminus, the length of track available for analysis and the type of experiment being carried out.

A somewhat simpler procedure for estimating the rest mass and kinetic energy of a singly charged particle has been described by Menon and Rochat (44). It may be applied to slow charged particles which have a measurable residual range, R, in a photographic emulsion. Neglecting the variation with velocity of the scattering constant, they show that, for a constant cell length, t, the parameter $\sum_{i=1}^{i=n} |\alpha_i| T_{M_i}/n$ of equation (5-19) is statistically equivalent to the quantity

$$\left(\sum_{i=1}^{i=n} |\alpha_i / n|\right) \times \left(\sum_{i=1}^{i=n} (T_{M_i})^{-2} \Big/ n\right)^{-\frac{1}{2}}$$

by establishing that they have the same average value, (i.e. $K'(\eta, t, \beta)$*. Thus, they take

$$K'(\eta, t, \beta) = \left(\sum_{i=1}^{i=n} |\alpha_i / n|\right) \times \left(\sum_{i=1}^{i=n} \left\{T_{M_i}\right\}^{-2} \Big/ n\right)^{-\frac{1}{2}}. \qquad (5\text{-}20)$$

The second factor on the R. H. S. of (5-20) can be evaluated by use of the range-energy relation $T = CR^{1/\nu}$ since the particle is arrested in the emulsion and the residual range may be measured. To do this, one replaces the sum by an integral to obtain

$$\left(\frac{1}{n} \sum_{i=1}^{i=n} \frac{1}{T_i^2}\right)^{-\frac{1}{2}} = C\left(\frac{1}{n} \sum_{i=1}^{i=n} R_i^{-2/\nu}\right)^{-\frac{1}{2}} = C\left\{\frac{1}{(R_o - R_n)} \int_{R_n}^{R_o} R^{-2/\nu}\, dR\right\}^{-\frac{1}{2}}$$

$$= CR_{eff}^{\;1/\nu} = T_{R_{eff}}$$

where R_o and R_n, $(R_o > R_n)$, are the two points of residual range between which the scattering angles were measured and an effective value of range, R_{eff}, is defined by

$$R_{eff} = \left\{\frac{\int_{R_n}^{R_o} R^{-2/\nu}\, dR}{(R_o - R_n)}\right\}^{-\nu/2} = \left[\frac{(2/\nu - 1)(R_o - R_n)}{R_n^{-(2/\nu - 1)} - R_o^{-(2/\nu - 1)}}\right]^{\nu/2}. \qquad (5\text{-}21)$$

---

*The mathematical justification for this statement is based on certain unpublished results of G. Moliere, University of Tubingen, Germany. Additional information has been requested, which at present, has not been received in this laboratory.

Since R_o and R_n are measurable, R_{eff} may be calculated.

Designating by $T_{R_{eff}}$ the kinetic energy of the particle corresponding to this effective value of range, one may write

$$T_{R_{eff}} = \frac{K'(\eta, t, \beta)}{\left(\frac{1}{n} \sum_{i=1}^{i=n} |\alpha_i|\right)} \tag{5-22}$$

where the denominator of the R. H. S. of (5-22) is simply the average deviation of the n successive observed angles lying between R_o and R_n. After $T_{R_{eff}}$ has been determined, the rest mass of the particle is obtained from the range-energy relation using the calculated values of $T_{R_{eff}}$ and R_{eff}.

In practice, R_{eff} obtained from (5-21) differs very little from the residual range at the center of the segment, so that $T_{R_{eff}}$ represents to a good approximation the kinetic energy at the center of the segment. In applying the method, Menon and Rochat arbitrarily divided each track into two equal segments and confined the scattering measurements to cells of equal length in the fast half of the track. By use of the value $\frac{1}{\nu} = 0.578$ with $R_o = 2R_n$ they obtain a value of $R_{eff} = 0.72\ R$ for the conditions of their experiment.

The so-called constant sagitta method (19) of measuring scattering is an ingenious method for obtaining an estimate of rest mass for singly charged particles producing tracks which terminate in the emulsion. The coordinate technique of measurement is used but, in making the multiple Coulomb scattering observations, the cell length, t, is permitted to vary with residual range, R, along the trajectory in accordance with a predetermined "scattering scheme" which takes account of the momentum lost by the particle as it approaches the point of arrest.

To arrive at a particular "scattering scheme" they make use of the results of Voyvodic and Pickup, given earlier, which have been calculated from the numerical constants for G-5 emulsions. These results may be written in the form

$$\bar{\alpha} = \frac{\bar{D}}{t} = 0.96\,(2/3)^{\frac{1}{2}}\,\frac{1.006t^{\frac{1}{2}}}{pv}\left(\frac{\pi}{180}\right)$$
$$\times\left[1.45 + 0.8\left\{\log_e \frac{0.94t}{2\;\;0.3}\right\}^{\frac{1}{2}}\right] \text{ radians*.} \qquad (5\text{-}23)$$

(Here the factor 0.96 represents the effect of smoothing out scattering if the position of the track is measured by observing the position of a small number of grains rather than that of a single grain.) Since

---

*Although the numerical factor 1.006 in equation (5-23) has been derived for the case that no correction is made for cut-off when calculating $\bar{D}$, Biswas et al. (19) have used the customary cut-off procedure in determining $\bar{D}$. They find that when they employ the method (to be described) in calibration measures on a large number of tracks that better agreement with the known masses of the particles would be obtained if a value of 1.020 had been used instead of 1.006. This suggests that the mass determinations obtained from the constant sagitta method may be subject to a systematic error of 3 percent if $\bar{D}$ is determined by use of a cut-off procedure.

$$pv = \frac{M}{m_e}(m_e c^2)\beta^2 (1-\beta^2)^{-\frac{1}{2}} = 0.511 \frac{M}{m_e}\beta^2 (1-\beta^2)^{\frac{1}{2}}$$

where M is the rest mass of the particle in units of electronic mass, m_e is the rest mass of the electron, and $\beta = v/c$, one has, upon solving equation (5-23) for the product $\frac{M}{m_e}\overline{D}$, that

$$\frac{M}{m_e}\overline{D} = \frac{(2.69 \times 10^{-2})\, t^{3/2} (1-\beta^2)^{\frac{1}{2}}}{\beta^2} \times \left[1.45 + 0.8 \left\{ \log_e \frac{0.94t}{\beta^2 + 0.3} \right\}^{\frac{1}{2}} \right]. \qquad (5\text{-}24)$$

One can now, for selected values of β, use equation (5-24) to plot a family of curves of $\frac{M}{m_e}\overline{D}$ vs t as shown in Figure 30. For any choice of M and $\overline{D}$, say, M_p and Δ, a sequence of pairs of values, (β_i, t_i), may be taken from the individual curves. Such pairs, in turn, can be used to construct a graph of t vs residual range, R, since, for an assumed mass M_p, β is expressible in terms of R through the range-energy relation for the emulsions. A set of points can then be taken from this t vs R graph which, when used as the end points of successive cell intervals, will give an average absolute value of second difference, $\overline{D}$, which is constant along the track and equal to the chosen value Δ.

For given values of M and Δ such a set of cell lengths is called a "scattering scheme" and is designated as an "M_Δ scheme". Graphs of t vs R, prepared in this laboratory, for a proton and a tau meson, taking $\Delta = 0.5$ microns are shown in Figure 31. To construct a given scheme from the t vs R graph

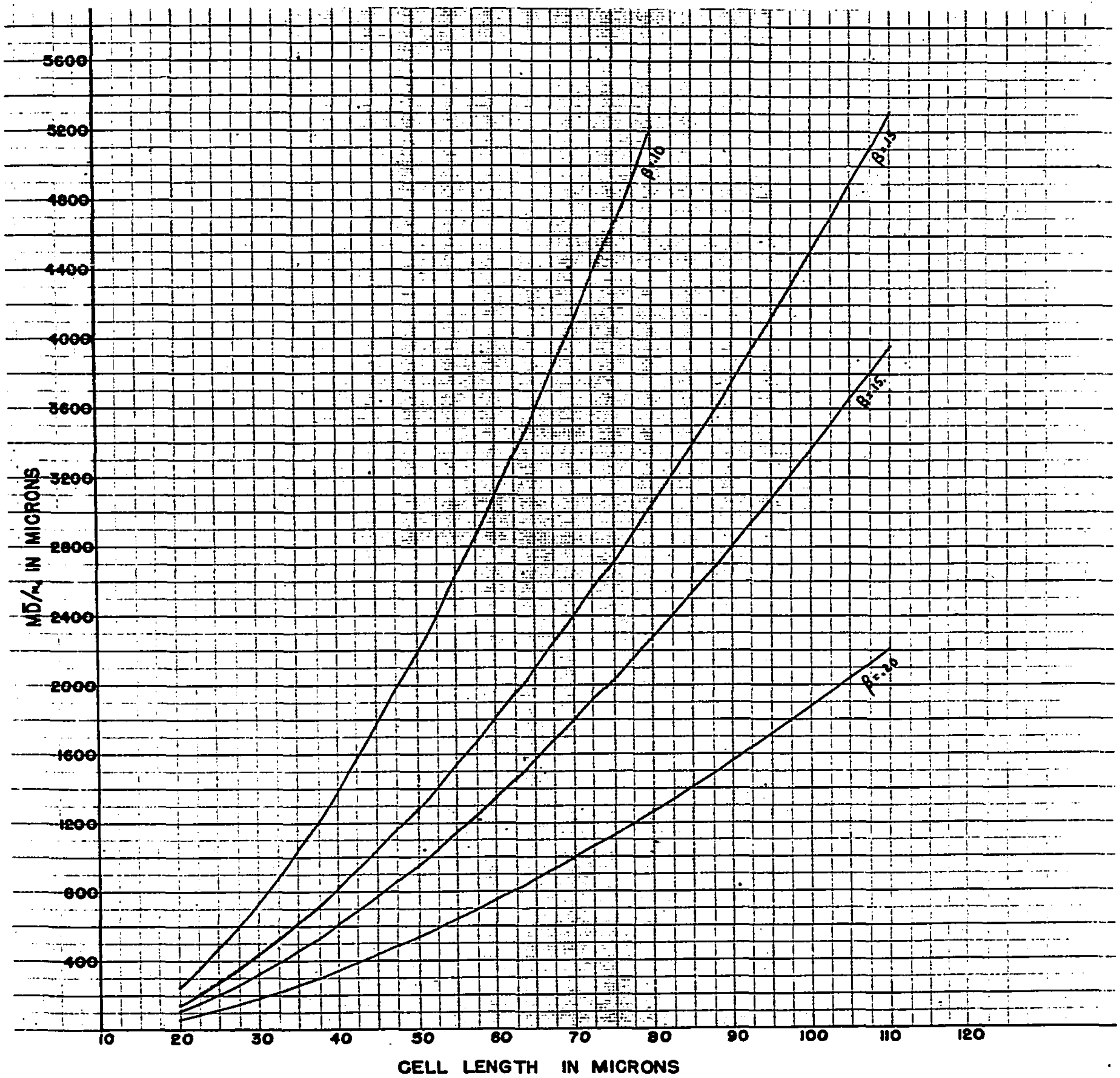

Fig. 30. Curves of MD/m_e vs cell length for various values of $\beta = v/c$.

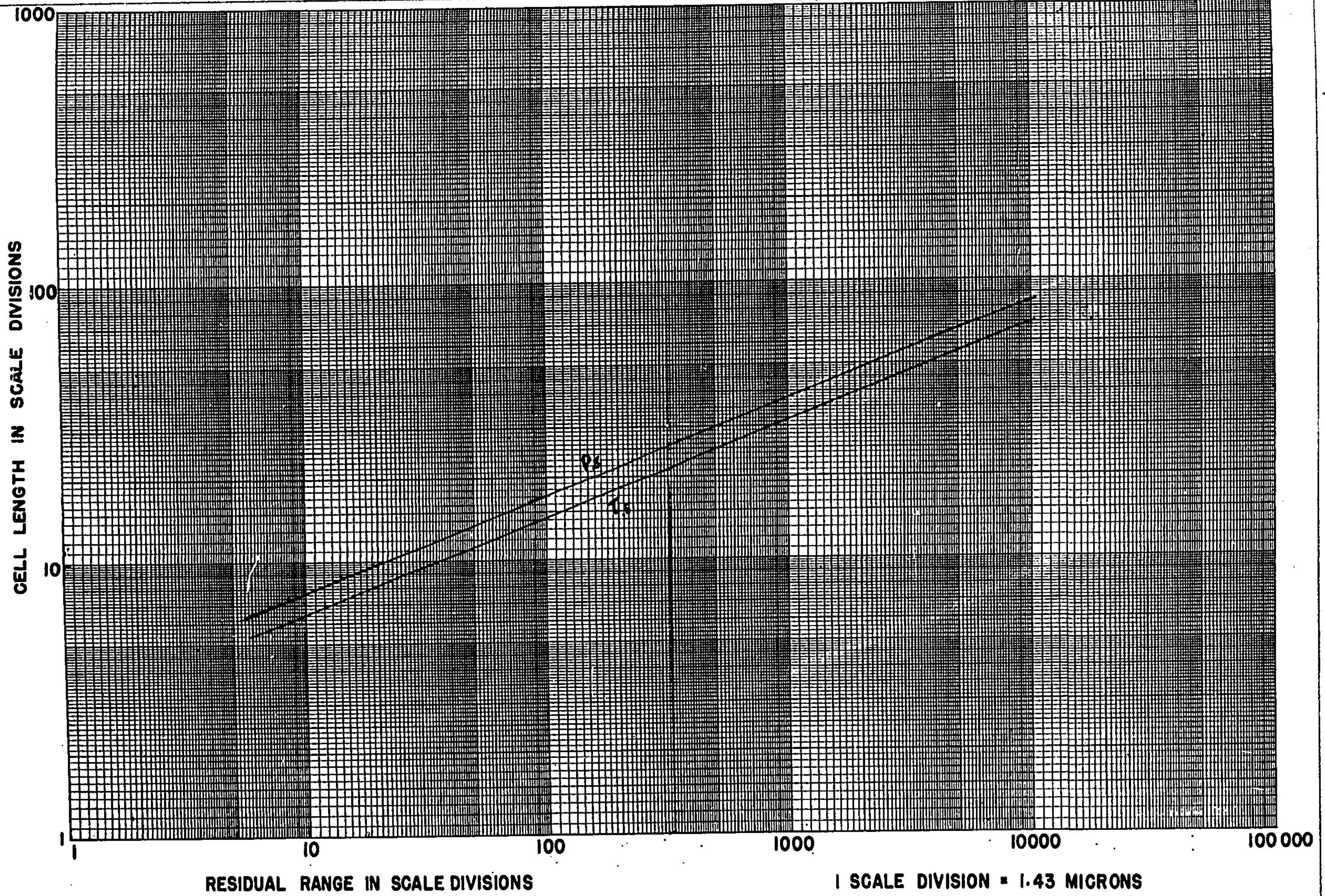

Fig. 31. "Scattering schemes" for a proton and a tau meson in G-5 emulsions, corresponding to a mean absolute value of second difference $\Delta = 0.5$ microns.

one simply starts at a small but arbitrary residual range, R_o, and finds the corresponding value, t_o. Then t_1 will correspond to the residual range $R_o + t_o$, t_2 to the residual range $R_o + t_o + t_1$, etc. If, now, one takes scattering observations on a flat track* produced by a proton, say, coming to rest in the emulsion and uses the $P_{0.5}$ "scattering scheme" he should expect to obtain a mean absolute value of second difference $\bar{D}$ equal to 0.5 microns.

Consider, now, the application which one may make to the track of an unknown particle, M. For a particle of rest mass, M, moving at a non-relativistic speed the kinetic energy, T, is approximately equal to $\frac{pv}{2}$. From the range-energy relation for the emulsions

$$M = \frac{R^{1-\nu}}{h^{1-\nu} T^{\frac{\nu}{1-\nu}}} = \frac{R^{1-\nu} \; 2^{\frac{\nu}{1-\nu}}}{h^{1-\nu} (pv)^{\frac{\nu}{1-\nu}}} . \tag{5-25}$$

Substitution in (5-25) of the expression for pv obtained from (5-23) yields

$$M = \left(\frac{R}{h}\right)^{1-\nu} \left\{ \left(\frac{0.96}{2}\right) \left(\frac{2}{3}\right)^{\frac{1}{2}} \left(\frac{1.006}{57.3}\right) \frac{t^{3/2}}{\bar{D}} \times \left[1.45 + 0.80 \left\{ \log_e \frac{0.94t}{\beta^2 + 0.3} \right\}^{\frac{1}{2}} \right] \right\}^{\frac{\nu}{\nu-1}} . \tag{5-26}$$

---

*If the track dips one can not measure t_i directly. If one uses projected cell lengths, t_i, taken from Figure 31 on a trajectory dipping at an angle, θ, with the plane of the emulsion the mean absolute value of second difference, $\bar{D}(\theta, R)$, so obtained, will be larger than the value Δ which

Assume, now, that one has made scattering observations on the track produced by M, employing an "m_Δ scheme". Neglecting the slight dependence of M on the β^2 which appears in the argument of the logarithmic term, (i.e., taking $\beta_M^2 \cong \beta_m^2$ at the same value of R), one can form the ratio M/m to obtain

$$\frac{M}{m} = \left(\frac{\Delta}{\Delta_M}\right)^{\frac{\nu}{\nu-1}} = \left(\frac{\Delta}{\bar{D}(\theta)}\right)^{\frac{\nu}{\nu-1}} \left(\sec\theta\right)^{\frac{0.975\nu}{\nu-1}} \qquad (5\text{-}27)$$

where θ is the angle which the trajectory of M makes with the emulsion plane. For the emulsions used in the present work $\nu = 1.761$, whence

$$M = m\left(\frac{\Delta}{\bar{D}(\theta)}\right)^{2.314} \left(\sec\theta\right)^{2.256}. \qquad (5\text{-}28)$$

Here, following Biswas et al.(19), $\bar{D}(\theta)$ is to be interpreted as the mean absolute value of the second difference obtained from measurements on the projected track after corrections have been made for distortion, noise and large angle cut-off.

In using the constant sagitta method, it is desirable to choose, if possible, a "scattering scheme" in which the given mass is nearly equal to the mass of the unknown particle. However, Biswas et al. (19) find that when the ratio M/m is as great as 1/6 corresponding to the measurement of a π-meson

---

one would get if the proper cell length $t_1 \cos\theta$ were used. By determining Δ and $\bar{D}(\theta,R)$ for tracks of identifiable particles dipping at various angles θ with the emulsion plane, Biswas et al. (19) find empirically that the ration $\bar{D}(\theta,R)/\Delta$ is very nearly independent of R and that in the range $0 < \theta < 60°$ the ratio satisfies the empirical formula $\bar{D}(\theta) = \Delta (\sec\theta)^{0.975}$.

with a proton scheme, and the range-energy curve is approximated by a single power law, the variation in $\overline{D}$ is only of the order of 10 percent.

Probable Deviation of the Mass and Energy Estimates from Scattering

As discussed earlier, an estimation of rest mass, M, for a non-relativistic particle which does not come to the end of its range in the emulsion, most commonly involves the independent measurement of two track parameters (i.e., multiple Coulomb scattering and ionization density). The scattering observations lead to a mean absolute value of second difference, $\overline{D}$, say Δ, and the ionization observations yield a value of $T_{M/M}$, say X. Since each of the two parameters, Δ and X, are obtained experimentally, there will be probable deviations, R_Δ and R_X respectively, associated with their measurement.

An estimate of R_X may be made by noting the dispersion of values $T_{M/M}$ obtained from the individual ionization density curves (see Chapter IV). If use is made of equation (5-8) an estimate of R_Δ may be secured from the expression

$$R_\Delta = \left[\left(\frac{\partial \Delta}{\partial \overline{D}_{obs}}\right)^2 (R_{\overline{D}_{obs}})^2 + \left(\frac{\partial \Delta}{\partial \overline{D}_n}\right)^2 (R_{\overline{D}_n})^2 \right]^{\frac{1}{2}} \tag{5-29}$$

where for n_o independent readings of second difference*

---

*If n successive readings of second difference, D_i, are determined for cells of length t along a track the indi-

$R_{\overline{D}_{obs}} = \frac{0.67}{\sqrt{n_o}} \overline{D}_{obs}$ and $R_{\overline{D}_n} = \frac{0.67}{\sqrt{n_o}} \overline{D}_n$. If the operations indicated in (5-29) are carried out one has

$$R_\Delta = \frac{0.67}{\sqrt{n_o}\,\Delta}\left[(\overline{D}_{obs})^4 + (\overline{D}_n)^4\right]^{\frac{1}{2}\,*}. \tag{5-30}$$

Making use of the facts that $pv \cong 2T$ and that $\bar{\alpha} \cong \frac{180}{\pi}\left(\frac{\overline{D}}{t}\right)$ radians one may reformulate equation (5-18) to obtain an estimate of M from the relation

$$M = \frac{\pi K_{co}\, t^{3/2}}{(1800)(2)(T_{M/M})\overline{D}} = \frac{C}{X\Delta} \tag{5-31}$$

where $C = \frac{\pi K_{co}\, t^{3/2}}{(1800)(2)}$ may be considered constant for the purpose of the calculation. Then the probable deviation, R_M, associated with the quoted value M, is given by

$$\begin{aligned} R_M &= \left[\left(\frac{\partial M}{\partial \Delta}\right)^2 (R_\Delta)^2 + \left(\frac{M}{X}\right)^2 (R_X)^2\right]^{\frac{1}{2}} \\ &= M\left[\left(\frac{R_\Delta}{\Delta}\right)^2 + \left(\frac{R_X}{X}\right)^2\right]^{\frac{1}{2}}. \end{aligned} \tag{5-32}$$

Since an estimate of energy, T_M, may be obtained directly from the scattering measurements, R_X does not enter

---

vidual values are not completely independent. It has been shown, however, by O'Ceallaigh et al. (45) that without overlap $n_o/n = 0.89$, and that as the coefficient of overlap, λ, is increased the ratio n_o/n approaches unity. Thus, if an overlap procedure is used to determine D, it is a sufficient approximation to take $n_o \cong n$.

*Biswas et al. (19) have noted that the quantity R_Δ/Δ has a flat minimum of $\overline{D}_{obs} = 2.60\ \overline{D}_n$. In the present work, the minimum value of cell length, t, which yields a value of $\overline{D}_{obs}$ satisfying this signal/noise criterion has been adopted.

the considerations and one may obtain the probable deviation, R_{T_M}, in the energy of the particle, by re-writing equation (5-18) in the form

$$T_M = \frac{\pi K_{co} t^{3/2}}{(1800)(2)} \times \frac{1}{\bar{D}} = \frac{C}{\bar{D}} = \frac{C}{\Delta} \tag{5-33}$$

and, thus,

$$R_{T_M} = \left(\frac{\partial T_M}{\partial \Delta}\right)^2 (R_\Delta)^2 = \frac{C}{\Delta^2} R_\Delta = \frac{R_\Delta}{\Delta} (T_M). \tag{5-34}$$

When a particle comes to rest in the emulsion its mass is usually determined by the constant sagitta method. The probably deviation, R_M, in the quoted mass may be obtained by making use of equation (5-27). In the usual way one has

$$R_M = \frac{\nu}{(\nu-1)} \left(\frac{R_{\Delta_M}}{\Delta_M}\right)^M. \tag{5-35}$$

If a value of ν equal to 1.761 is assumed and equation (5-30) is evaluated, for the condition $\bar{D}_{obs} = 2.60\ \bar{D}_n$, one has

$$R_M = \frac{(2.31)(0.79)}{\sqrt{n_o}} M = \frac{1.82M}{\sqrt{n_o}}. \tag{5-36}$$

CHAPTER VI

DECAY OF A HEAVY NEUTRAL PARTICLE

Introduction

In the course of scanning the emulsions the V-event shown in Figure 32 was observed in plate No. (8-53-1U). The vertex, (M), of the V appears at a distance of 949 microns from the center of an energetic star with 19 visible prongs.* One branch of the V, hereinafter referred to as track A, appears as the path of a charged particle which, after leaving the vertex of the V, traverses the emulsion for 847 microns to a point, designated C, at which it undergoes either a nuclear interaction of some type or a decay in flight. The gap density and the straightness of track A at C show that the track cannot be due to a particle which comes to rest at C. There is no evidence of a blob or prong at C produced by a nuclear recoil. A track, designated track A', making an angle of 21°** with the forward direction of track A, contin-

*The turntable coordinates of the vertex and star center are (56.6, 100.2) and (57.2, 100.9) respectively.

**Various values of angles, momenta, energy, etc.,

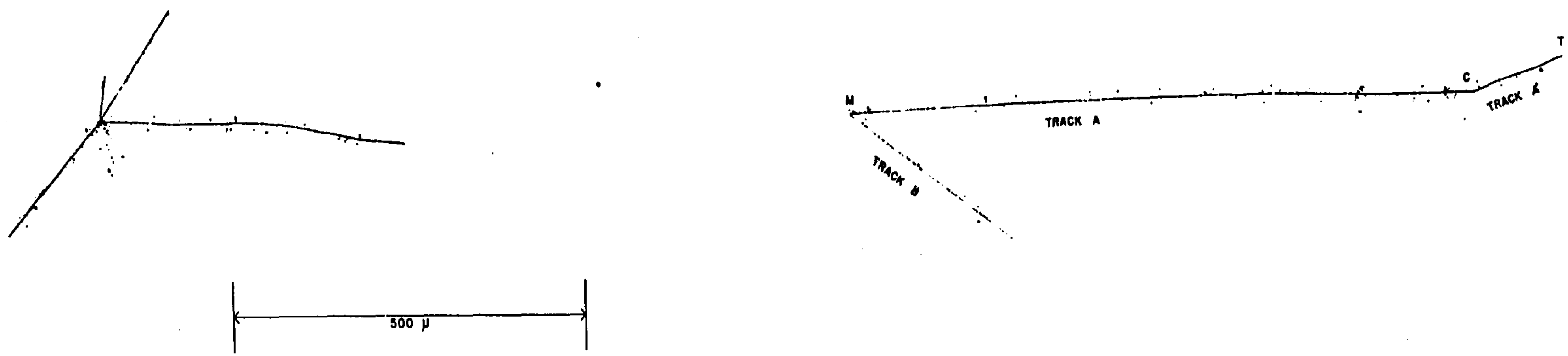

Fig. 32. Photomiciograph of a V-event observed in one of the emulsions used in the present work. The most plausible explanation of the twin track is that a heavy unstable particle emitted from the star (shown in lower half of the figure) suffered a two

ues on from this point, passing through 131 microns of emulsion before coming to rest at point T. A careful examination of the emulsion failed to reveal the track of a decay particle coming from T. The other branch of the V, hereinafter referred to as track B, makes an angle of 48° 31' ± 11' with track A. Track B enters the glass backing plate after going a distance of 416 microns in the emulsion. Tracks A and B make angles of 5° 5' ± 5' and 43° 26' ± 6' respectively with the projection onto the plane of the V-event of the star center-M-axis. The vertex of the V is particularly "clean" with no visible evidence of nuclear recoil or other associated event.

The fact that no visible recoil was observed in connection with the pair of diverging tracks which apparently have a common origin in the emulsion, suggests that a neutral particle has undergone spontaneous decay. The occurrence of the V tracks in the vicinity of a high energy star leads one to inquire whether there may be some connection between the two events. The idea that the two events are connected is reinforced by the fact that the plane of the V tracks only 3° 52' ± 5' of being coplanar with the star center.

---

are quoted in the present chapter. The procedures used to calculate these quantities and/or their associated probable deviations when not described in the text of this chapter are treated in Appendix A. The probable deviation of the angle between the forward direction of track A and the direction of track A' has not been calculated since this information is not of importance in the subsequent development.

Mass of Particle A

Since the ionization produced by the particle causing track A is too great to permit meaningful measurements of grain density, attempts to estimate the mass of the particle have been confined essentially to scattering and gap counting measurements. The uncertainty in the residual range made it impossible to apply the constant sagitta method (19). Gap dessity measurements were made, however, which, when taken together with scattering observations obtained by the coordinate technique, could be used to obtain an estimate of the rest mass of the particle.

Three sets of gap count measurements were made on track A from point C to the vertex M. Since the track was not perfectly flat and because previous measurements had indicated the presence of distortion, the observed data were corrected for the distortion effect.* The results are set forth in Table 5. The three sets of corrected data were plotted on logarithmic paper, (see Figure 33), and a visual

*The track exhibits little curvature and the reference axis, x', used for scattering measurements on A (to be discussed) is essentially parallel to the apparent projected track direction in the range interval from M to C. The distortion vector determined as outlined in Chapter III was found to make an angle $\phi = 38^{\circ}\ 39'$ with the x'-axis. This value of ϕ was taken to be the angle made by the distortion vector with the projection of the apparent track direction in correcting the gap lengths for distortion. Actually, the angle, θ, of dip between the trajectory of A and the plane of the emulsion is small ($8^{\circ}\ 15'$) so that only slight corrections for distortion were involved. The procedure which was used has been described in Chapter IV (J, 30-31d, 54-55).

Table 5

Gap Length Data on Track A

Gap Count 1		Gap Count 2		Gap Count 3	
$(R-R_k)_1$	$(G-G_k)_1$	$(R-R_k)_2$	$(G-G_k)_2$	$(R-R_k)_3$	$(G-G_k)_3$
(72.57) 73.44	(2.01) 2.03	(72.57) 73.44	(2.19) 2.22	(72.36) 73.41	(2.00) 2.03
(144.86) 146.74	(3.28) 3.33	(144.86) 146.74	(3.47) 3.51	(144.72) 146.93	(3.46) 3.51
(217.15) 220.14	(6.76) 6.83	(217.15) 220.14	(7.28) 7.38	(217.01) 220.29	(7.08) 7.19
(289.72) 293.89	(13.11) 13.30	(289.72) 293.89	(14.01) 14.22	(289.80) 294.30	(13.47) 13.69
(362.58) 368.41	(18.06) 18.37	(362.58) 368.41	(19.32) 19.66	(362.59) 368.82	(18.77) 19.11
(435.15) 442.46	(21.88) 22.27	(435.15) 442.46	(23.33) 23.74	(434.95) 442.79	(22.40) 22.83
(507.72) 516.61	(28.26) 28.78	(507.72) 516.61	(30.24) 30.82	(507.09) 516.14	(28.18) 28.70
(580.01) 590.09	(36.94) 37.61	(580.01) 590.09	(39.11) 39.82	(579.23) 589.56	(36.31) 36.97
(652.30) 663.67	(44.73) 45.53	(652.30) 663.67	(46.35) 47.19	(651.09) 662.52	(42.96) 43.73
(724.59) 737.78	(48.90) 49.81	(724.59) 737.78	(50.71) 51.66	(723.23) 736.06	(47.84) 48.70
(796.45) 810.74	(56.28) 57.30	(796.45) 810.74	(57.73) 58.78	(795.09) 809.11	(55.04) 56.02
(832.45) 847.54	(58.44) 59.51	(832.45) 847.54	(59.89) 60.99	(830.91) 845.61	(56.83) 57.85

*$(R-R_k)$ and $(G-G_k)$ refer to the range and the cumulative gap length respectively, as measured from point C to point M, both expressed in microns. The uncorrected values of $(R-R_k)$ and $(G-G_k)$ are given in parentheses for comparison.

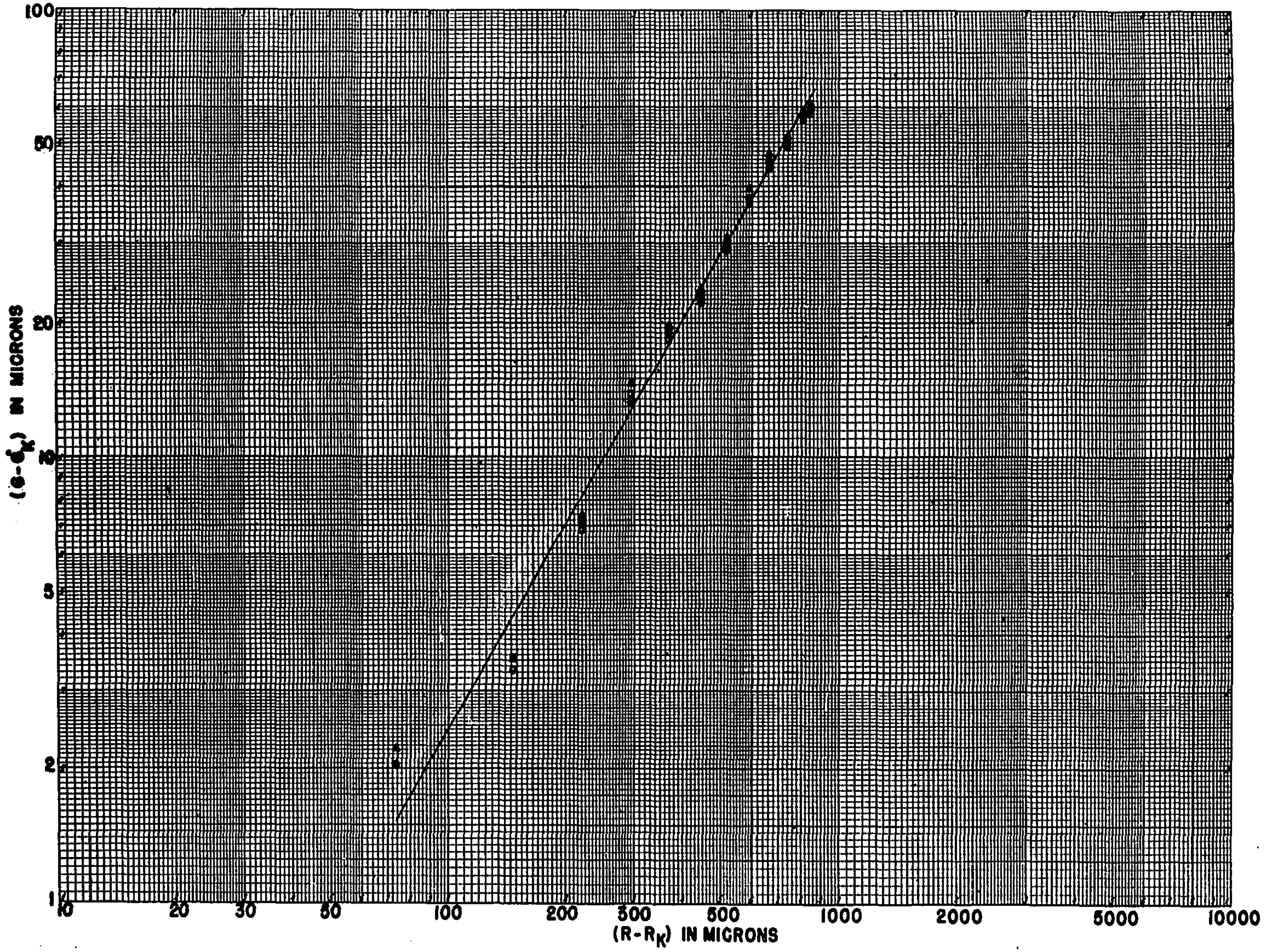

Fig. 33. Gap length data for track A of the V-event

best fit curve was drawn through the points. A value of gap density, $dG/dR = 0.079$, at the midpoint of track A, ($R = R_k + 423.5$ microns), was determined from this curve. Comparison with the mean gap length curve (Figure 19) shows that at a point on a proton track where the ionization density is equal to 0.079, the proton should, on the average, have a residual range of 400 microns. Using the range-energy relation one finds that the energy of a proton corresponding to a residual range of 400 microns is 8.42 Mev. Then, from equation (4-4) and the fact that $\bar{p}_A v \cong 2T_A$ one has $p_A v/M_A = 2T_p/m_p = (2)(8.42)$ Mev/1837 $m_e = 9.17 \times 10^{-3}$ Mev per electron mass unit.

To take the scattering observations the plate was rotated until track A was aligned approximately parallel to the x-axis of the microscope state. They y-coordinate of point M was recorded first. Then y-coordinate readings were taken at successive points along the track using a projected cell length, t_p', of 5 scale divisions on the eyepiece reticule.* Equation (5-15) was used to correct for the effect of the distortion displacements perpendicular to the reference axis, x'. A correction was calculated for each of the observed values of second difference which had been computed for a

---

*The 90 x oil immersion objective was used in combination with the 10 x eyepiece in making the measurements. For this optical arrangement 1 scale division on the eyepiece reticule corresponds to 1.43 microns.

projected cell length of 40 scale divisions* (H, 24-271). To do this the corrected height, z_0, of point M above the glass-emulsion surface was determined. The values of the z-coordinates and the differences in the z-coordinates which are required for the evaluation of (5-15) were then taken from the visual best fit curve obtained by plotting the cumulative depth differences, corrected for shrinkage, for successive points on track A from M to C as a function of the cumulative projected range. The results of these observations and calculations are given in Table 6.

After correction for distortion and cut-off the value of $\bar{D}_{obs}$ corresponding to an apparent projected cell length of 40 scale divisions was found to be 0.570 microns. A correction for the stretching effect on track A associated with the component of the distortion vector parallel to the reference axis x' results in a slight increase in the projected cell length. The total stretch of the projection of track A was only 15 microns. Since the distortion effect is so slight it is a sufficient approximation to assume that each

---

*Preliminary calculations based on the uncorrected data had indicated, that, after cut-off at $D_i \geqq 4\bar{D}_{obs}$, the optimum value of t_p, which would yield a mean absolute value of second difference $\bar{D}_{obs} \cong 2.6\ \bar{D}_n$, corresponded to a projected cell length of 40 scale divisions. For this choice of t_p, after cut-off, $\bar{D}_{obs}$ (uncorrected) is equal to 0.561 microns and $\bar{D}_n$ is equal to 0.215 microns (see Figure 25). It was clear that the introduction of a small correction for distortion would not alter significantly this result.

Table 6

Scattering Observations on Track A*

t'_p in scale div.	y-coordinate in $\frac{\text{scale div.}}{8}$	S_i** (uncorrected) in $\frac{\text{scale div.}}{8}$	D_i (uncorrected) in $\frac{\text{scale div.}}{8}$	D_i (uncorrected) in scale div.	$\Delta^2 S_{i4}$ ***in scale div.	D_i corrected in scale div.****
0	0	1	1	0.125	0.097140	0.222140
5	-1	0	2	0.250	0.097817	0.347817
10	-1	-1	0	0.000	0.083554	0.083554
15	-2	-3	-4	-0.500	0.084454	0.415546
20	-3	-2	1	0.125	0.067566	0.192566
25	-1	1	5	0.625	0.060438	0.685438
30	-2	-1	2	0.250	0.047085	0.297085
35	-1	0	4	0.500	0.051081	0.551081
40	-1	0	3	0.375	0.039527	0.414527
45	-1	-2	-1	-0.125	0.024281	-0.099719
50	0	-1	1	0.125	0.021022	0.146022
55	1	1	6	0.750	0.021830	0.771830
60	-1	-3	-1	-0.125	0.025778	-0.099222
65	-2	-4	-2	-0.250	0.026633	-0.223367
70	-1	-3	-1	-0.125	0.029152	-0.095848
75	-1	-4	-2	-0.250	0.021047	-0.228953
80	-1	-3	1	-0.125	0.022195	-0.102805
85	1	-1	4	0.500	0.011176	0.511176
90	1	-2	1	0.125	0.019725	0.144725
95	0	-5	-2	-0.250	0.010336	-0.239664
100	2	-2	3	0.375	0.006700	0.381700
105	2	-2	4	0.500	0.000375	0.500375
110	2	-2	4	0.500	0.000182	0.499818

Table 6 -- continued

t'_p in scale div.	y-coordinate in scale div./8	S_i** (uncorrected) in scale div./8	D_i (uncorrected) in scale div./8	D_i (uncorrected) in scale div.	$\Delta^2 S_{ii}$***in scale div.	D_i corrected in scale div.****
115	3	-2	4	0.500	0.002376	0.497624
120	2	-4	3	0.375	0.005924	0.380924
125	2	-5	1	0.125	0.006059	0.131059
130	3	-3	5	0.625	0.003967	0.628967
135	5	-3	3	0.375	0.013400	0.388400
140	4	-5	1	0.125	0.004576	0.129576
145	4	-6	-1	-0.125	0.008357	-0.116643
150	4	-6	-1	-0.125	0.003678	-0.121322
155	5	-6	-3	-0.375	0.005871	-0.369129
160	6	-7	-3	-0.375	0.005675	-0.369355
165	7	-6	-3	-0.375	0.012868	-0.362132
170	6	-8	-5	-0.625	0.010873	-0.614127
175	8	-6	-2	0.250	0.001947	-0.248053
180	9	-6	-4	-0.500	0.009842	-0.490158
185	10	-5	-3	-0.375	0.009157	-0.365843
190	10	-5	-2	-0.250	0.007537	-0.242463
195	11	-3	3	0.375	0.005438	0.380438
200	13	-4	0	0.000	0.003067	0.003067
205	13	-3	1	0.125	-0.002617	0.122383
210	14	-3	0	0.000	-0.008181	-0.008181
215	14	-4	-3	-0.375	-0.000594	-0.375594
220	15	-2	1	0.125	-0.006608	0.118392
225	15	-2	2	0.250	-0.013410	0.236590
230	15	-3	-1	-0.125	-0.007604	-0.132604
235	14	-6	-5	-0.625	-0.009297	-0.634297

Table 6 -- continued

t'_p in scale div.	y-coordinate in $\frac{\text{scale div.}}{8}$	S_i (uncorrected) in $\frac{\text{scale div.}}{8}$	D_i (uncorrected) in $\frac{\text{scale div.}}{8}$	D_i (uncorrected) in scale div.	$\Delta^2 S_{ii}$ in scale div.	D_i corrected in scale div.
240	17	-4	-4	-0.500	-0.015975	-0.515975
245	16	-4	-3	-0.375	-0.016351	-0.391351
250	17	-3	-2	-0.250	-0.009201	-0.259201
255	18	-1	0	-0.000	-0.008700	-0.008700
260	17	-3	-4	-0.500	-0.018522	-0.518522
265	17	-4	-4	-0.500	-0.011617	-0.511617
270	18	-2	-1	-0.125	-0.023198	-0.148198
275	20	-1	-1	-0.125	-0.019306	-0.144306
280	21	0	0	0.000	-0.018680	-0.018680
285	20	-1	-4	-0.500	-0.016798	-0.516798
290	20	-1	-3	-0.375	-0.024307	-0.399307
295	19	-1	-2	-0.250	-0.029506	-0.279506
300	20	1	2	0.250	-0.017958	0.232042
305	21	0	-1	-0.125	-0.025227	-0.150227
310	20	-1	-2	-0.250	-0.024090	-0.274090
315	21	0	2	0.250	-0.027345	0.222655
320	21	0	2	0.250	-0.025745	0.224255
325	21	3	9	1.125	-0.034852	1.090148
330	21	22	8	1.000	-0.028419	0.971581
335	20	1	9	1.125	-0.029659	1.095341
340	19	-1	6	0.750	-0.034538	0.715462
345	21	1	10	1.250	-0.026218	1.223782
350	21	1	11	1.375	-0.028337	1.346666
355	21	-2	5	0.625	-0.029560	0.595440
360	21	-2	8	1.000	-0.025766	0.974234
365	18	-6	4	0.500	-0.021344	0.478656

Table 6 -- continued

t'_p in scale div.	y- coordinate in $\frac{\text{scale div.}}{8}$	S_i (uncorrected) in $\frac{\text{scale div.}}{8}$	D_i (uncorrected) in $\frac{\text{scale div.}}{8}$	D_i (uncorrected) in scale div.	$\Delta^2 S_{ii}$ in scale div.	D_i corrected in scale div.
370	19	-6	3	0.0375	-0.030395	0.344605
375	19	-8	0	0.000	-0.045837	-0.045837
380	20	-7	2	0.250	-0.031264	0.218736
385	20	-9	- 1	-0.125	-0.045684	-0.170684
390	20	-10	- 2	-0.250	-0.039671	-0.289671
395	23	- 7	3	0.375	-0.042522	0.332478
400	23	-10	-22	-0.250	-0.046850	-0.296850
405	24	-10	- 2	-0.250	-0.049010	-0.299010
410	25	- 9	- 2	-0.250	-0.044681	-0.294681
415	27	- 8	- 2	-0.250	-0.036003	-0.286003
420	27	- 9	- 4	-0.500	-0.040789	-0.540789
425	29	- 8	- 6	-0.750	-0.028259	-0.778259
430	30	- 8	- 9	-1.125	-0.031536	-1.156536
435	30	-10	-14	-1.750	-0.025094	-1.775094
440	33	- 8	-14	-1.750	-0.031404	-1.781404
445	34	- 8	-17	-2.125	-0.022799	-2.147799
450	34	- 7	-17	-2.125	-0.021469	-2.146469
455	35	- 6	-17	-2.125	-0.035775	-2.160775
460	36	- 5	-17	-2.125	-0.030736	-2.155736
465	37	- 2	-13	-1.625	-0.037925	-1.662925
470	38	1	-10	-1.250	-0.038877	-1.288877
475	40	4	- 8	-1.000	-0.042333	-1.042333
480	41	6	- 7	-0.875	-0.031473	-0.906473
485	42	9	- 2	-0.250	-0.038352	-0.288352
490	41	10	1	0.125	-0.039243	0.085757

Table 6 -- continued

t'_p in scale div.	y-coordinate in $\frac{\text{scale div.}}{8}$	S_i (uncorrected) in $\frac{\text{scale div.}}{8}$	D_i (uncorrected) in $\frac{\text{scale div.}}{8}$	D_i (uncorrected) in scale div.	$\Delta^2 S_{ii}$ in scale div.	D_i corrected in scale div.
495	41	11	2	0.250	-0.065085	
500	41	12				
505	39	11				
510	37	11				
515	36	12				
520	35	13				
525	33	11				
530	31	9				
535	30	9				
540	29					
545	28					
550	26					
555	24					
560	22					
565	22					
570	21					
572	21					

After deleting $D_{i(obs)} \geqq 4\bar{D}_{obs}$ in an iterative process

$$\bar{D}_{obs} = \frac{\sum |D_{i(obs)}|}{n} = \frac{36.704}{92}\,(1.430) = 0.570 \text{ microns}$$

*A coefficient of overlap $\lambda = 8$ was used in forming $\bar{D}_{obs}$.

**Here S_i refers to the first difference for a projected cell length of 40 scale divisions; not to be confused with the symbol for the distortion vector.

***The computations were performed on an electric calculator and it was convenient to simply record the six figures furnished by the machine.

****<u>Ibid</u>.

of the 14 projected cells of length 40 scale divisions (57.20 microns) may be increased by the amount 15/14 = 1.07 microns. Thus, the corrected projected cell length which was used in determining the mass was taken to be 58.27 microns.*

The value of noise level, $\overline{D}_n$, corresponding to a projected cell length of 58.27 microns is found from Figure 25 to be 0.215 microns, hence the actual mean absolute value of second difference, $\overline{D}$, to be used in the calculation of the mass of A is $\overline{D} = \left\{(0.570)^2 - (0.215)^2\right\}^{\frac{1}{2}} = 0.528$ microns.

Since track A is produced by a slow particle, a value of $K_{co} = 25.0$, corresponding to an equivalent cell length, $t_1 = 4t = (4)(58.27) = 233.08$ microns, has been taken from Figure 28. The previous results may be combined to obtain an estimate of the rest mass of particle A. One has, by use of equation (5-31), that

$$M_A = \left(\frac{\pi}{1800}\right) \frac{K_{co}\, t^{3/2}}{(\overline{D})\, p_A v/M_A} = \frac{(3.416)(25.0)(445.375)}{(0.528)(1800)(9.17)(10^{-3})}\, m_e$$

$$= 4013\, m_e. \qquad (6\text{-}1)$$

To assign a probable deviation to M_A it was necessary first to determine the probable deviations in $\overline{D}$ and $p_A v/M_A$. $R_{\overline{D}}$ was obtained from equation (5-30).

$$R_{\overline{D}} = \frac{0.67}{\sqrt{12}\,(0.528)} \left\{(0.570)^4 + (0.215)^4\right\}^{\frac{1}{2}} = 0.120 \text{ microns.}$$

---

*Actually one should take into account the dip of the track in determining the proper cell length, but since here this effect is small it has not been considered in the calculation.

Here, the value of n_o was taken to be twelve. To determine the probable deviation, R_X, in $p_A v/M_A$ three estimates of the ratio $p_A v/M_A$ were obtained by use of the individual G vs R curves for the calibration protons. The greatest difference between the separate estimates and the estimate obtained from the mean G vs R proton curve was found to be 1.163×10^{-3} Mev per electron mass unit. This value was taken to be the probable deviation R_X. Thus the probable deviation, R_{M_A}, in the quoted mass, M_A, was calculated from equation (5-32) to be

$$R_{M_A} = M_A \left\{ \left(\frac{0.120}{0.528}\right)^2 + \left(\frac{1.163 \times 10^{-3}}{9.17 \times 10^{-3}}\right)^2 \right\}^{\frac{1}{2}} = 1050 \ m_e.$$

Total gap length measurements are not capable of differentiating sharply between protons, charged hyperons and deuterons having residual ranges less than several thousand microns. It is possible, however, to use gap counting data to check for consistency with the mass estimate secured from gap density-scattering measurements. The following procedure was employed.

If it be assumed that the particle associated with track A suffered a collision with negligible loss of energy at point C, continued through the emulsion and finally came to rest at point T, then one may plot the averaged cumulative gap length G vs the residual range R, for the particle, taking R = 0 at point T. Comparison with the calibration curves for the proton and deuteron, Figure 34, shows that the data points, so plotted, lie on the high mass side of the deuteron curve

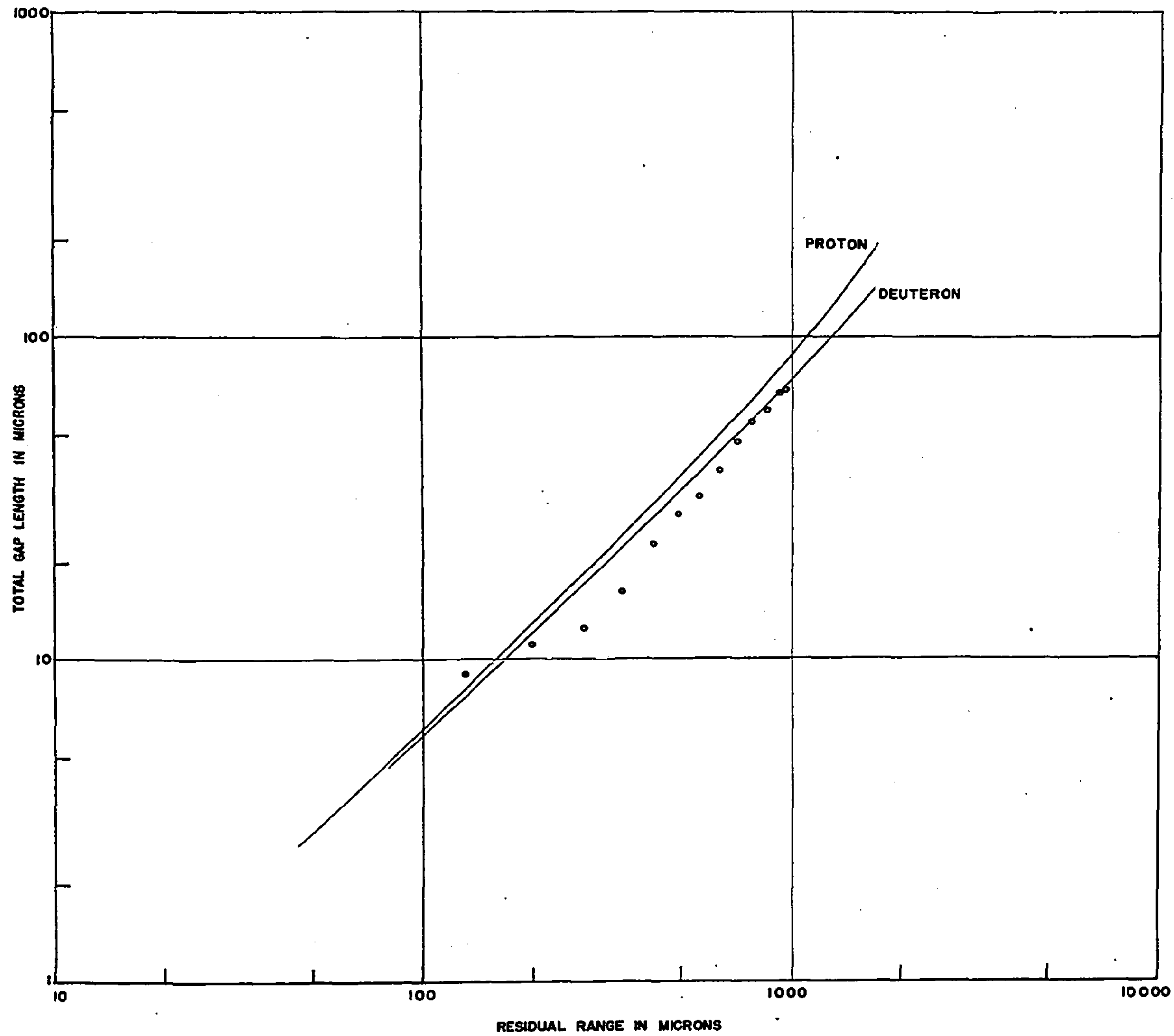

Fig. 34. Total gap length vs residual range. The circled points represent the observed gap length data for track A. These have been plotted under the unlikely assumption that the particle suffered a deflection, without loss of energy, at C and finally came to rest in the emulsion at point T. This procedure which should result in an underestimation of the mass of particle A has been used to check for consistency with the estimate of rest mass (4013 m_e) obtained for the same particle from gap density--scattering measurements.

(i.e., smaller cumulative gap lengths than that for the corresponding residual range values on the mean deuteron curve). The value of G at R = 131 microns was obtained from gap length measurements on track A'. Since the assumed scheme takes no account of possible energy loss at point C by the unknown particle, the actual measured gap length may be somewhat greater than it would have been if no interaction had taken place. Similarly, other possible explanations of the event at C, which are discussed later, tend to yield gap count curves which will cause the mass of the particle responsible for track A to be underestimated. The cumulative gap data thus confirm the scattering-gap density estimate which indicates a particle having a mass equal to or somewhat greater than that of a deuteron.

One may check for compatibility of the observed range of the particle of track A with the residual ranges which are predicted by the gap length calibration curves. As stated earlier, comparison with the proton curve shows that the gap density as determined for the unknown particle at the midpoint of track A corresponds to a residual range for a proton (at the midpoint) of 400 microns which is less than the measured value of range from the midpoint of track A to point C. This evidence would rule against the possibility that the unknown particle is a proton. A deuteron, however, with an energy corresponding to the gap-density at the midpoint of track A should have a residual range of 800 microns which is greater than the total track length of 554 microns from the midpoint of track A to T. This is acceptable if one does not require the unknown particle to undergo scattering without loss of energy at C.

The residual ranges corresponding to the gap density at the midpoint of track A, for particles more massive than a proton will, by equation (4-4), be greater than the 400 micron residual range by the ratio of the assumed mass to the mass of the proton. These residual ranges plus the distance (423.5 microns) from the midpoint of track A to M give the residual ranges at M for the various assumed masses. The energies at M were then calculated from equation (4-3b). Scattering measurements yielded an independent value of the energy at the midpoint at the track. Corresponding energies at M were then calculated for various assumed masses by using the range-energy relation. The weighted means of the energies obtained in this way have been used in the calculations. The results are set forth in Table 7.

Mass of Particle A'

Track A' is too short to yield a meaningful mass estimate from gap length measurements. From the general appearance of the track, however, the area density seems greater than is to be expected for a light meson coming to the end of its range in the emulsion. As there is no evidence of decay or nuclear absorption at T it is probable that the track

Table 7

Energy and Momentum Data on Track A

Assumed Particle		Energy in Mev	Momentum in Mev/c
deuteron	(3672 m_e)	21.9 ± 1.8	287.3 ± 12.1
Y^+	(4013 m_e)*	23.0 ± 1.9	308.1 ± 12.7

*Mass from scattering - gap density = 4013 ± 1050 m_e.

was made by a particle more massive than a pion and most likely by a stable particle such as a proton or deuteron. Scattering observations using the constant sagitta method were made on the particle to obtain a rest mass value of $985 \pm 680\ m_e$ (Table 8)*. In view of the low mass estimate from these scattering measurements the identification of the responsible particle as a proton is favored. The energies shown in Table 9 have been determined from the range-energy relation by assuming various masses for the unknown particle.

Mass of Particle B

Although the statistical weight which one may assign to measurements made on track B is seriously limited by the short range of the particle in the emulsion, attempts to gain information about its nature have been made by means of grain counting and scattering observations.

The grains along the track were counted three times. The data so obtained are shown in Table 10.** Each set of corrected grain count data was plotted on a separate sheet

---

*A $\tau_{0.5}$ scattering scheme with a coefficient of overlap $\lambda = 3$ was used in making the measurements. This scheme was found to give the largest number of cells consistent with the criterion $\bar{D}_{obs} \cong 2.6\ \bar{D}_n$. Here $\bar{D}_n$ was assumed to be constant and equal to 0.20 microns. Due to the large statistical uncertainty associated with the measurements no attempt was made to correct the observed data for the slight effect of distortion.

**The distortion vector was observed to be parallel to the reference axis used for scattering and hence essentially

Table 8

Scattering Observations on Track A'

Projected residual* range in scale div.	Projected cell length in scale div.	y-coordinate in $\frac{\text{scale div.}}{8}$	S_i in $\frac{\text{scale div.}}{8}$	D_i in $\frac{\text{scale div.}}{8}$
7	6	0	12	6
9	6	- 4	10	5
11	7	- 6	9	4
13	7	-12	6	5
15	7	-14	5	6
18	8	-15	5	8
20	8	-18	1	4
22	8	-19	-1	2
26	9	-20	-3	-1
28	9	-19	-3	-1
30	9	-18	-3	-2
35	10	-17	-2	0
37	10	-16	-2	-2
39	10	-15	-1	0
45	11	-15	-2	-2
47	11	-14	0	0
49	11	-14	-1	-3
56	12	-13	0	-4
60	12	-13	2	-2
68	12	-13	4	

*Having selected a $\tau_{0.5}$ scattering scheme starting at a value of residual range, R = 7 scale divisions, it was possible to choose two more $\tau_{0.5}$ scattering schemes starting at values of residual range R = 9 and R = 11 scale divisions in such a way as to effect an overlap. Thus, in forming the first difference S_i,

Table 8 -- continued

Projected residual* range in scale div.	Projected cell length in scale div.	y-coordinate in scale div./8	S_i in scale div./8	D_i in scale div./8
70	13	-14	4	
72	13	-15	4	
80	13	-17		
83		-18		
85		-19		

$$\bar{D}_{obs} = \frac{\Sigma |D_i|}{n} = \frac{(61)(1.430)}{(20)(8)} = 0.545 \text{ microns}$$

$$\bar{D} = \left\{(0.545)^2 - (0.200)^2\right\}^{\frac{1}{2}} = 0.507 \text{ microns}$$

$$M'_A = m_l \left(\frac{\Delta_l}{\Delta_A}\right)^{2.314} (\sec\theta\,^{**})^{2.256} = (975)\left(\frac{0.500}{0.507}\right)^{2.314} (1.0194)^{2.256} = 985 m_e$$

$$R_{M'_A} = \frac{1.82}{\sqrt{7}}(985) = \pm 680 m_e$$

one must use values of the y-coordinates corresponding to a given scattering scheme (i.e. $S_1 = y_1 - y_4 = 0 - (-12) = +12$). A similar procedure must be used in forming the second difference, D_i.

**The angle $\theta = 11.2^{\circ}$ was determined from the visual best fit curve obtained by plotting the cumulative depth differences (corrected for shrinkage) between points along track A' as a function of the cumulative projected residual range.

Table 9

Energy Data on Track A'

Assumed Particle	Energy in Mev
proton (1837 m_e)	4.4
deuteron (3672 m_e)	6.0

Table 10

Grain Count Data for Track B

Grain Count 1			Grain Count 2			Grain Count 3		
$(R-R_k)'$	$(R-R_k)$	$(N-N_k)$	$(R-R_k)'$	$(R-R_k)$	$(N-N_k)$	$(R-R_k)'$	$(R-R_k)$	$(N-N_k)$
(31.98)	27.97	42	(32.28)	27.99	43	(32.28)	28.03	38
(62.90)	54.92	78	(63.20	54.87	82	(63.79)	55.04	71
(93.19)	81.83	115	(94.12)	81.90	119	(95.30)	82.24	98
(124.11)	108.97	152	(124.61)	108.89	159	(126.30)	109.40	138
(154.40)	136.11	193	(154.81)	135.92	201	(157.30)	136.73	172
(185.03)	163.41	224	(185.73)	163.26	231	(188.30)	164.06	212
(215.95)	190.92	255	(217.10)	190.94	259	(219.81)	191.75	247
(246.58)	218.42	308	(247.59)	218.36	313	(251.32)	219.64	301
(277.21)	246.05	345	(278.96)	246.24	347	(282.32)	247.39	333
(307.84)	273.83	381	(309.88)	274.09	383	(313.32)	275.30	363
(338.13)	301.54	409	(340.37	301.91	414	(343.92)	303.30	409
(370.11)	330.84	465	(373.07	331.43	463	(374.52)	331.30	451
(401.03)	359.05	505	(403.99)	359.63	503	(405.12)	359.42	484
(431.66)	387.28	540	(435.36)	388.14	535	(437.00)	388.39	521
(462.58)	415.54	581	(467.22)	417.17	575	(468.88)	417.46	564

*$(R-R_k)$ and $(N-N_k$ refer to the range and cumulative grain counts respectively, as measured from the entry point into glass backing plate to point M. $(R-R_k)'$ refers to the uncorrected values of cell length used in making the grain counts. These values are included in the table for purpose of comparison. Both $(R-R_k)'$ and $(R-R_k)$ are expressed in microns.

of logarithmic paper and a visual best fit curve passed through the experimental points. These values of $(N-N_K)$, corresponding to a selected value of $(R-R_K)$, were taken from these curves and an average value $\overline{(N - N_K)}$ was calculated. This procedure was repeated for successive choices of $(R-R_K)$ and a series of average values $\overline{(N-N_K)}$ was obtained which are presented in Table 11. A visual best fit curve drawn through the averaged data is shown in Figure 35.

Grain density values at two different points on the track were obtained from the slopes at these points as determined from Figure 35. The grain density 50 microns from the vertex was found to be 1.32 grains per micron while a value of 1.42 grains per micron was obtained at a point on the same track 316 microns distant. By comparison the range interval over which identifiable π-mesons suffer a change in grain density from 1.42 to 1.32 grains per micron is found from Figure 14 to be 205 microns. Thus, the mass m_B may be estimated for the unknown particle from the relation $m_B = m_\pi \frac{\Delta R_B}{\Delta R_\pi}$, where ΔR_B and ΔR_π are the respective range intervals over which the change in grain density occurs. This procedure yielded a value of $m_B = 420 \pm 196\ m_e$ for the rest mass of the

---

parallel to the apparent track direction in such a sense as to indicate that a stretching of the track had occurred under distortion. Thus the apparent cell lengths used in making the grain count were corrected for this effect following the procedure described in Chapter IV (B, 54-55b; c, 42-43b; J, 59-59b).

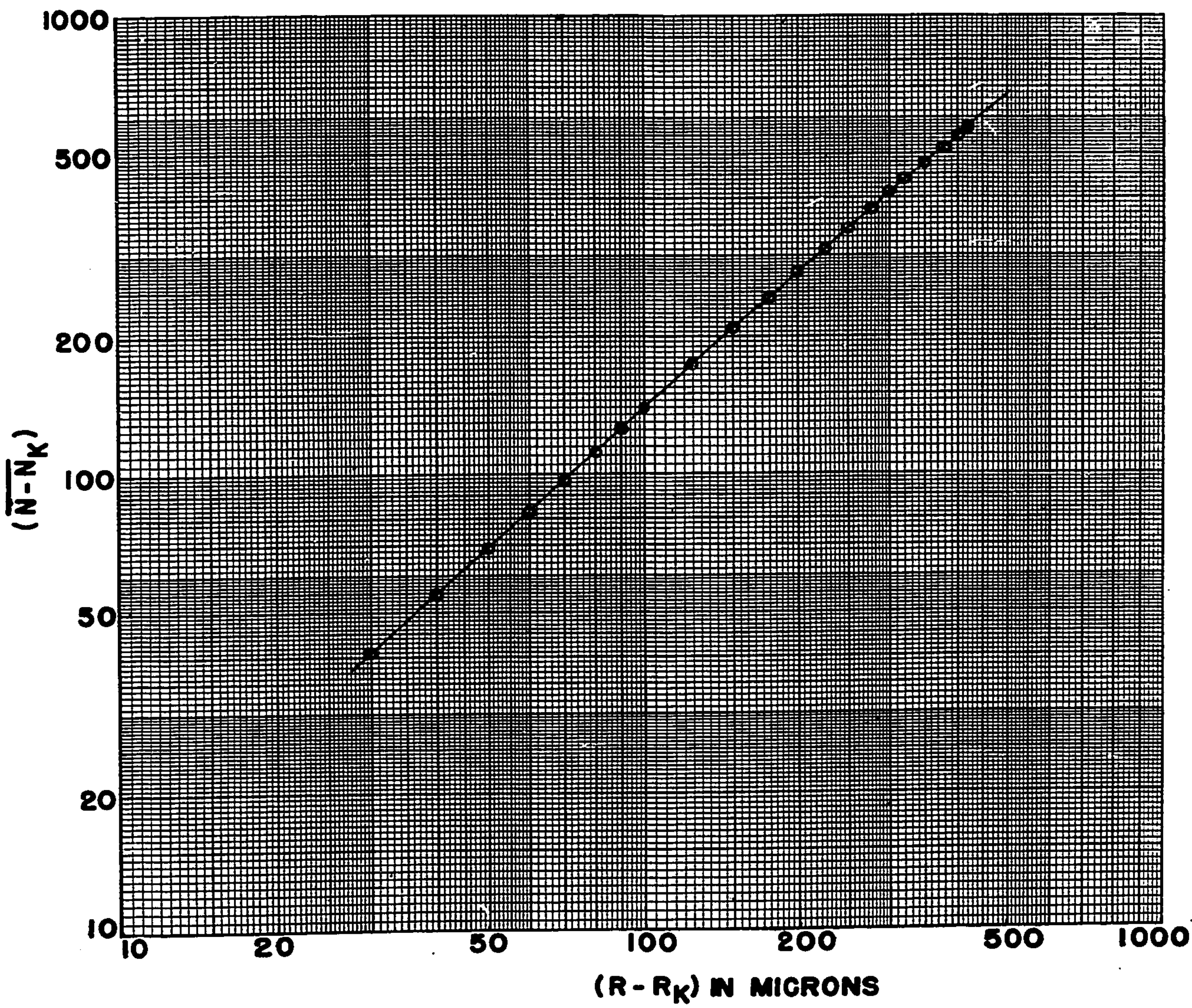

Fig. 35. Mean grain count vs range for track B of the V-event.

Table 11

Mean Grain Count Data for Track B

$(R - R_K)$	$(\overline{N - N_K})$
30	41
40	55
50	69
60	83
70	97
80	112
90	126
100	140
125	174
150	209
175	243
200	275
225	311
250	345
275	378
300	413
320	439
350	479
380	518
400	547
420	571

unknown particle, where the probable deviation was obtained from the individual π-meson grain density-residual range curves in a manner already described.

Again the coordinate technique was used to make scattering measurements and y-coordinate readings were taken at intervals of 5 scale divisions on the projection of the track. See Table 12. Since the distortion vector lies along the reference axis used in making the scattering measurements, the only correction for distortion which was required was to the projected cell length used in the evaluation of $\bar{D}_{obs}$. To make this correction, the cumulative depth differences (corrected for shrinkage) along track B from the point of entry into the glass backing plate to point M were plotted against the cumulative projected cell lengths, corrected for distortion. The experimental points used in this plot were taken from the data obtained from the grain counts which had been corrected for the stretching effect on the track introduced by the distortion. The resulting curve best fitted to these points was approximately a straight line with slope 0.472. In similar fashion one finds that the slope of trajectory before correction for distortion is 0.412. Thus the corrected projected cell length, t_p, is equal to 0.873 times the uncorrected length, $(t_p)_u$. The proper value of $(t_p)_u$ to satisfy the noise level criterion had been determined to be 55 scale divisions, hence $t_p = 48$ scale divisions $= 68.64$ microns. This value, in turn, must be corrected for dip,

Table 12

Scattering Observations on Track B

t' in scale div.	y-coordinate in $\frac{\text{scale div.}}{8}$	S_i (uncorrected) in $\frac{\text{scale div.}}{8}$	D_i (uncorrected) in $\frac{\text{scale div.}}{8}$
0	0	4	- 2
5	- 1	2	- 5
10	- 3	2	- 2
15	- 3	3	- 3
20	- 4	2	- 3
25	- 3	3	- 4
30	- 4	3	- 1
35	- 3	5	1
40	- 4	3	- 4
45	- 3	6	1
50	- 5	3	- 2
55	- 4	6	1
60	- 3	7	1
65	- 5	4	- 4
70	- 6	6	3
75	- 6	5	- 1
80	- 6	7	4
85	- 7	4	- 2
90	- 8	4	- 3
95	- 7	7	5
100	- 9	5	3
105	- 8	5	- 1
110	-10	5	3
115	-10	6	6
120	- 9	8	8
125	-12	3	3
130	-11	6	7
135	-13	3	4
140	-11	6	9
145	-12	7	10
150	-14	2	3
155	-14	2	2
160	-13	6	10
165	-15	2	5
170	-16	0	- 1
175	-17	0	2
180	-15	0	0

Table 12 -- Continued

t'_p in scale dvi.	y-coordinate in scale div. / 8	S_i (uncorrected) in scale div. / 8	D_i (uncorrected) in scale div. / 8
185	-17	-1	2
190	-16	-1	
195	-17	-3	
200	-19	-3	
205	-16	-1	
210	-16	0	
215	-19	-4	
220	-17	-3	
225	-16	1	
230	-17	-2	
235	-15	0	
240	-16	-3	
245	-15		
250	-14		
255	-16		
260	-15		
265	-16		
270	-15		
275	-14		
280	-17		
285	-15		
290	-15		
295	-13		

$$\bar{D}_{obs} = \frac{\sum |D_i|}{n} = \frac{131}{38} \; \frac{(1.430)}{(8)} = 0.616 \text{ microns}$$

$$\bar{D} = \left\{(0.616)^2 - (0.216)^2\right\}^{\frac{1}{2}} = 0.577 \text{ microns}$$

so that the cell length, t, used in the calculation of the mass, was t = 75.90 microns.

From Figure 35 the grain density at the midpoint of track B is found to be 1.37 grains per micron. Taking dN/dR =0.264 grains per micron as a reasonable value for plateau ionization* in the plates, one gets from Figure 28 and Figure 29 a value of K_{co} equal to 24.95. A value of $p_B/m_B = 0.068$ Mev per electron mass unit at the midpoint of the track was obtained from the appropriate calibration curves. The previous results, combined with the calculated value of $\bar{D} = 0.577$ microns, yielded an estimate of rest mass of 741 ± 283 m_e**. Despite the statistical fluctuations involved in estimating the mass from grain count and scattering observations on such a short track it is clear that the particle must be either a μ, π, τ or K meson.

Another piece of evidence which strengthens the meson interpretation is the following: if the particle were of protonic mass the energy corresponding to the observed grain density would be 66.5 Mev and it should have sufficient range to be found in the adjacent plate in the stack. A

---

*Previous measurements on the lightly ionized electron tracks from μ-meson decays had indicated a value of minimum ionization of 0.24 grains per micron. If one assumes that the minimum ionization is approximately 10 percent below the "plateau", the value of 0.264 grains per micron is obtained.

**The procedures used to determine both the value of p_Bv/m_B and the probable deviation in m_B have been described in connection with the discussion of track A.

careful search has been made of the appropriate region of the next emulsion but no trace of such a particle has been found.

Table 13 gives the energies corresponding to the assumption that track B was produced by a μ, π, ζ or K meson. The grain density of that part of the track nearest the V-vertex was first determined. A value of 1.28 grains per micron was obtained from Figure 35. Then the energy of a pion which would give this grain density was found by using, in the empirical range-energy relation, the value of range indicated by the grain density-residual range curve for identified pions (Figure 14). The energy corresponding to a particle of different mass was then calculated from equation (4-6).

Momentum Balance

If it be assumed that a neutral particle, Y^o, emanated from the star and underwent subsequent decay into two charged particles, calculations may be made, for various possible decay schemes, to determine the degree to which the transverse momenta fail to balance (or, alternatively, the angle between the vector $\vec{p} = \vec{p}_A + \vec{p}_B$ and the star-M-axis). Now, if one observes a V-event which is not perfectly coplanar with some chosen point, (e.g., a star center), there is a question as to the line with respect to which one should measure the transverse momenta. One method which suggests itself is to pass a plane, perpendicular to the plane of the V, through

Table 13

Energy and Momentum Data on Track B

Assumed Particle	Energy in Mev	Momentum in Mev/c
π(273 m_e)	9.9 ± 0.9	53.5 ± 2.4
μ(206.6 m_e)	7.5 ± 0.6	40.5 ± 1.8
K(968 m_e)	35.1 ± 3.0	189.5 ± 8.4
ζ(536 m_e)	19.4 ± 1.7	105.0 ± 4.6

the vertex of the twin tracks and the point in question and to utilize the intersection of this plane with the plane of the event to determine the line with respect to which the transverse momenta are taken. This procedure was adopted in computing the residual transverse momenta which are given, along with other pertinent information, in Table 14.

Interpretation and Discussion

Decay schemes (5) through (8) cannot be ruled out but they are not compatible with the two-body decay of a neutral particle coming from the star. Neither can one demonstrate conclusively that one or more neutral particles were not emitted in the decay of the supposed primary neutral particle, but the near coplanarity is a strong argument against this possibility.

The observed momenta and energies of the particles which created tracks A and B are not consistent with a nucleon-nucleon collision such as $n + n \longrightarrow d^{+} + \pi^{-}$, while the collision with a heavier nucleus, of a neutron with sufficient energy to produce a pion would not only give the residual nucleus a considerable momentum, thus producing a heavy spur track or blob at the V-vertex, but would probably leave the nucleus in an excited state from which additional charged particles would be boiled off.

Schemes (1) through (4) are all reasonably consistent with the decay of a heavy neutral particle emitted by the

Table 14

Momentum Balance

Assumed decay scheme*	Angle between assumed trajectory of neutral particle and $\vec{P} = \vec{P}_A + \vec{P}_B$	Residual transverse momentum in Mev/c	Q in Mev	Mass of neutral in m_e	Proper time of flight of Y^0 in sec $\times 10^{-11}$
(1) $Y^0 \to d^+ + \pi^-$	$4^\circ 21' \pm 8'$	11.2 ± 2.0	5.9 ± 0.6	3956	2.0
(2) $Y^0 \to d^+ + \mu^-$	$3^\circ 54' \pm 8'$	2.3 ± 1.7	4.5 ± 0.4	3887	2.0
(3) $Y^0 \to Y^\pm + \pi^\mp$	$4^\circ 11' \pm 8'$	9.4 ± 2.0	5.9 ± 0.6	4298	2.0
(4) $Y^0 \to Y^\pm + \mu^\mp$	$3^\circ 53' \pm 8'$	0.5 ± 1.7	4.5 ± 0.5	4228	2.0
(5) $Y^0 \to d^+ + K^-$	$14^\circ 26' \pm 43'$	104.8 ± 5.9	17.4 ± 1.7	4674	—
(6) $Y^0 \to Y^\pm + K^\mp$	$13^\circ 37' \pm 41'$	103.0 ± 5.9	17.8 ± 1.8	5016	—
(7) $Y^0 \to d^+ + \zeta^-$	$8^\circ 18' \pm 30'$	46.7 ± 3.4	10.6 ± 1.1	4229	—
(8) $Y^0 \to Y^\pm + \zeta^\mp$	$7^\circ 43' \pm 28'$	44.8 ± 3.4	10.8 ± 1.1	4570	—

*Possible contributory effects such as small angle scattering of the neutral particle, Coulomb scattering of the charged secondaries near the vertex of the V and lack of precise knowledge of the emulsion shrinkage factor have not been included in the quoted probable deviations. See Appendix A.

energetic star. If track A was made by a deuteron then the particle suffered either an inelastic scatter or a stripping at point C. In either case one might expect to see a recoil blob or perhaps β-decay tracks from the excited nucleus; neither of these were observed at C. If one assumes an average total cross section for (d, p) reactions with emulsion nuclei other than hydrogen (hydrogen would give an unmistakable recoil) in the energy range of 11* to 22 Mev of 0.4 barn and density of 4.85×10^{22} nuclei (excluding hydrogen) per cm^3 then the estimated mean free path for stripping $\left[\lambda = 1/(4.85)(10^{22})(0.4 \times 10^{-24})\right]$ is 52 cm. When this is compared with the observed range of 0.0847 cm one must conclude that the probability of a stripping reaction is very small.

If the neutral particle in scheme (1) were a Λ^o particle** bound to a neutron, the binding energy would have to be unexpectedly great to account for the low Q of the decay. Decay scheme (2) is of course not possible for an integral spin neutral primary.

In decay schemes (3) and (4), if the Y is assumed to have a mean lifetime of 10^{-10} sec, the probability that it would decay in the calculated travel time of

---

*If track A is caused by a deuteron its energy at point C as determined from the range-energy curve is 11.0 Mev.

**The symbol Λ^o is used to designate a neutral particle ($\sim 2182\ m_e$) which decays, with a mean lifetime of $\sim 3.0 \times 10^{-10}$ sec, into a proton and pion with an energy release, Q, of 37 Mev.

0.15×10^{-10} sec is 0.14. (The travel time, t, has been calculated from the relation $t = \int_{450}^{1297} dR/v$ where for a non-relativistic particle, of mass 4013 m_e, v may be expressed in terms of the residual range R through the range-energy relation. The probability of decay is then given by $\left[1 - e^{-t/\tau}\right]$). Decay scheme (3) is consistent with a primary particle composed of a pair of bound Λ^o particles whose rest mass would be 4364 m_e less a mass equivalent to the binding energy. This mass is in relatively good accord with the computed mass of 4298 m_e. The low Q of the Y^o, if it consists of a pair of bound Λ^o particles, implies a maximum Q* for the Y^+ disintegration of 71 Mev. The small observed energy of the particle which produced track A' and the large implied Q for the disintegration of the Y^+ are not at all inconsistent with the decay scheme $Y^+ \longrightarrow p^+ + n + \pi^o$, since the π^o may easily carry away most of the energy released in this decay.

The most plausible interpretation of the event seems to be that a neutral hyperon of mass in the neighborhood of 4300 to 4360 m_e was emitted by the 19 prong star, that this neutral hyperon decayed in flight after 2×10^{-11} sec into a pion and a charged hyperon of mass in the neighborhood of 4015 to 4075 m_e which subsequently decayed in flight after 1.5×10^{-11} sec into a proton and two neutral particles.

---

*The maximum Q value corresponds to an assumption of zero binding energy for the Λ^o particles. Actually this binding energy is expected to be small ($\simeq 2$ Mev).

CHAPTER VII

SUMMARY

Ilford, G-5, nuclear emulsions, 400 microns thick, which have been exposed to cosmic radiation at approximately 100,00 ft. were used in the investigation. The procedures which were set up to process, scan and store these plates have been described in detail. A microscope turntable of great utility not only in scanning the plates but also in making measurements, which was built in the Physics Department's instrument shop is described. By maintaining the atmosphere of the microscopy room at a temperature of $70^\circ \pm 1^\circ$ F and a relative humidity of 60 ± 3 percent the problem of emulsion stripping has been eliminated. Emulsions stored in this environment for as long as two years exhibit no tendency to peel from their glass backing plates.

Close control of any factors which might affect the measurements is required if one is to obtain the maximum amount of significant information from the analysis of a single event. Procedures, suggested by the work of Lal et al. (6), are given for correcting the observed data for distortion effects. A new technique for determining the ionization densities in the more severely clogged regions of tracks produced by slow particles is described. Preliminary findings indicate that the mass discrimination provided by the method is comparable to the more commonly used procedure of gap counting.

A review has been made of the application of multiple Coulomb scattering theory to the study of tracks in nuclear emulsions. The techniques used by various research groups to make mass and energy determinations from scattering measurements have been summarized. Wherever necessary the information available in the literature has been supplemented. This has been done in order to present the material in a more readily understandable and usable form.

Certain curious aspects of the V-event shown in Figure 32 led to an extended analysis of the finding. The interpretation which is favored is that a heavy unstable neutral particle, emitted from the star, decayed into two charged secondaries according to the scheme

$$Y^{0}\ (4300 - 4360\ m_e) \xrightarrow{2 \times 10^{-11}\ \mathrm{sec}} Y^{+}(4015 - 4075\ m_e) + \pi^{-}\ (273\ m_e)$$

$$Y^{+} \xrightarrow{1.5 \times 10^{-11}\ \mathrm{sec}} p^{+} + 2\ \text{neutral particles.}$$

Strong evidence from nuclear emulsion and cloud chamber studies indicates that unstable particles more massive than the proton exist in the secondary cosmic radiation. In practically all of the cases reported, however, the rest masses of the unstable particles were found to be less than the mass of the deuteron. A single event has been reported by Bradt and Peters (46) which may be interpreted as the decay of a heavy neutral particle (4120 ± 20 m_e) into two charged secondaries of masses 3960^{+900}_{-600} and 240 ± 40 m_e respectively. A Q-value of 89 ± 10 Mev is quoted for the reaction. This value of energy release is much greater than the calculated Q-values for decay schemes (1) through (40), so that it does not appear possible to explain the two events in terms of the decay of the same kind of particle.

Little information has appeared in reports by different research groups as to the methods which they use to calculate the probable deviations associated with the results of their measurements. Thus, it has been found necessary to formulate a procedure for assigning probable deviations to the various quoted values of momenta, angles, etc. The details of this procedure are given in Appendix A.

BIBLIOGRAPHY

1. C. C. Dilworth, G. P. S. Occhialini and L. Vermassen, Bull. du Cen. de Phys. Nuc. de L'Univ. Libre de Bruxelles, 13a, (February, 1950).

2. M. M. Shapiro, Private Communication, 1953.

3. B. Stiller, M. M. Shapiro and F. W. O'Dell, Rev. Sci. Instr. 25, 340 (1954).

4. P. H. Fowler, Phil. Mag. 41, 169 (1950).

5. A. D. Dainton, A. R. Gattiker and W. O. Lock, Phil. Mag. 42, 396 (1951).

6. D. Lal, Y. Pal and B. Peters, Proc. Indian Acad, Sci. 38, 398 (1953).

7. L. Voyvodic, Progress in Cosmic Ray Physics, (North-Holland Publishing Co., Amsterdam), Vol. II, Chapter V, 231 (1954).

8. B. Rossi and K. Greisen, Rev. Mod. Phys. 13, 240 (1941).

9. C. M. G. Lattes, P. H. Fowler and P. Cuer, Proc. Phys. Soc. 59, 883 (1947).

10. H. Bradner, F. H. Smith, W. H. Barkas and A. S. Bishop, Phys. Rev., 77, 462 (1950).

11. R. Brown, U. Camerini, P. H. Fowler, H. Muirhead and C. F. Powell, Nature 163, 83 (1949).

12. O. Halpern and H. Hall, Phys. Rev. 73, 477 (1948).

13. M. S. Livingston and H. Bethe, Rev. Mod. Phys. 9, 263 (1937).

14. W. Birnbaum, F. M. Smith and W. H. Barkas, Phys. Rev. 83, 895 (1951).

15. C. M. G. Lattes, G. P. S. Occhialini and C. F. Powell, Proc. Phys. Soc. 61, 173 (1948).

16. P. E. Hodgson, Phil. Mag. 41, 725 (1950).

17. S. Von Freisen and K. Kristiansson, Arkiv. F. Fysik. 4, 505 (1952).

18. J. M. Fowler, "A Study of Nuclear Disintegrations Induced by High Energy Cosmic Radiation," M. S. Thesis, Dept. of Physics, University of Oklahoma (1950).

19. S. Biswas, E. C. George and B. Peters, Proc. Indian Acad. Sci. 38A, 418 (1953).

20. E. J. Williams, Proc. Roy. Soc. (London) A169, 531 (1939).

21. L. Voyvodic and E. Pickup, Phys. Rev. 85, 91 (1952).

22. E. J. Williams, Phys. Rev. 47, 568 (1935).

23. S. A. Goudsmit and J. L. Saunderson, Phys. Rev. 57, 24 (1940), 58, 36 (1940).

24. H. S. Snyder and W. T. Scott, Phys. Rev. 76, 220 (1949).

25. W. T. Scott, Phys. Rev. 85, 245 (1952).

26. H. W. Lewis, Phys. Rev. 78, 526 (1950).

27. G. Moliere, Z. Naturforsch, 3a, 78 (1948).

28. Y. Goldschmidt-Clermont, D. T. King, H. Muirhead, D. M. Ritson, Proc. Phys. Soc. 61, 183 (1948).

29. Y. Goldschmidt-Clermont, Nuovo Cim. 1, 331 (1950).

30. M. G. K. Menon, C. O'Ceallaigh and O. Rochat, Phil. Mag. 42, 932 (1951).

31. R. Levi-Setti, Nuovo Cim. 8, 96 (1951).

32. K. Gottstein, M. G. K. Menon, J. H. Mulvey, C. O'Ceallaigh and O. Rochat, Phil. Mag. 42, 708 (1951).

33. M. J. Berger, Phys. Rev. 88, 59 (1952).

34. R. Levi-Setti, Bull. du Cen. de Phys. Nuc. de L'Univ. Libre de Bruxelles, (1950), Note No. 22.

35. J. E. Moyal, Phil. Mag. 41, 1058 (1950).

36. K. Gottstein and J. H. Mulvey, Phil. Mag. 42, 1089 (1951).

37. J. G. Wilson, Prog. in Cosmic Ray Phys. Vol. II, 273 (1954).

38. W. Bosley and H. Muirhead, Phil. Mag. 43, 63 (1952).

39. D. R. Corson, Phys, Rev. 80, 303 (1950).

40. D. R. Corson, Phys. Rev. 84, 605 (1951).

41. R. R. Daniel, J. H. Davis, J. H. Mulvey and D. H. Perkins, Phil. Mag. 43, 753 (1952).

42. M. Danysz, W. O. Lock and G. Yekutieli, Report of Bristol Conference on Heavy Mesons, (1951).

43. L. Voyvodic, Report of Bristol Conference on Heavy Mesons, (1951).

44. M. G. K. Menon and O. Rochat, Phil. Mag. 42, 1050 (1951).

45. C. O'Ceallaigh and O. Rochat, Phil. Mag, 42, 1232 (1951).

46. D. Lal, Y. Pal, and B. Peters, Phys. Rev. 92, 430 (1953).

APPENDIXES

A. PROBABLE DEVIATIONS

Calculation of the Angle $\Delta\theta$ between the Star Center-M- Axis and the Plane of the V-Event and the Associated Probable Deviation

Where l, m, n, and l', m', n', are the direction cosines of any two intersecting lines, the normalized equation of the plane defined by these lines is given by

$$\frac{a}{w}x + \frac{b}{w}y + \frac{c}{w}z = 0. \qquad \text{(A-1)}$$

Here $a = mn' - m'n$; $b = l'n - ln'$; $c = lm' - l'm$; and $w = (a^2 + b^2 + c^2)^{\frac{1}{2}}$. Use will be made of equation (A-1) in the development which follows.

A reference coordinate system associated with the microscope was obtained as described in Chapter III, the x-axis of this system being aligned parallel to the x-axis drive of the microscope stage. The plate containing the V-event was then rotated until the images of the star center and point M were both superimposed on the image of the x-axis crosshair. All coordinate measurements were then referred to point M as the origin of the coordinate system.

Coordinate readings for ten points on track A and six points on track B, in the neighborhood of the vertex were taken, from which, after correcting the z-coordinates for shrinkage, the best fit directions of these tracks were determined graphically. These two best-fit directions defined a new best-fit vertex. All coordinates quoted hereafter are referred to the best fit vertex as the origin of the coordinate system and have been corrected for shrinkage. Two points (x_A, y_A, z_A) and (x_B, y_B, z_B) were chosen arbitrarily from the best fit curves which, after correction for distortion, were used to determine the direction cosines of the trajectories of A and B. The coordinate values of the two points and the star center (also corrected for distortion) are given below (K, 18-19b):

$x_A = + 138.60$	$x_B = + 53.85$	$x_S = - 948.90$
$y_A = + 3.00$	$y_B = - 40.21$	$y_S = - 1.51$
$z_A = + 13.90$	$z_B = - 32.60$	$z_S = + 9.55$

It is convenient to tabulate now the numerical values of various direction cosines which have been calculated on the basis of the foregoing data and to which reference will be made in the subsequent discussion.

Unit vector, $\vec{n}_A$, along trajectory of A:	$l_A = + 0.99294$	$m_A = + 0.02149$	$n_A = + 0.09958$

Unit vector, $\vec{n}_B$, along trajectory of B:	$l_B = +0.72092$	$m_B = -0.53832$	$n_B = -0.43644$
Unit vector, $\vec{n}_S$ along star center -M-axis	$l_S = -0.99995$	$m_S = -0.00159$	$n_S = +0.01006$
Unit vector, $\vec{n}_n$, normal to plane of V-event	$l_n = +0.05912$	$m_n = +0.67525$	$n_n = -0.73522$
$\vec{r} \equiv \vec{n}_n \times \vec{n}_S$:	$l_r = +\frac{0.00563}{r}$	$m_r = +\frac{0.73459}{r}$	$n_r = +\frac{0.67512}{r}$.

The information given above has been used to evaluate the coefficients in (A-1). The normalized equation of the plane of the V-event was found to be

$$0.059120\, x + 0.675248\, y - 0.735219\, z = 0. \qquad \text{(A-1b)}$$

The angle, $\Delta\theta$, which the star center-M-axis makes with this plane was found from the relation* (F, 4-5)

$$\Delta\theta \cong \sin\Delta\theta = \frac{(z' - z_S)\cos\psi}{(x_S^2 + y_S^2 + z_S^2)^{\frac{1}{2}}} \qquad \text{(A-2)}$$

where z' is the z-coordinate of a point, (x_S, y_S, z'), on a line parallel to the z-axis and passing through z_S, which lies in the plane defined by (A-1b) and ψ is the angle between the z-axis and a line through z_S perpendicular to the plane of the V-event. Then $\cos\psi$ is equal to the absolute value of the coefficient of z in the normalized equation of the plane (A-1b), so that for the particular case which was

---

*It is convenient to express the angle in this form for the later determination of the probable deviation $R_{\Delta\theta}$.

studied, $\cos\psi = 0.735219$.

Since the point (x_S, y_S, z') must satisfy (A-1b) one has the condition

$$0.059120\, x_S + 0.675248\, y_S - 0.735219\, z' = 0 \quad \text{(A-3)}$$

from which z', and hence (A-2), may be evaluated. This has been done and the value of $\Delta\theta = 3^{\circ}\ 52'$ was obtained.

In order to determine the probable deviation, $R_{\Delta\theta}$, z' has first been expressed in terms of the coordinates involved. Thus, one has

$$z' = a x_S + b y_S = \frac{(y_A x_S - x_A y_S) z_B + (x_B y_S - x_S y_B) z_A}{(x_B y_A - x_A y_B)}. \quad \text{(A-4)}$$

In what follows, it has been assumed that the deviations in the x- and y-coordinates are small compared to the deviations in the z-coordinates. Under this assumption one has, with the usual notation, the probable deviation of z',

$$R_{z'} = \left[\left(\frac{\partial z'}{\partial z_A}\right)^2 R^2_{z_A} + \left(\frac{\partial z'}{\partial z_B}\right)^2 R^2_{z_B}\right]^{\frac{1}{2}} \quad \text{(A-5)}$$

and from (A-2), since for this particular event $z_S << x_S$

$$R_{\Delta\theta} = \frac{\cos\psi}{(x_S^2 + y_S^2)^{\frac{1}{2}}} \left[R^2_{z'} + R^2_{z_S}\right]^{\frac{1}{2}} \quad \text{(A-6)}$$

It has been assumed, further, that the probable deviation associated with the measurement of any one z-coordinate is the same as the probable deviation associated with the measurement of any other z-coordinate, (i.e., $R_{z'} = R_{z_S} = R_z$). R_{z_S} was determined * by making a series of measurements of depth differences between the star center and point M (C, 38-39).

The terms involving partial derivatives in (A-5) have been evaluated to yield

$$\left(\frac{\partial z'}{\partial z_A}\right)^2 = \left[\frac{x_B y_S - x_S y_B}{x_B y_A - x_A y_B}\right]^2 = \left[\frac{(53.85)(-1.51) - (-948.90)(-40.21)}{(53.85)(3.00) - (138.60)\ (-40.21)}\right]^2$$
$$= 44.46$$

$$\left(\frac{\partial z'}{\partial z_B}\right)^2 = \left[\frac{y_A x_S - x_A y_S}{x_B y_A - x_A y_B}\right]^2 = \left[\frac{(3.00)(-948.90) - (138.60)(-1.51)}{(53.85)(3.00) - (138.60)(-40.21)}\right]^2$$
$$= 0.21$$

so that, in degrees, one has

$$R_{\Delta\theta} = \frac{(0.735218)}{(948.95)}\left[(-0.295)^2\ \{44.46 + 0.21\} + (0.295)^2\right]^{\frac{1}{2}}\left(\frac{180}{\pi}\right)$$
$$= 0.09^{\circ} = 5'.$$

Calculation of the Angles between the Trajectories of A and of B and the Projection onto the V plane of the Star Center-M-Axis and the Associated Probable Deviations

For convenience, in what follows, the projection onto the V plane of the star center-M-axis, the trajectory of A and the trajectory of B will be referred to as S, A, and B respectively. The angle, θ_A, between S and A was determined

---

*The relation $R_{z_S} = 0.67\left\{\Sigma(\overline{m} - m_i)^2/n\right\}^{\frac{1}{2}}$ was used to obtain a value of 0.295 microns. In this expression $\overline{m}$ is the arithmetic mean, m_i, the value of an individual measure and n is the number of independent measures.

by forming the scalar product

$$\frac{\vec{r}}{r} \cdot \vec{n}_A = \cos\,(90^\circ - \theta_A) = \sin\theta_A = l_A\left(\frac{l_r}{r}\right) + m_A\left(\frac{m_r}{r}\right) + n_A\left(\frac{n_r}{r}\right) \tag{A-7}$$

from which

$$\sin\theta_A = \frac{1}{(0.99772)}\Big[(0.99294)(0.00563) + (0.02149)(0.73459) + (0.09958)(0.67512)\Big]$$

$$= 0.08881$$

and $\theta_A = 5^\circ\ 5'$.

The probable deviation R_{θ_A} was determined by calculating first the probable deviation in $R_{\sin\theta_A}$. Since $\theta_A = \sin^{-1}\{\sin\theta_A\}$, R_{θ_A} is related to $R_{\sin\theta_A}$ through the equation

$$R_{\theta_A} = \left(\frac{\partial \sin^{-1}\ \{\sin\theta_A\}}{\partial \sin\theta_A}\right) R_{\sin\theta_A} = \frac{1}{(1 - \sin\theta_A^2)^{\frac{1}{2}}}\ R_{\sin\theta_A} \tag{A-8}$$

where $R_{\sin\theta_A} = R_z \left[\left(\frac{\partial\sin\theta_A}{\partial z_A}\right)^2 + \left(\frac{\partial\sin\theta_A}{\partial z_B}\right)^2 + \left(\frac{\partial\sin\theta_A}{\partial z_S}\right)^2\right]^{\frac{1}{2}}$ (A-9)

and $\sin\theta_A = \frac{\vec{n}_A \cdot \vec{r}}{r}$ from (A-7).

The results obtained after carrying out the operations on $\sin\theta_A$ which are indicated in (A-9) are given below for purpose of reference.

$$\frac{\partial\sin\theta_A}{\partial z_A} = \frac{(n_r - n_A\sin\theta_A)}{d_A} + \frac{1}{r}\Big[(n_A m_S - m_A n_S)\frac{\partial l m}{\partial z_A} +$$

$$(l_A n_S - l_S n_A)\frac{\partial m_n}{\partial z_A} + (m_A l_S - l_A m_S)\frac{\partial n_n}{\partial z_A}\Big] -$$

$$\frac{\sin\theta_A}{r^2}\Big[(l_n - \{\vec{n}_S \cdot \vec{n}_n\} l_s)\frac{\partial l_n}{\partial z_A} +$$

$$(m_n - \{\vec{n}_S \cdot \vec{n}_n\} m_S)\frac{\partial m_n}{\partial z_A} + (n_n - \{\vec{n}_S \cdot \vec{n}_n\} n_S)\frac{\partial n_n}{\partial z_A}\Big]$$

where $d_A = \left[x_A^2 + y_A^2 + z_A^2\right]^{\frac{1}{2}}$. Setting $\alpha = \left[(y_A z_B - y_B z_A)^2 + (x_B z_A - x_A z_B)^2 + (x_A y_B - x_B y_A)^2\right]^{\frac{1}{2}}$ and $\delta_A = \left[Z_B(x_A x_B + y_A y_B) - z_A(x_B^2 + y_B^2)\right]/\alpha^2$ one may write

$$\frac{\partial l_n}{\partial z_A} = \delta_A l_n - \frac{y_B}{\alpha};\ \frac{\partial m_n}{\partial z_A} = \delta_A m_n + \frac{x_B}{\alpha};\ \frac{\partial n_n}{\partial z_A} = \delta_A n_n. \qquad \text{(A-10)}$$

$$\frac{\partial \sin\theta_A}{\partial z_B} = \frac{1}{r}\Big[(n_A m_S - m_A n_S)\frac{\partial l_n}{\partial z_B} + (l_A n_S = n_A l_S)\frac{\partial m_n}{\partial z_B} +$$

$$(m_A l_S - l_A m_S)\frac{\partial n_n}{\partial z_B} - \frac{\sin\theta_A}{r^2}\Big[(l_n - \{\vec{n}_S \cdot \vec{n}_n\} l_S)\frac{\partial l_n}{\partial z_B} +$$

$$(m_n - \{\vec{n}_S \cdot \vec{n}_n\} m_S)\frac{\partial m_n}{\partial z_B} + (n_n - \{\vec{n}_S \cdot \vec{n}_n\} m_S\ \frac{\partial n_n}{\partial z_B}\Big].$$

Setting $\delta'_A = \left[z_B(x_A x_B + y_A y_B) - z_B(x_A^2 + y_A^2)\right]/\alpha^2$ one may write

$$\frac{\partial l_n}{\partial z_B} = \delta'_A l_n + \frac{y_A}{\alpha};\ \frac{\partial m_n}{\partial z_B} = \delta'_A m_n - \frac{x_A}{\alpha};\ \frac{\partial n_n}{\partial z_B} = \delta'_A n_n. \qquad \text{(A-11)}$$

$$\frac{\partial \sin\theta_A}{\partial z_S} = \frac{1}{r d_S}\left[(l_A m_n - m_A l_n) - \frac{\sin\theta_A}{r}(l_r m_n - m_r l_n)\right]$$

where $d_S = \left[x_S^2 + y_S^2 + z_S^2\right]^{\frac{1}{2}}$. (A-12)

Expression (A-10) was evaluated as shown below.

$$(\vec{n}_S \cdot \vec{n}_n) = \Big[(-0.99995)(0.05912) + (-0.00159)(0.67525) + (0.01006)(-0.73522)\Big] = -0.06759$$

$$d_A = \Big[(138.60)^2 + (3.00)^2 + (13.90)^2\Big]^{\frac{1}{2}} = 139.59$$

$$\alpha = \Big[\{(3.00)(-32.60) - (40.21)(13.90)\}^2 + \{(53.85)(13.90) - (138.60)(-32.60)\}^2 + \{(138.60)(-40.21) - (53.85)(3.00)\}^2\Big]^{\frac{1}{2}} = 7.80 \times 10^3$$

$$\delta_A = \Big[(-32.60)\{(138.60)(53.85) + (3.00)(-40.21)\} - (13.90)\{(53.85)^2 + (-40.21)^2\}\Big] \Big/ (7.80)^2 \times 10^6$$

$$= -5.00 \times 10^{-3}$$

$$\delta_A' = \Big[(13.90\ \{(138.60)(53.85) + (3.00)(-40.21)\} + (32.60)\{(138.60)^2 + (3.00)^2\}\Big] \Big/ (7.80)^2 \times 10^6$$

$$= 1.20 \times 10^{-2}$$

$$\frac{\partial l_n}{\partial z_A} = (-0.00500)(0.05912) - \frac{(-40.21)}{7.80 \times 10^3} = 4.86 \times 10^{-3}$$

$$\frac{\partial m_n}{\partial z_A} = (-0.00500)(0.67525) + \frac{(53.85)}{7.80 \times 10^3} = 3.54 \times 10^{-3}$$

$$\frac{\partial n_n}{\partial z_A} = (0.00500)(-0.73522) = 3.68 \times 10^{-3}$$

$$\frac{\partial l_n}{\partial z_B} = (1.20 \times 10^{-2})(0.05912) + \frac{(3.00)}{7.80 \times 10^3} = 1.09 \times 10^{-3}$$

$$\frac{\partial m_n}{\partial z_B} = (1.20 \times 10^{-2})(0.67525) - \frac{(138.60)}{7.80 \times 10^3} = -9.67 \times 10^{-3}$$

$$\frac{\partial n_n}{\partial z_B} = (1.20 \times 10^{-2})(-0.73522) = -8.82 \times 10^{-3}$$

$$\frac{\partial \sin\theta_A}{\partial z_A} = \left[\frac{(0.67512) - (0.09958)(0.08881)}{139.59}\right] +$$

$$\frac{1}{0.99772} \Big\{\Big[(0.09958)(-0.00159) - (0.02149)(0.01006)\Big] (4.86 \times 10^{-3}) +$$

$$\Big[(0.99294)(0.01006) - (-0.99995)(0.09958)\Big] (3.54 \times 10^{-3}) +$$

$$\Big[(0.02149)(-0.99995) - (0.99294)(-0.00159)\Big] (3.68 \times 10^{-3})\Big\} -$$

$$\frac{(0.08881)}{(0.99544)} \Big\{\Big[(0.05912) - (-0.06759)(-0.99995)\Big] (4.86 \times 10^{-3}) +$$

$$\Big[(0.67525) - (-0.06759)(-0.00159)\Big] (3.54 \times 10^{-3}) +$$

$$\Big[(-0.73522) - (-0.06759)(0.01006)\Big] (3.68 \times 10^{-3})\Big\}$$

$$= 5.05 \times 10^{-3}$$

The evaluation of (A-11) and (A-12) was carried out as above to give

$$\frac{\partial \sin\theta_A}{\partial z_B} = 0.88 \times 10^{-3}; \qquad \frac{\partial \sin\theta_A}{\partial z_S} = 0.71 \times 10^{-3}.$$

These values were substituted in (A-9) to obtain

$$R_{\sin\theta_A} = 0.295\left[0.2560 \times 10^{-4} + 0.0008 \times 10^{-4} + 0.0051 \times 10^{-4}\right]^{\frac{1}{2}}$$

$$= 1.530 \times 10^{-3}.$$

A value of R_{θ_A} was then obtained by use of (A-8). It was found that

$$R_{\theta_A} = \frac{(1.530 \times 10^{-3})(180)}{(1 - 0.008)^{\frac{1}{2}} \quad (\pi)} = 0.09^\circ = 5'.$$

In a similar fashion, the angle, θ_B, between S and B, and its probable deviation were found to be

$$\theta_B = 43^\circ\ 26' \pm 6'.$$

Calculation of the Momentum of a Particle and its Associated Probable Deviation

If the kinetic energy, T, of a particle of known mass M_o* has been estimated, the magnitude of the correspon- ding momentum vector, $\vec{p}$, may be calculated from the relation

$$p = \frac{1}{c}\left[T(T + 2M_o c^2)\right]^{\frac{1}{2}} \tag{A-13}$$

where c is the velocity of light in free space. Then the probable deviation, R_p, of the momentum, $\vec{p}$, will be given

---

*The following treatment assumes we know M_o precisely. This is approximately true once the particle has been identified.

by

$$R_p = \left(\frac{\partial p}{\partial T}\right) R_T = \frac{1}{c}\left[\frac{T + M_o c^2}{pc}\right] R_T \qquad \text{(A-14)}$$

where R_T is the probable deviation of the kinetic energy, T.

A calculation for the particle producing track A, assuming it to be a deuteron, will serve as an example. If the particle A be a deuteron, then its kinetic energy, T, at the vertex of the V was estimated, as described in Chapter VI, to be 21.9 ± 1.8 Mev. Hence, from (A-13),

$$p = \frac{1}{c}\left[(21.9)\left\{(21.9) + (2)(0.511)(3672)\right\}\right]^{\frac{1}{2}} = 287.3 \text{ Mev/c}$$

and from (A-14),

$$R_p = \frac{1}{c}\left[\frac{(21.9) + (0.511)(3672)}{287.3}\right](1.8) = 12.1 \text{ Mev/c.}$$

Calculation of the Angles between the Assumed Trajectory of the Neutral Particle and $\vec{p} = \vec{p}_A + \vec{p}_B$ and the Associated Probable Deviations

If ψ represents the angle between the star center-M-axis and the direction of $\vec{p}$, the value of ψ for an assumed decay scheme, may be obtained by forming the scalar product $(-\vec{n}_S \cdot \vec{n}_P)$ where $\vec{n}_p$ is a unit vector in the direction of $\vec{p}$.

The method will be illustrated by an example. Consider the decay scheme (1) given in Chapter VI, in which it is assumed that the neutral particle decays into a deuteron and a π-meson. Here

$$\vec{p}_A = |\vec{p}_A|\left\{l_A\vec{i} + m_A\vec{j} + n_A\vec{k}\right\}$$

$$= 285.27166\ \vec{i} + 6.17408\ \vec{j} + 28.60933\ \vec{k},$$

and

$$\vec{p}_B = |\vec{p}_B|\left\{l_B\vec{i} + m_B\vec{j} + n_B\vec{k}\right\}$$

$$= 38.533176\ \vec{i} - 28.77320\ \vec{j} - 23.32772\ \vec{k}.$$

Thus

$$\vec{p} = 323.80482\ \vec{i} - 22.59912\ \vec{j} + 5.28161\ \vec{k};\ |\vec{p}| = 324.63548$$

and

$$\vec{n}_p = \frac{\vec{p}}{|\vec{p}|} = 0.99744\vec{i} - 0.06961\ \vec{j} + 0.01627\ \vec{k}.$$

Then

$$-\cos\psi = \vec{n}_p \cdot \vec{n}_S = l_p l_S + m_p m_S + n_p n_S$$

$$= -\left\{(0.99744)(-0.99995) + (-0.06961)(-0.00159) + (0.01627)(0.01006)\right\}$$

$$= -0.99712$$

so that

$$\psi = 4^\circ\ 21'$$

The probable deviation, R_ψ, is related to the probable deviation, $R_{(-\cos\psi)}$, by the equation

$$R_\psi = \frac{1}{(1-\cos^2\psi)^{\frac{1}{2}}}\ R_{(-\cos\psi)}. \qquad \text{(A-15)}$$

It is convenient, as before, to find first the value of $R_{(-\cos\psi)}$. Now

$$(-\cos\psi) = \vec{n}_p \cdot \vec{n}_S = \frac{l_S(p_A l_A + p_B l_B)}{p} + \frac{m_S(p_A m_A + p_B m_B)}{p} +$$

$$\frac{n_S(p_A n_A + p_B n_B}{p} = \frac{1}{p}\Big[p_A(l_S l_A + m_S m_A + n_S n_A) +$$

$$p_B(l_S l_B + m_S m_B + n_S n_B)$$

where $p = \left[(p_A l_A + p_B l_B)^2 + (p_A m_A + p_B m_B)^2 + (p_A n_A + p_B n_B)^2\right]^{\frac{1}{2}}$

so that $R_{(-\cos\psi)}$ depends on both the momenta and the coordinates. One may write

$$R_{(-\cos\psi)} = \left\langle \left\{\frac{\partial(-\cos\ )}{\partial p_A}\right\}^2 R^2_{p_A} + \left\{\frac{\partial(-\cos\psi)}{\partial p_B}\right\}^2 R^2_{p_B} + R_z^2 \left[\left\{\frac{\partial(-\cos\psi)}{\partial z_A}\right\}^2 + \left\{\frac{\partial(-\cos\psi)}{\partial z_B}\right\}^2 + \left\{\frac{\partial(-\cos\psi)}{\partial z_S}\right\}^2\right]\right\rangle^{\frac{1}{2}} \quad \text{(A-16)}$$

where

$$\frac{\partial(-\cos\psi)}{\partial p_A} = \frac{l_S l_A + m_S m_A + n_S n_A}{p}$$
$$\frac{\cos\psi\{p_A + p_B \cos(\theta_A + \theta_B)}{p^2}$$

$$\frac{\partial(-\cos\psi)}{\partial p_B} = \frac{l_S l_B + m_S m_B + n_S n_B}{p} +$$
$$\frac{\cos\psi\{p_B + p_A \cos(\theta_A + \theta_B)\}}{p^2}$$

$$\frac{\partial(-\cos\psi)}{\partial z_A} = \frac{n_A p_A}{p d_A}\left\{l_S l_A + m_S m_A + n_S n_A\right\} + \frac{p_A n_S}{p d_A} - \frac{n_B \cos\psi\, p_A p_B \left\{\cos(\theta_A + \theta_B) - n_B/n_A\right\}}{p^2 d_A}$$

$$\frac{\partial(-\cos\psi)}{\partial z_B} = -\frac{n_B p_B}{p d_B}\left\{l_S l_B + m_S m_B + n_S n_B\right\} + \frac{p_A n_S}{p d_B} - \frac{n_B \cos\psi\, p_A p_B}{p^2 d_B}\left\{\cos(\theta_A + \theta_B) - n_A/n_B\right\}$$

$$\frac{\partial(-\cos\psi)}{\partial z_S} = \frac{n_S}{d_S}\cos\psi + \frac{p_A n_A + p_B n_B}{p d_S}.$$

The evaluation of (A-16) for decay scheme (1) is given below.

$$\frac{\partial(-\cos\psi)}{\partial p_A} = \frac{(-0.99995)(0.99294) + (-0.00159)(0.02149)}{324.63548} + \frac{(0.01006)(0.09958)}{324.63548} + \frac{(0.99712)\left\{287.3 + 53.45\,(0.66240)\right\}}{10.53882 \times 10^4}$$

$$= -0.00225 \times 10^{-3}$$

$$\frac{\partial(-\cos\psi)}{\partial p_B} = \frac{(-0.9995)(0.72092) + (-0.00159)(-0.53832)}{324.63548} + \frac{(0.01006)(-0.43644)}{324.63548} + \frac{(0.99712)\left\{53.45 + 287.3\,(0.66240)\right\}}{10.53882 \times 10^4}$$

$$= 0.07482 \times 10^{-3}$$

$$\frac{\partial(-\cos\psi)}{\partial z_A} = \frac{1}{(324.63548)(139.59)}\Big\{(-0.09958)(287.3)(-0.99192) + (287.3)(0.01006) - \frac{(0.09958)(0.99712)(287.3)(53.45)}{324.63548}\Big[0.66240 -$$

$$\left.\left.\frac{(-0.43644)}{0.09958}\right]\right\}$$

$$= 0.16709 \times 10^{-3}$$

$$\frac{\partial(-\cos\psi)}{\partial z_B} = \frac{1}{(324.63548)(74.70)}\Big\{-(-0.43644)(53.45)(-0.72442)+$$

$$(53.45)(0.01006) - (-0.43644)(47.16662)\Big[(0.66240 -$$

$$\left.\left.\frac{0.09958}{-0.43644}\right]\right\}$$

$$= 0.08129 \times 10^{-3}$$

$$\frac{\partial(-\cos\psi)}{\partial z_S} = \frac{1}{948.95}\Big\{(0.01006)(0.99712)+$$

$$\left.\left[\frac{(287.3)(0.09958) \quad (53.45)(-0.43644)}{324.63548}\right]\right\}$$

$$= 0.02772 \times 10^{-3}.$$

These values were substituted in (A-16) to obtain

$$R_{(-\cos\psi)} = \Big[(2.25 \times 10^{-6})^2(12.1)^2 + (74.82 \times 10^{-6})^2 (2.4)^2 +$$

$$\{(167.09 \times 10^{-6})^2 + (81.29 \times 10^{-6})^2 +$$

$$(27.72 \times 10^{-6})^2\} \quad 8.70 \times 10^{-2}\Big]$$

$$= 1.863 \times 10^{-4}.$$

Then, by use of (A-15) one has

$$R_\psi = \frac{(1.863 \times 10^{-4})(180)}{(1 - 0.99425)^{\frac{1}{2}} \quad \pi} = 0.141^\circ \cong 8'.$$

Calculation of the Residual Transverse Momenta and the Associated Probable Deviations

The residual transverse momentum, p_T, for an assumed decay scheme may be obtained from the equation

$$p_T = p_A \sin\theta_A - p_B \sin\theta_B \tag{A-17}$$

and the probable deviation, R_{p_T}, is given by

$$R_{p_T} = \Big[(\sin\theta_A)^2 R^2_{p_A} + (\sin\theta_B)^2 R^2_{p_B} + p_A^2\, R^2(\sin\theta_A) + p_B^2 R^2_{\sin\theta_B}\Big]^{\frac{1}{2}} \tag{A-18}$$

For decay scheme (1), (A-17) yields

$$p_T = (287.3)(0.08881) - (53.45)(0.68761) = -11.23 \text{ Mev/c}$$

and from (A-18)

$$R_{p_T} = \Big[(80.07)(10^{-4})(146.4) + (0.473)(5.62) + (8.254)(10^4)(2.341)(10^{-6}) + (2.857)(10^3)(1.682)(10^{-6})\Big]^{\frac{1}{2}}$$
$$= 2.00 \text{ Mev/c.}$$

Calculation of the Q values and the Associated Probable Deviations

If a neutral particle decays in flight into two charged secondaries whose masses are M_A and M_B, the energy release, Q, may be calculated from the relation

$$Q^* = (M_A + M_B)\ c^2 \left\{\left[1 + 2\left\langle\frac{(T_AT_B + T_AM_Bc^2 + T_BM_Ac^2 - p_Ap_B\cos(\theta_A + \theta_B)c^2}{(M_A + M_B)^2c^4}\right\rangle\right]^{\frac{1}{2}} - 1\right\}$$

where $(\theta_A + \theta_B)$ is the angle between $\vec{p}_A$ and $\vec{p}_B$, and the remaining subscripts and notation have the usual significance. If Q and the masses M_A and M_B are known one may calculate the mass M_o of the neutral particle since

$$Q = (T_A + T_B) - T_O = M_oc^2 - (M_A + M_B)c^2.$$

Decay scheme (1) is again used to illustrate the procedure. The evaluation of (A-19) gave

$$Q = (3672 + 273)(0.511)\left\{\left[1 + 2\left\langle\frac{(21.9)(9.9) + (21.9)(2.73)(0.511)}{[(3672 + 273)(0.511)]^2} + \frac{(9.9)(3672)(0.511) - (287.3)(53.5)(0.66240)}{[(3672 + 273)(0.511)]^2}\right\rangle\right]^{\frac{1}{2}} - 1\right\}$$

$$Q = 5.9 \text{ Mev}$$

and $M_o = \frac{5.9}{0.511} + (3672 + 273) = 3956\ m_e.$

The probable deviation, R_Q can then be computed from the relation

---

*$Q = (T_A + T_B) - T_o$ where T_A and T_B represent the kinetic energies of the decay products and T_o designates the kinetic energy of the decaying neutral. (A-19) may be derived readily by applying the momentum and energy conservation principles (K,49-50).

$$R_Q = \left[\left(\frac{\partial Q}{\partial T_A}\right)^2 R^2_{T_A} + \left(\frac{\partial Q}{\partial T_B}\right)^2 R^2_{T_B} + \left(\frac{\partial Q}{\partial \cos(\theta_A + \theta_B)}\right)^2 R^2_{\cos(\theta_A + \theta_B)}\right]^{\frac{1}{2}} .$$

(A-20)

It is convenient in (A-19) to set $\alpha = (M_A + M_B)c^2$ and

$$\beta = 1 \quad \frac{2}{\alpha^2}\Big\langle T_A T_B + T_A M_B c^2 + T_B M_A c^2 - (T_A^2 + 2M_A c^2 T_A)^{\frac{1}{2}} (T_B^2 + 2M_B c^2 T_B)^{\frac{1}{2}} \cos(\theta_A + \theta_B)\Big\rangle .$$

Then

$$\frac{\partial Q}{\partial T_A} = \frac{1}{\alpha \beta^{\frac{1}{2}}}\left\{ T_B + M_B c^2 - \frac{p_B}{p_A}(T_A + M_A c^2) \cos(\theta_A + \theta_B)\right\}$$

$$\frac{\partial Q}{\partial T_B} = \frac{1}{\alpha \beta^{\frac{1}{2}}}\left\{ T_A + M_A c^2 - \frac{p_A}{p_B}(T_B + M_B c^2) \cos(\theta_A + \theta_B)\right\}$$

$$\frac{\partial Q}{\partial \cos(\theta_A + \theta_B)} = \frac{-1}{\alpha \beta^{\frac{1}{2}}}\left\{ p_A p_B c^2 \right\}$$

$$R^2_{\cos(\theta_A + \theta_B)} = R_z^2 \left\{\left(\frac{\partial \cos(\theta_A + \theta_B)}{\partial z_A}\right)^2 + \left(\frac{\partial \cos(\theta_A + \theta_B)}{\partial z_A}\right)^2\right\}$$

where, in the last equation

$$\frac{\partial \cos(\theta_A + \theta_B)}{\partial z_A} = \frac{1}{d_A}\left\{ n_B - n_A \cos(\theta_A + \theta_B)\right\} \quad \text{and}$$

$$\frac{\partial \cos(\theta_A + \theta_B)}{\partial z_B} = \frac{1}{d_B}\left\{ n_A - n_B \cos(\theta_A + \theta_B)\right\} .$$

The evaluation of (A-20) for decay scheme (1) is given below.

$$\frac{\partial \cos(\theta_A + \theta_B)}{\partial z_A} = \frac{1}{(139.59)}\left\{(-0.43644) - (0.09958)(0.66240)\right\}$$

$$= -3.61 \times 10^{-3}$$

$$\frac{\partial \cos(\theta_A + \theta_B)}{\partial z_B} = \frac{1}{74.70}\left\{(0.09958) - (-0.43655)(0.66240)\right\}$$

$$= 5.20 \times 10^{-3}$$

$$R^2_{\cos(\theta_A + \theta_B)} = (0.295)^2\left\{(-3.61 \times 10^{-3})^2 + (5.20 \times 10^{-3})^2\right\}$$

$$= 3.49 \times 10^{-6}$$

$$\frac{1}{\alpha\beta^{\frac{1}{2}}} = \frac{1}{(2.0159)(1.0029) \times 10^{-3}} = 4.95 \times 10^{-4}$$

$$\frac{\partial Q}{\partial T_A} = (4.95 \times 10^{-4})\left\{9.9 + 139.50 - (0.186)(0.66240)\left[21.9 + 1876.39\right]\right\}$$

$$= (4.95 \times 10^{-4})(-84.34)$$

$$\frac{\partial Q}{\partial T_B} = (4.95 \times 10^{-4})\left\{21.9 + 1876.39 - (4.98)(0.66240)\left[9.9 + 139.50\right]\right\}$$

$$(4.95 \times 10^{-4})(1405.72)$$

$$\frac{\partial Q}{\partial \cos(\theta_A + \theta_B)} = (-4.95 \times 10^{-4})(287.3)(53.5)$$

$$= -(4.95 \times 10^{-4})(15356.19)$$

$$R_Q = (0.495 \times 10^{-3})\left\{\left[(84.34)(1.8)\right]^2 + \left[(1405.72)(0.9)\right]^2 + \left[15356.19\right]^2 (3.49 \times 10^{-6})\right\}^{\frac{1}{2}}$$

$$= 0.60 \text{ Mev.}$$

B. TABLES OF DATA

Table 15

Grain Count Data for Track 1, Table 2

β_i in microns	$k\delta_i$ in microns	ΔR_i in microns	$(R - R_K)$* in microns	$(N - N_K)$** grains
60.1	4.2	60.2	60.2	90
71.5	8.4	72.0	132.2	169
71.5	5.3	71.7	203.9	258
71.5	6.3	71.8	275.7	349
71.5	7.4	71.9	347.6	446
71.5	4.2	71.6	419.2	525
71.5	2.1	71.6	490.8	610
71.5	4.2	71.6	562.4	689
71.5	1.1	71.5	633.9	763
71.5	1.1	71.5	705.4	827
71.5	0	71.5	776.9	915
71.5	1.1	71.5	848.4	1003
71.5	0	71.5	919.9	1072
71.5	0	71.5	991.4	1174
71.5	0	71.5	1062.9	1255
71.5	2.1	71.6	1134.5	1330
71.5	4.2	71.6	1206.1	1412
71.5	4.2	71.6	1277.7	1492
71.5	2.3	71.7	1349.4	1568
71.5	3.2	71.6	1421.0	1642
71.5	4.2	71.6	1492.6	1709
71.5	2.1	71.6	1564.2	1762
71.5	4.2	71.6	1635.8	1843
71.5	4.2	71.6	1707.4	1912
71.5	5.3	71.7	1779.1	1985
71.5	4.2	71.6	1850.7	2038

Table 15 -- continued

β_i in microns	$k\delta_i$ in microns	ΔR_i in microns	$(R - R_K)$* in microns	$(N - N_K)$** grains
71.5	3.2	71.6	1922.3	2109
71.5	3.2	71.6	1993.9	2172

*$(R - R_K)$ represents the total track length which has accrued from the point at which the grain count was begun. R_k = 2010 microns.

**$(N - N_K)$ represents the total number of grains which have accrued from the point at which the grain count was begun. N_K has not been determined.

Table 16

Scattering Data for Track (1), Table 3*

Projected residual** range in scale div.	Projected cell length in scale div.	y-coordinate in $\frac{\text{scale div.}}{8}$	S_i in $\frac{\text{scale div.}}{8}$	D_i in $\frac{\text{scale div.}}{8}$
7	6	0	- 4	- 1
9	7	1	- 5	- 4
11	7	3	- 4	- 3
13	8	4	- 3	- 3
16	8	6	- 1	- 2
18	9	7	- 1	- 4
21	9	7	0	- 5
24	10	7	1	- 4
27	10	8	3	- 3
30	11	7	5	- 1
34	11	6	5	- 4
37	11	5	6	- 4
41	12	2	6	- 5
45	12	1	9	0
48	13	- 1	10	1
53	13	- 4	11	3
57	13	- 8	9	1
61	14	-11	9	1
66	14	-15	8	- 1
70	14	-17	8	- 2
75	15	-20	8	- 4
80	15	-23	9	- 2
84	15	-25	10	- 1
90	16	-28	12	1
95	16	-32	11	1
99	16	-35	11	2
106	17	-40	11	3
111	17	-43	10	3
115	17	-46	9	2
123	17	-51	8	3
128	18	-53	7	0
132	18	-55	7	0
140	18	-59	5	0
146	19	-60	7	3
150	19	-62	7	5
158	19	-64	5	2
165	20	-67	4	4

Table 16 --continued

Projected residual** range in scale div.	Projected cell length in scale div.	y-coordinate in $\frac{\text{scale div.}}{8}$	S_i in $\frac{\text{scale div.}}{8}$	D_i in $\frac{\text{scale div.}}{8}$
169	20	-69	2	2
177	20	-69	3	6
185	20	-71	0	2
189	20	-71	0	2
197	21	-72	- 3	- 3
205	21	-71	- 2	- 2
209	21	-71	- 2	- 1
218	22	-69	0	- 1
226	22	-69	0	- 1
230	22	-69	- 1	- 3
240	22	-69	1	0
248	23	-69	1	- 2
252	23	-68	2	- 2
262	23	-70	1	- 2
271	23	-70	3	4
275	23	-70	4	7
285	24	-71	3	9
294	24	-73	- 1	6
298	24	-74	- 3	6
309	24	-74	- 6	2
318	24	-72	- 7	- 2
322	25	-71	- 9	- 6
333	25	-68	- 8	- 6
342	25	-65	- 5	- 2
347	25	-62	- 3	0
358	26	-60	- 2	0
367	26	-60	- 3	0
372	26	-59	- 3	0
384	26	-58	- 2	1
393	26	-57	- 3	- 2
398	27	-56	- 3	- 4
410	27	-56	- 3	- 4
419	27	-54	- 1	- 3
425	27	-53	1	- 3
437	27	-53	1	- 3
446	28	-53	2	- 1
452	28	-54	2	- 2
464	28	-54	4	1
474	28	-55	3	- 2

Table 16 -- continued

Projected residual** range in scale div.	Projected cell length in scale div.	y-coordinate in $\frac{\text{scale div.}}{8}$	S_1 in $\frac{\text{scale div.}}{8}$	D_1 in $\frac{\text{scale div.}}{8}$
474	28	-55	3	- 2
480	28	-56	4	0
492	29	-58	3	- 3
502	29	-58	5	- 3
508	29	-60	4	- 3
521	29	-61	6	- 4
531	29	-63	8	- 3
537	30	-64	7	- 8
550	30	-67	10	- 6
560	30	-71	11	- 5
567	30	-71	15	0
580	30	-77	16	5
590	31	-82	16	6
597	31	-86	15	5
610	31	-93	11	1
621	31	-98	10	2
628	31	-101	10	3
641	31	-104	10	3
652	32	-108	8	- 1
659	32	-111	7	- 1
672	32	-114	7	- 4
684	32	-116	9	- 2
691	32	-118	8	- 6
704	33	-121	11	- 3
716	33	-125	11	- 4
723	33	-126	14	0
737	33	-132	14	- 1
749	33	-136	15	3
756	33	-140	14	- 6
770	33	-146	15	- 6
782	34	-151	12	- 7
789	34	-154	20	- 1
803	34	-161	21	- 3
816	34	-171	19	- 5
823	34	-174	21	- 3
837	34	-182	24	1
850	35	-190	24	1
857	35	-195	24	1
871	35	-206	23	- 2

Table 16 -- continued

Projected residual** range in scale div.	Projected cell length in scale div.	y-coordinate in $\frac{\text{scale div.}}{8}$	S_i in $\frac{\text{scale div.}}{8}$	D_i in $\frac{\text{scale div.}}{8}$
885	35	-214	23	- 2
892	35	-219	23	- 2
906	36	-229	25	1
920	36	-237	25	1
927	36	-242	25	1
942	36	-254	24	3
956	36	-262	24	6
963	36	-267	24	9
978	37	-278	21	10
992	37	-286	18	8
999	37	-291	15	5
1015	37	-299	11	3
1029	37	-304	10	4
1036	37	-306	10	6
1052	37	-310	8	5
1066	38	-314	6	4
1073	38	-316	4	3
1089	38	-318	3	4
1104	38	-320	2	6
1111	38	-320	1	4
1127	38	-321	- 1	3
1142	39	-322	- 4	0
1149	39	-321	- 3	2
1165	39	-320	- 4	2
1181	39	-318	- 4	1
1188	39	-318	- 5	0
1204	39	-316	- 6	- 6
1220	40	-314	- 5	- 7
1227	40	-313	- 5	-10
1243	40	-310	0	- 7
1260	40	-309	2	- 7
1267	40	-308	5	- 3
1283	40	-310	7	0
1300	40	-311	9	3
1307	41	-313	8	2
1323	41	-317	7	0
1340	41	-320	6	0
1348	41	-321	6	- 2
1364	41	-324	7	2

Table 16 -- continued

Projected residual** range in scale div.	Projected cell length in scale div.	y-coordinate in $\frac{\text{scale div.}}{8}$	S_i in $\frac{\text{scale div.}}{8}$	D_i in $\frac{\text{scale div.}}{8}$
1381	41	-326	6	2
1389	42	-327	8	7
1405	42	-331	5	6
1422	42	-332	4	6
1431	42	-335	1	4
1447	42	-336	- 1	2
1464	42	-336	- 2	1
1473	43	-336	- 3	1
1489	43	-335	- 3	2
1506	43	-334	- 3	3
1516	43	-333	- 4	1
1532	43	-332	- 5	- 1
1549	43	-331	- 6	- 1
1559	43	-329	- 5	0
1575	43	-327	- 4	2
1592	44	-325	- 5	2
1602	44	-324	- 5	4
1618	44	-323	- 6	8
1636	44	-320	- 7	11
1646	44	-319	- 9	9
1662	44	-317	-14	1
1680	44	-313	-18	- 7
1690	45	-310	-18	- 8
1706	45	-303	-15	- 5
1724	45	-295	-11	0
1735	45	-292	-10	1
1751	45	-288	-10	1
1769	45	-284	-11	0
1780	46	-282	-11	1
1796	46	-278	-11	0
1814	46	-273	-11	0
1826	46	-271	-12	- 1
1842	46	-267	-11	1
1860	46	-262	-11	2
1872	46	-259	-11	3
1888	47	-256	-12	3
1906	47	-251	-13	2
1918	47	-248	-14	1
1935	47	-244	-15	1

Table 16 -- continued

Projected residual** range in scale div.	Projected cell length in scale div.	y-coordinate in $\frac{\text{scale div.}}{8}$	S_i in $\frac{\text{scale div.}}{8}$	D_i in $\frac{\text{scale div.}}{8}$
1953	47	-238	-15	1
1965	47	-234	-15	2
1982	47	-229	-16	2
2000	47	-223	-16	3
2012	48	-219	-17	2
2029	48	-213	-18	1
2047	48	-207	-19	0
2060	48	-202	-19	1
2077	48	-195	-19	1
2095	49	-188	-21	- 2
2108	49	-182	-19	3
2125	49	-176	-20	0
2144	49	-167	-19	3
2157	49	-163	-22	0
2174	49	-156	-20	4
2193	49	-148	-22	4
2206	49	-141	-22	2
2223	49	-136	-24	1
2242	50	-126	-26	- 4
2255	50	-119	-24	1
2272	50	-112	-25	- 2
2292	50	-100	-22	3
2305	50	- 95	-25	1
2322	50	- 87	-23	4
2342	50	- 78	-25	1
2355	50	- 72	-26	0
2372	50	- 64	-27	- 3
2392	51	- 53	-26	- 4
2405	51	- 46	-26	- 2
2422	51	- 37	-24	1
2443	51	- 27	-22	9
2456	51	- 20	-24	4
2473	51	- 13	-25	4
2494	52	- 5	-31	- 5
2507	52	4	-28	0
2524	52	12	-29	- 1
2546	52	26	-26	2
2559	52	32	-28	
2576	52	41	-28	

Table 16 -- continued

Projected residual** range in scale div.	Projected cell length in scale div.	y-coordinate in $\frac{\text{scale div.}}{8}$	S_i in $\frac{\text{scale div.}}{8}$	D_i in $\frac{\text{scale div.}}{8}$
2598	52	52	-28	
2611	52	60		
2628	52	69		
2650	53	80		
2662	53			
2680	53			
2703	53			

$$\bar{D}_{obs} = \left\{(0.509)^2 - (0.20)^2\right\}^{\frac{1}{2}} = 0.468 \text{ microns}$$

$$M = 1837 \left(\frac{0.5}{0.468}\right)^{2.314} = 2142 \; m_e$$

$$R_M \cong \frac{1.82}{\sqrt{76}} \; (2142) = 417 \; m_e$$

*The constant sagitta method has been employed in making the scattering measurements. The technique is described in Chapter V.

**A $P_{Q,5}$ scheme has been used with overlap. The procedure is described in a footnote to Table 8, Chapter VI.

Table 17

Gap Length Data for Track 1, Table 3

β_i in microns	$k\delta_i$ in microns	ΔR_i in microns	$\sum g_i''$ in* microns	$\sum g_i$ in** microns	G in microns	R in microns
15.7	2.0	15.9	0.18	0.18	0.18	15.9
71.5	3.0	71.6	4.11	4.12	4.30	87.5
71.5	2.0	71.6	4.47	4.47	8.77	159.1
71.5	1.0	71.5	7.15	7.15	15.92	230.6
71.5	2.0	71.6	5.18	5.19	21.11	302.2
71.5	3.0	71.6	5.18	5.19	26.30	373.8
71.5	5.0	71.7	3.58	3.59	29.89	445.5
71.5	4.0	71.6	5.18	5.20	35.09	517.1
71.5	5.0	71.7	8.22	8.26	43.34	588.8
71.5	5.0	71.7	4.82	4.85	48.18	660.5
71.5	2.0	71.6	6.26	6.26	54.44	732.1
71.5	2.0	71.6	6.61	6.61	61.05	803.7
71.5	3.0	71.6	7.69	7.69	68.74	875.3
71.5	1.0	71.6	11.44	11.44	80.18	946.9
71.5	2.0	71.6	8.04	8.04	88.23	1018.5
71.5	0.0	71.5	8.40	8.40	96.63	1090.0
71.5	2.0	71.6	9.12	9.13	105.76	1161.6
71.5	1.0	71.5	7.87	7.87	113.63	1233.1
71.5	1.0	71.5	9.65	9.65	123.28	1304.6
71.5	0.0	71.5	13.59	13.59	136.87	1376.1
71.5	0.0	71.5	11.26	11.26	148.13	1447.6
71.5	0.0	71.5	10.90	10.90	159.03	1519.1
71.5	1.0	71.5	9.65	9.65	168.68	1590.6
71.5	1.0	71.5	10.37	10.37	179.05	1662.1
71.5	2.0	71.6	9.47	9.48	188.53	1733.7
71.5	2.0	71.6	9.83	9.84	198.37	1805.3

*$\sum g_i''$ represents the cumulative gap length in a single cell uncorrected for depth. The double prime notation is adopted to avoid confusion with the notation which is introduced in the discussion of distortion corrections at the end of Chapter IV.

**$\sum g_i$ represents the cumulative gap length in a single cell after correcting for depth. The correction required is discussed on the following page.

Let A be the mean grain diameter, g_i'' be the measured length of a single gap in a projected cell of length β and δ be the depth difference between the end points of the cell as measured on the fine focussing adjustment of the microscope. If g_i^a is the actual length of the gap on the track and θ is the observed angle at which the cell dips with respect to the viewing plane then

$$g_i'' = (g_i^a + A)\cos\theta - A$$

under the assumption that the grains are spherical. If the equation above is solved for $g_i^a \cos\theta$ one has

$$g_i^a \cos\theta = g_i'' + A\left(1 - \frac{\beta}{(\beta^2 + \delta^2)^{\frac{1}{2}}}\right).$$

Now if z_2 and z_1 represent the heights of the end points of g_i^a above the glass emulsion interface, after correction for shrinkage, then the corrected length, g_i of the gap will be given by

$$\begin{aligned} g_i &= \left[(z_2 - z_1)^2 + (g_i^a \cos\theta)^2\right]^{\frac{1}{2}} \\ &= \left[(kg_i^a \sin\theta)^2 + (g_i^a \cos\theta)^2\right]^{\frac{1}{2}} \\ &= g_i^a \cos\theta\left[1 + (k\tan\theta)^2\right]^{\frac{1}{2}} \\ &= g_i^a \cos\theta\left[1 + \left(\frac{k\delta}{\beta}\right)^2\right]^{\frac{1}{2}} \\ &= g_i'' + A\left(1 - \frac{\beta}{(\beta^2 + \delta^2)^{\frac{1}{2}}}\right)\left(\frac{\beta^2 + (k\delta)^2}{\beta}\right)^{\frac{1}{2}}. \end{aligned}$$

Then if there are n gaps in the single cell

$$\sum_{i=1}^{i=n} g_i = \left\{1 + \left(\frac{k\delta}{\beta}\right)^2\right\}^{\frac{1}{2}} \sum_{i=1}^{i=n} g_i'' + nA \left\{1 + \left(\frac{k\delta}{\beta}\right)^2\right\}^{\frac{1}{2}} \left\{1 - \frac{1}{\left[1 + \left(\frac{\delta}{\beta}\right)^2\right]^{\frac{1}{2}}}\right\}$$

$$= \psi' \sum_{i=1}^{i=n} g_i'' + nA\,\psi'\left(1 - \frac{1}{\psi}\right) \qquad \text{(B-1)}$$

where $\psi' = \left\{1 + \left(\frac{k\delta}{\beta}\right)^2\right\}^{\frac{1}{2}}$ and $\psi = \left\{1 + \left(\frac{\delta}{\beta}\right)^2\right\}^{\frac{1}{2}}$.

Tables of values of ψ', ψ and $\left(1 - \frac{1}{\psi}\right)$ have been constructed from which (B-1) may be readily evaluated.

Table 18

Area Data for Track 1, Table 4

β_i in microns	$k\delta_i$ in microns	ΔR_i in microns	R in microns	Area in arbitary units
14.9	0.0	14.9	14.9	0.12
21.1	0.0	21.1	36.0	0.27
28.6	5.4	29.1	65.1	0.51
33.6	5.4	34.0	99.1	0.74
28.6	3.2	28.8	127.9	0.98
31.1	3.2	31.2	159.1	1.12
23.6	3.2	23.8	182.9	1.36
36.1	6.5	36.6	219.5	1.60
34.8	6.5	35.4	254.9	1.86
19.9	2.2	20.0	274.9	1.99
38.5	7.5	39.3	314.2	2.24
36.1	6.5	36.6	350.8	2.44
39.8	7.5	40.5	391.3	2.68
44.8	7.5	45.4	436.7	3.01
42.3	5.4	42.7	479.4	3.27
43.5	5.4	43.8	523.2	3.54
44.8	4.3	45.0	568.2	3.77
38.5	4.3	38.8	607.0	3.97
38.5	2.2	38.6	645.6	4.20
43.5	2.2	43.7	689.3	4.48
42.3	2.2	42.3	731.6	4.68
44.8	2.2	44.8	776.4	4.96
42.3	3.2	42.4	818.8	5.17
44.8	2.2	44.8	863.6	5.39
42.3	3.2	42.4	906.0	5.59
44.8	1.1	44.8	950.8	5.82
38.5	1.1	38.6	989.4	6.04